AGU PUBLICATIONS

Reviews of Geophysics

REVIEW ARTICLE
10.1002/2017RG000560

Key Points:
- The 2015/2016 El Niño is the first extreme El Niño of the 21st century
- The 2015/2016 El Niño contributes to a better understanding of ENSO extremes
- Multiple simple indices can be used to monitor and identify ENSO extremes

Correspondence to:
A. Santoso,
a.santoso@unsw.edu.au

Citation:
Santoso, A., Mcphaden, M. J., & Cai, W. (2017). The defining characteristics of ENSO extremes and the strong 2015/2016 El Niño. *Reviews of Geophysics*, *55*, 1079–1129. https://doi.org/10.1002/2017RG000560

Received 1 MAR 2017
Accepted 9 NOV 2017
Accepted article online 14 NOV 2017
Published online 20 DEC 2017

The Defining Characteristics of ENSO Extremes and the Strong 2015/2016 El Niño

Agus Santoso[1,2], Michael J. Mcphaden[3], and Wenju Cai[2,4]

[1]ARC Centre of Excellence for Climate System Science and Climate Change Research Centre, University of New South Wales, Sydney, New South Wales, Australia, [2]Centre for Southern Hemisphere Oceans Research, CSIRO Oceans and Atmosphere, Hobart, Tasmania, Australia, [3]Pacific Marine Environmental Laboratory, National Oceanic and Atmospheric Administration, Seattle, WA, USA, [4]Physical Oceanography Laboratory/CIMST, Ocean University of China and Qingdao National Laboratory for Marine Science and Technology, Qingdao, China

Abstract The year 2015 was special for climate scientists, particularly for the El Niño Southern Oscillation (ENSO) research community, as a major El Niño finally materialized after a long pause since the 1997/1998 extreme El Niño. It was scientifically exciting since, due to the short observational record, our knowledge of an extreme El Niño has been based only on the 1982/1983 and 1997/1998 events. The 2015/2016 El Niño was marked by many environmental disasters that are consistent with what is expected for an extreme El Niño. Considering the dramatic impacts of extreme El Niño, and the risk of a potential increase in frequency of ENSO extremes under greenhouse warming, it is timely to evaluate how the recent event fits into our understanding of ENSO extremes. Here we provide a review of ENSO, its nature and dynamics, and through analysis of various observed key variables, we outline the processes that characterize its extremes. The 2015/2016 El Niño brings a useful perspective into the state of understanding of these events and highlights areas for future research. While the 2015/2016 El Niño is characteristically distinct from the 1982/1983 and 1997/1998 events, it still can be considered as the first extreme El Niño of the 21st century. Its extremity can be attributed in part to unusually warm condition in 2014 and to long-term background warming. In effect, this study provides a list of physically meaningful indices that are straightforward to compute for identifying and tracking extreme ENSO events in observations and climate models.

Plain Language Summary The El Niño Southern Oscillation (ENSO) continues to boast its prominence as Earth's strongest source of year-to-year climate variability with the appearance of a remarkable El Niño event in 2015–2016. The 2015/2016 El Niño was indeed a strong event with dramatic impact on a global scale. However, it exhibited distinct characteristics from those of past extreme El Niños in modern instrumental record. This challenges our previous understanding of an extreme El Niño which is important for ENSO prediction, monitoring, and future projections. The 2015/2016 El Niño has diversified the small sample of ENSO events in our short instrumental record. It has facilitated important discussions on our progress in understanding the nature of ENSO and its extremes, how they respond to greenhouse warming, and what the climate science community should do next in their quest to fully grasp the complexity of ENSO behavior. These are covered in this review paper which establishes the 2015/2016 El Niño as the first extreme El Niño of the 21st century.

1. Introduction

The El Niño–Southern Oscillation (ENSO) is the Earth's strongest source of year-to-year climate variability as emphasized by the recent appearance of a remarkable El Niño event in 2015–2016 (Blunden & Arndt, 2016). The pronounced global impacts of ENSO extend to land and marine habitats, water availability, food security, economies, and social stability (e.g., Barnard et al., 2015; Cashin et al., 2015; Glantz, 2001; Hsiang et al., 2011; Iizumi et al., 2014; McPhaden et al., 2006), thus underscoring the necessity to accurately predict ENSO well in advance for better management of resources and disaster risk reduction. This has been the major motivation for intensive research into how ENSO operates.

Since Jacob Bjerknes put forth a hypothesis about 50 years ago that ENSO arises through ocean-atmosphere coupled feedbacks (Bjerknes, 1966), our understanding about ENSO has progressed significantly through advances in conceptual theories, modeling, and paleo-reconstructions. However, the shortness of modern observational record has remained a major issue. That is, although the spatial coverage of our observing

system has been increasing over time since the 1950s and particularly since the 1970s when buoy and satellite observations became available (e.g., Smith & Reynold, 2004), the temporal record is still too short to sufficiently constrain multiyear variability (Wittenberg, 2009). Longer records deep into the past can be obtained, but this involves dealing with large uncertainties. Instrumental ocean observations prior to 1950 were sparse, for instance, due to world war disruptions and were affected by inhomogeneous ship recording practices (e.g., Ishii et al., 2005; Kennedy, 2014; Worley et al., 2005). Paleo-reconstructions are limited in spatial coverage and still have difficulty in accurately capturing individual ENSO events, even though they can reasonably capture the statistics over a specific period (e.g., Gergis et al., 2006). For instance, $\delta^{18}O$ record from modern coral at Palmyra Island (6°N, 162°W) over the twentieth century is highly correlated with the Niño3.4 index, a commonly used ENSO metric, but the magnitude of individual events can either be severely overestimated or underestimated (Figure 2 of Cobb et al., 2003). Thus, every new observation, in particular, an emergence of a strong event, such as the 2015/2016 El Niño, presents a valuable opportunity to test the prevailing knowledge about ENSO and to review our progress toward a better understanding of this profound climate phenomenon.

Generated in the equatorial Pacific, ENSO vacillates irregularly between its warm phase, El Niño, and its cold phase, La Niña, peaking in boreal winter and recurring every 2 to 7 years. The central-to-eastern tropical Pacific Ocean warms during an El Niño and cools in a La Niña, causing large-scale changes in ocean and atmospheric circulations within and outside the tropical Pacific, elevating likelihood of extreme weather events around the globe, such as cyclones (e.g., Bell & Chelliah, 2006; Jin et al., 2014) and extreme rainfall (e.g., Power & Callaghan, 2016). The impacts tend to be more dramatic overall during extreme El Niño events, such as the 1982/1983 (Philander, 1983) and 1997/1998 (McPhaden, 1999) events, which can translate to significant fatalities, economic losses, and large-scale environmental degradation (Changnon, 2001; Glynn, 1990; Merlen, 1984; Valle et al., 1987). The 1997/1998 El Niño, for instance, cost tens of thousands of human casualties worldwide and economic losses of tens of billions in U.S. dollars (McPhaden et al., 2006). There were environmental disruptions such as devastating floods in Peru (Vos et al., 1999), mass coral bleaching events (Aronson et al., 2000; Strong et al., 1998), and severe drought and forest fires in southeast Asia (Murty et al., 2000). An enhanced capacity to predict such impactful events is a necessity, especially when they have been projected to increase in frequency under greenhouse forcing (Cai, Santoso, et al., 2015). There is also some paleo evidence indicating that twentieth century ENSO variability appears stronger than that in the past centuries or millennia (Cobb et al., 2013; McGregor, Timmermann, et al., 2013). Despite the ability of theories and climate models to provide insights into ENSO extremes (Cai, Santoso, et al., 2015; Takahashi & Dewitte, 2016), we must live with the fact that there have been only two extreme El Niño events that were relatively well observed and documented, and a handful of extreme La Niña events (Cai, Wang, et al., 2015) against which to test our understanding.

The 1982/1983 and 1997/1998 El Niños were not just the most intense in modern observational record but also the most peculiar. They exhibit unusual characteristics distinct from any other observed El Niños. These include an eastward propagation of sea surface temperature (SST) anomalies (McPhaden & Zhang, 2009; Santoso et al., 2013) and particularly intense rainfall in the otherwise dry and cold eastern equatorial Pacific Ocean (Cai, Borlace, et al., 2014). Such characteristics have been exploited to identify extreme El Niño in climate models under present-day and future greenhouse forcing scenarios (Cai, Santoso, et al., 2015; Santoso et al., 2013). However, given the limited observed sample, it is not certain to what extent the observed characteristics are applicable to all extreme El Niño events. For instance, the multimodel analysis of Cai, Santoso, et al. (2015) showed that extreme El Niños satisfying the rainfall definition does not necessarily occur with an eastward propagating El Niño. This result is in itself an issue as to how an extreme El Niño is defined. In addition, it is not yet clear what other variables exist that can potentially be used in event characterization.

Relative to extreme El Niño, the characteristics of extreme La Niña events tend to be less studied, since the nonnormal nature of the tropical Pacific SSTs is largely due to strong El Niño events (e.g., Burgers & Stephenson, 1999). Yet their impacts are equally dramatic. For instance, the 1998/1999 extreme La Niña was associated with catastrophic flooding events that claimed thousands of lives in Bangladesh, Venezuela, and China (Del Ninno & Dorosh, 2001; Jonkman, 2005; Kunii et al., 2002; Takahashi et al., 2001) and severe drought in the southwestern United States (Bell et al., 1999; Cole et al., 2002), to name only a few impacts. The fact that the 1998/1999 extreme La Niña immediately followed an extreme El Niño is

concerning. For instance, the 1997–1999 swing of ENSO extremes resulted in a dramatic increased U.S. agriculture economic losses from $1.5–1.7 billion in one year to $2.2–$6.5 billion in the following year (Adams et al., 1999). Particularly worrisome is that such swings from extreme El Niño to extreme La Niña have been projected to occur more frequently under greenhouse warming (Cai, Santoso, et al., 2015). As such, a better knowledge of ENSO extremes is crucial, and the emergence of the strong 2015/2016 El Niño nearly two decades after the major El Niño of 1997/1998, provides a timely opportunity to re-evaluate our knowledge of ENSO extremes.

The 2015/2016 El Niño unfolded just after the public and scientific community had anticipated an intense El Niño in 2014 (McPhaden, 2015; Santoso et al., 2015). Comparisons of the basic ENSO processes between the 2015/2016 event and the 1982/1983 and 1997/1998 events can be found in recent papers by L'Heureux et al. (2017) and Xue and Kumar (2017). As a general measure of ENSO amplitude, the Niño3.4 index of the 2015/2016 El Niño registers a value comparable, if not stronger, than the two previous extreme El Niño events (L'Heureux et al., 2017; see also Figure 10 below). The Niño3.4 index is an average of SST anomaly over central to eastern equatorial Pacific (5°S–5°N, 170°W–120°W), where the global atmosphere in general responds strongly to underlying SST variations; and is thus commonly used as a key index for ENSO operational forecasts. The media were abuzz with reports of extreme weather events which appear consistent with expectations during a strong El Niño. Indonesia experienced huge forest fires in austral spring that caused a haze crisis in neighboring countries; Peru was devastated by catastrophic flooding in early 2016; while severe coral bleaching events were spotted in many parts of the Pacific Ocean (Blunden & Arndt, 2016).

This review paper discusses the current view of ENSO and its extremes in light of the characteristics of the 2015/2016 El Niño, through analysis of various observed variables that typify ENSO processes. We will also assess how best to characterize extreme El Niño and La Niña events. In effect, we provide a list of physically based indices that capture the key characteristics of extreme ENSO, which are straightforward to compute. Such indices would be useful not only for the scientific research community and climate prediction agencies but also for industries, such as insurance (e.g., Khalil et al., 2007) and agriculture (e.g., Fraisse et al., 2008; Iizumi et al., 2014) that have already considered implementing some of the indices to develop risk management strategy.

The paper is organized as follows. Section 2 provides an overview of the basic ENSO properties, along with some of the associated research highlights. To help frame the rest of the discussions, we assign different strengths to ENSO events in section 3 where a summary of the data sets used in the paper is also provided. Section 4 examines the observed features of ENSO extremes, providing a context for the 2015/2016 El Niño, with discussion of the mixed layer heat budget. Section 5 summarizes the paper with discussion of the existing gaps and future research directions, touching upon various aspects including inter-basin interactions.

2. ENSO in a Nutshell and Topical Issues

2.1. Origin and Basic Properties

The tropical Pacific contains the essential geographical and physical elements that generate and support ENSO existence, all of which have evolved throughout Earth's history (e.g., Lyle et al., 2008). In a world without land masses there would not be an ENSO cycle, as there are no meridional boundaries that can support such a zonal mode of variability (Marshall et al., 2007). In essence, ENSO exists due to the fact that the tropical Pacific features equatorward blowing trade winds that veer westward under Coriolis force, accumulating an enormous volume of water above 28°C toward the Maritime Continent (Figure 1) (Yan et al., 1992), termed the western Pacific warm pool (WPWP). The warm pool fuels vigorous convection of moist air, forming the ascending branch of the Walker Circulation. This large-scale movement of air mass descends over the dry eastern equatorial Pacific, marked by a tongue of upwelled cooler waters that extend northwestward off the South American coast due to the Trades. The Intertropical Convergence Zone (ITCZ), a rainfall band of atmospheric convection sits just north of this "cold tongue," extending to the west toward the WPWP (Schneider et al., 2014). One other major convective zone is the South Pacific Convergence Zone (SPCZ), a rain band extending southeastward from the warm pool toward the French Polynesia (Kiladis et al., 1989). Associated with this climatological setup, the atmospheric sea level pressure is lower in the western tropical Pacific than in the eastern tropical Pacific. To maintain a balance with the atmosphere, the oceanic

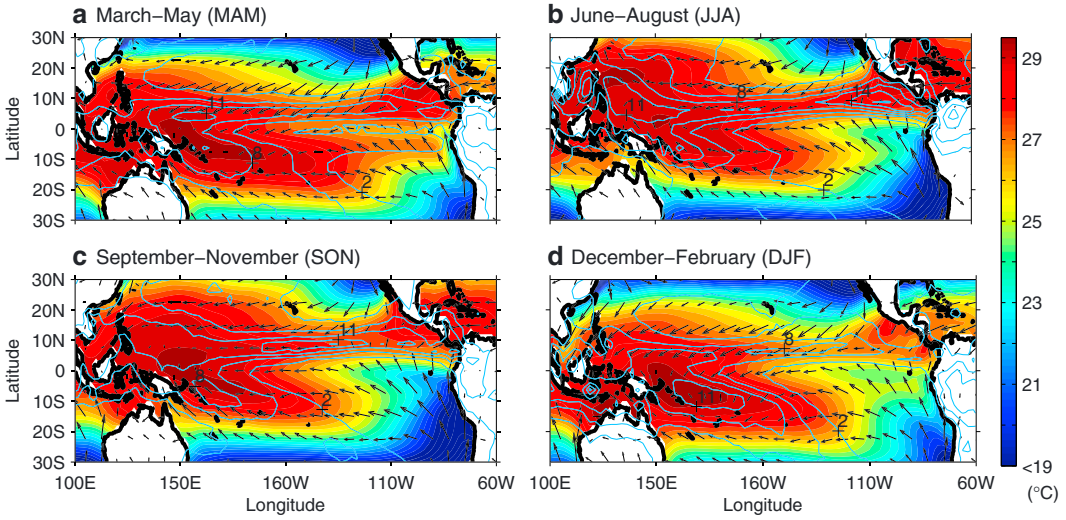

Figure 1. Seasonal climatology of the tropical Pacific, showing SST (color shading), precipitation (contours), and surface wind velocities (vectors) for (a) boreal spring (March–May average; MAM), (b) summer (June–August average, JJA), (c) autumn (September–November average, SON), and (d) winter (December–February average, DJF). The data are based on the ERSSTv5, CMAP rainfall, and NCEP winds from 1979 to 2017.

thermocline—a sharp boundary separating warm upper waters from cold deeper waters (typically marked by the 20°C isotherm)—shoals eastward, reaching as shallow as 30 m in the far eastern Pacific, and up to 200 m in the vicinity of the WPWP. This climatological state varies seasonally (e.g., Horel, 1982; Li & Philander, 1996; Yu & McPhaden, 1999) in response to the seasonal march of solar irradiance with a slight lag owing to the high heat capacity of the ocean. The cold tongue and the Trade Winds intensify in boreal summer as the ITCZ marches poleward. Meanwhile, precipitation decreases over the eastern equatorial Pacific reaching a monthly average value of less than 1 mm d^{-1}. The cold tongue then warms toward boreal spring, as the ITCZ shifts equatorward and the easterly winds weaken.

ENSO is year-to-year deviation from this seasonally evolving climatological state in which anomalous warming of the eastern equatorial Pacific during an El Niño is associated with weaker than normal Walker Circulation, marked by slackened Trade Winds, east-west atmospheric pressure gradient, and thermocline tilt (Figure 2). These elements interact in a positive Bjerknes-coupled feedback loop (Bjerknes, 1966), whereby the eastern Pacific warming induces weaker winds which in turn deepen the thermocline, thus further promoting surface warming. The feedback cycle continues toward the end of the calendar year when damping processes start to take over. Associated with this surface warming, the WPWP shifts eastward and the ITCZ and SPCZ move equatorward, significantly increasing precipitation in the otherwise dry eastern equatorial Pacific. La Niña generally describes the opposite, though this is a loose generalization in particular when ENSO is viewed from the lens of its extremes as discussed in this present review paper.

2.2. Irregularity and Seasonality

ENSO occurs in a quasi-oscillatory manner with an average period of about 4 years, owing to the particularity of the tropical Pacific climate system (e.g., Cane & Zebiak, 1985). That is, the climatological elements of the tropical Pacific, such as the Trade Winds, warm pool, cold tongue, thermocline, including the geometry of the basin, allow accumulation and lag times for their interactions to result in roughly 2 years for an El Niño to develop, peak, and decay, followed by a La Niña, and so forth in a quasi-cyclical fashion (e.g., MacMynowski & Tziperman, 2008). The cyclical tendency of ENSO occurrence, and specifically the transition from one opposite phase to the other, can be generally explained through conceptual models such as the recharge-discharge oscillator (Jin, 1997), delayed oscillator (Battisti & Hirst, 1989), western Pacific oscillator (Weisberg & Wang, 1997), or advective-reflective oscillator (Picaut et al., 1997). These theoretical models include the Bjerknes positive feedback but have different views on the negative feedback process that involves ocean equatorial waves (see also Wang, 2001, for a unified view of these frameworks; and Fedorov, 2010, on how these oscillator models are various limits of an integro-differential equation that

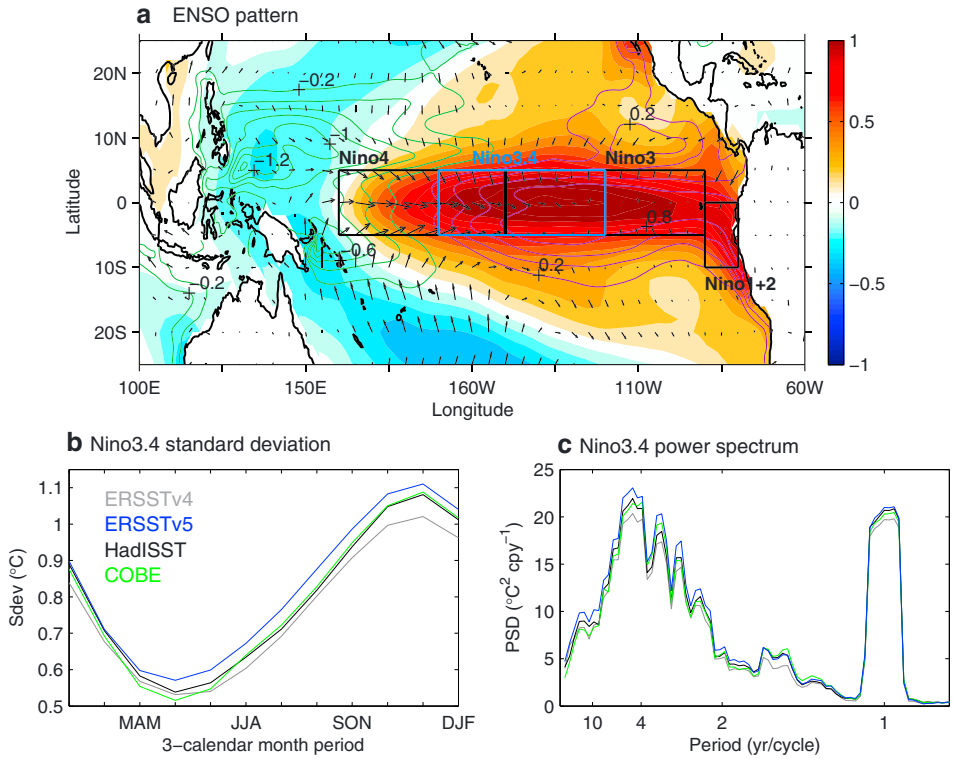

Figure 2. General ENSO properties. (a) Anomalous patterns in SST (color shading), T300 (contours), and surface wind velocities (vectors), shown as regressions onto the Niño3.4 index. (b) Standard deviation of the Niño3.4 index as a function of season (calculated with a 3 month sliding window from January 1950 to February 2017), representing ENSO amplitude toward the end of the calendar year when it peaks. (c) Power spectrum of the Niño3.4 index (January 1950–December 2016), indicating the characteristic frequency of ENSO at about 4 years/cycle. The data in Figure 2a are based on ERSSTv5, GODAS for T300, and NCEP winds. In Figures 2b and 2c, the different colors correspond to different SST reanalysis products. Boxed regions in Figure 2a indicate Niño4 (5°S to 5°N, 160°E–150°W), Niño3.4 (5°S–5°N, 170°W–120°W), Niño3 (5°S–5°N, 150°W–90°W), and Niño1+2 (10°S–0°, 90°W–80°W).

describes equatorial dynamics in a low-frequency approximation). These theories describe the deterministic component of ENSO, which makes it the most predictable climate phenomenon, with potential forecast lead times extending to more than a year (Chen & Cane, 2008; Latif et al., 1998). However, observations show a high degree of irregularity in these vacillations. The power spectrum of the Niño3.4 index (Figure 2c) shows that while there is a peak at about 4 years per cycle, the interannual spectrum is rather broad, spanning 2–7 years per cycle.

The issue of aperiodicity or irregularity is critical as it essentially underscores what limits ENSO predictability (Fedorov et al., 2003). Thus, much effort has gone into understanding the factors that cause variations in ENSO behavior. These include stochasticity or weather noise (e.g., Blanke et al., 1997; Eckert & Latif, 1997), chaos stemming from the deterministic nonlinear ocean-atmosphere dynamical system and the annual cycle (e.g., Jin et al., 1994; Münnich et al., 1991; Neelin et al., 2000; Tziperman et al., 1994), as well as changes in the background climate state (e.g., Fedorov & Philander, 2001; Wang & An, 2002) and processes external to the tropical Pacific (e.g., Kajtar et al., 2017; Kucharski et al., 2016; Terray et al., 2016). Investigating these processes requires the use of climate models of a certain degree of complexity, such as a simple conceptual model (e.g., Jin, 1997; Suarez & Schopf, 1988), an intermediate complexity model (e.g., Zebiak & Cane, 1987), or a comprehensive general circulation model, depending on the extent to which particular processes need to be isolated and controlled.

Using a comprehensive ocean model coupled to a simple atmospheric model, Blanke et al. (1997) examined the effect of stochastic winds on ENSO irregularity. Without stochastic wind forcing, a regular self-sustained oscillation was produced, indicated by a sharp spectral peak; whereas with weather noise the spectral peak broadened substantially, resembling the observed. In the real system, stochasticity can

manifest in the form of "wind bursts"—episodic but sustained reversals or enhancements of winds about the equator for several days, which can be due to various factors, such as tropical cyclones and Madden-Julian Oscillation (e.g., Puy et al., 2016). Wind bursts can trigger ENSO development and influence its eventual fate, depending on the characteristics of the wind bursts (e.g., strength, timing, and location) as well as the prevailing background condition of the tropical Pacific (e.g., Fedorov, 2002). Such stochastic forcings ultimately lead to diversity in ENSO strength, patterns, and timing (e.g., Hu et al., 2014; Karnauskas, 2013). On the other hand, other studies such as Münnich et al. (1991) demonstrate that stochastic forcing alone is not the only source of aperiodicity, but another contender is chaos stemming from nonlinearity in the deterministic system. The use of a simple linear shallow-water equatorial ocean model driven by zonal wind forcing as a nonlinear function of eastern equatorial Pacific thermocline depth allowed Münnich et al. to systematically explore the effect of air-sea coupling strength as well as Rossby waves. Self-sustained oscillation was achieved under sufficiently strong coupling, and irregularity then emerged, even in the absence of weather noise, as air-sea coupling and/or number of Rossby waves were increased. These results were produced in a model without annually varying climatology, but aperiodicity appeared more readily if the model incorporated seasonality. The role of the seasonal cycle in giving rise to chaotic behavior on interannual time scales was elaborated further by Jin et al. (1994) and Tziperman et al. (1994), through the so-called mechanism "quasi-periodicity route to chaos" (Jensen et al., 1984).

The fact that ENSO variability can be produced in models without an annual cycle, that is, in the absence of seasonal shifts in the trade winds, ITCZ, SPCZ, and so forth, indicates that the intrinsic seasonality is not a requirement for ENSO existence. However, the annual cycle does introduce peculiarity in ENSO behavior, including the salient seasonal phase-locking property (e.g., Rasmusson & Carpenter, 1982), featuring the tendency for ENSO amplitude to peak toward the end of calendar year from a minimum in boreal spring (Figure 2b). This aspect is relevant for seasonal forecasting, and thus the mechanism for the seasonal phase locking of ENSO has been a subject of active research (e.g., An & Wang, 2001; Dommenget & Yu, 2016; Harrison & Vecchi, 1999).

There exist two main paradigms for the seasonal phase locking, with the first being related to the frequency-locking mechanism of Jin et al. (1994) and Tziperman et al. (1994). The other is related to the modulation of ENSO's growth rate according to the seasonal variation of the equatorial Pacific climatological state (Hirst, 1986; Philander et al., 1984; Stein et al., 2010). Stein et al. (2014) argued using experiments with a recharge oscillator model that it is the latter paradigm that seems to be the more likely mechanism. This re-emphasizes what had been inferred by earlier studies, as clearly surmised by Tziperman et al. (1997): "Hirst (1986) noted that the annually averaged basic state of the equatorial Pacific is too stable to support the onset of ENSO as a coupled ocean-atmosphere instability. Thus the seasonality of the background state is important in creating times during the year in which this state is unstable and ENSO can initiate through a coupled instability mechanism (Hirst, 1986; Philander, 1983; Philander et al., 1984)." The seasonality property is also reflected in the predictability of ENSO. The so-called "spring predictability barrier" exists in which ENSO forecast skill drops off dramatically over boreal spring than any other seasons in the year (Webster & Yang, 1992). This appears to be also associated with the annual cycle in the growth rate of ENSO. For instance, Levine and McPhaden (2015) found that spring predictability barrier exists in a conceptual recharge oscillator model only when the ENSO growth rate is set to vary seasonally.

Many of the studies mentioned above implemented models that include just the tropical Pacific basin, yet ENSO and its irregularity can be produced. However, in reality, there are various forcings coming from other regions, including the effect modes of climate variability sourced in other oceans via atmosphere and ocean teleconnection. These remote modes, such as the Indian Ocean Dipole (Saji et al., 1999) and the Atlantic Niño (Merle, 1980; Zebiak, 1993), are now realized to be able to influence ENSO evolution (e.g., Izumo et al., 2010; Rodríguez-Fonseca et al., 2009), either in combination or independently (Kajtar et al., 2017). Each also contains their own stochasticity, thus also contributing to ENSO irregularity. To complicate matters, ENSO irregularity also appears to be influenced by the mean state climate. This is reflected in the dependency of ENSO predictability on the decadally evolving mean state climate and the associated changes in ENSO characteristics (Aiken et al., 2015; Balmaseda et al., 1995; Barnston et al., 2012; Flügel & Chang, 1998; Horii et al., 2012; Kirtman & Schopf, 1998; McPhaden, 2012; Tang et al., 2008; Zhao et al., 2016).

2.3. ENSO-Mean State Interactions

The seasonal phase locking of ENSO reaffirms the close link between ENSO and the background climate. Various studies have demonstrated how ENSO behavior and characteristics are dependent on the structure of the background mean state which evolves on long time scales. This dependency is obvious on geological time scales (e.g., Cane, 2005; Manucharyan & Fedorov, 2014), such as in association with the wobble of the Earth's orbit (Braconnot et al., 2012; Clement et al., 1999; Timmermann et al., 2007), continental drifts affecting the configuration of oceanic gateways like the Indonesian throughflow (Santoso et al., 2011; Song et al., 2007), freshwater discharge into the North Atlantic Ocean (Timmermann et al., 2005), and so forth, all of which dramatically alter the mean state climate and in turn ENSO characteristics.

On decadal time scales, disentangling mean state-ENSO linkage is somewhat a more contentious issue. This is because ENSO can rectify onto the mean state through nonlinear dynamics (e.g., Sun et al., 2014) or redden through ocean and atmosphere teleconnections (e.g., Newman et al., 2016), thus giving rise to decadal variability, manifesting in modes such as the Interdecadal Pacific Oscillation (IPO) (Power et al., 1999) or its Northern Hemisphere analog, the Pacific Decadal Oscillation (PDO) (Mantua et al., 1997). Yet the impact of decadal mean state on ENSO can be readily explained through coupled dynamical frameworks (e.g., Boucharel et al., 2015; Choi et al., 2011; Jin et al., 2006, 1996; Lübbecke & McPhaden, 2014). Research on this issue was particularly stimulated following the apparent climate shift around the mid-1970s towards a more positive IPO phase until the late 1990s, as evident from an El Niño-like decadal mean state with warming of the tropical Pacific and slackened Pacific Trade Winds (e.g., Trenberth & Hurrel, 1994). The ENSO properties and dynamics pre- and post-1970s decadal periods are distinct (see also Aiken et al., 2013; Capotondi & Sardeshmukh, 2017). The earlier period exhibits higher frequency and weaker amplitude than the later period (e.g., An & Wang, 2000), consistent with theoretical understanding which emphasizes the stronger role of the "thermocline feedback" (An & Jin, 2000; Fedorov & Philander, 2000; Wang & An, 2002).

The thermocline feedback, which involves subsurface temperature anomalies acting upon the mixed layer in the far eastern equatorial Pacific, is one of the three major components of the Bjerknes positive feedback. The other two are the "zonal advective" and "Ekman pumping" feedbacks, which involve anomalous zonal and vertical currents acting on the respective mean temperature gradients (see section 4.1). The increased importance of the thermocline feedback has also been associated with the emergence of the tendency for a stronger signature of eastward propagating SST anomalies in the post-1970s period, although such property is largely associated with the 1982/1983 and 1997/1998 extreme El Niños that feature strong SST anomalies toward the far eastern Pacific (McPhaden & Zhang, 2009; Santoso et al., 2013; see section 4.2.1 below). As the mean state has, in recent decades, switched back into a more negative IPO phase, which can explain the early 21st century global warming hiatus (England et al., 2014; Kosaka & Xie, 2013; see Medhaug et al., 2017 on hiatus controversies), ENSO variability consistently weakens (Hu et al., 2013), marked by more frequent emergence of weaker El Niño events that peak in the central Pacific (Lee & McPhaden, 2010; Xiang et al., 2013)—often referred to as central Pacific (CP) El Niño (Kao & Yu, 2009), El Niño Modoki (Ashok et al., 2007), dateline El Niño (Larkin & Harrison, 2005), or warm pool El Niño (Kug et al., 2009). This has been associated with the declining role of the thermocline feedback (Boucharel et al., 2015; Guan & McPhaden, 2016; Lübbecke & McPhaden, 2014).

Certainly, one of the most intriguing and pressing issues in recent decades is how ENSO would respond to greenhouse forcing (e.g., Timmermann et al., 1999). As anthropogenic greenhouse gas emission continues to climb, climate models project a mean state climate with weakened Walker Circulation (Vecchi et al., 2006), leading to slower ocean circulation (DiNezio et al., 2009; Sen Gupta et al., 2016; Vecchi & Soden, 2007), warmer SSTs and more rainfall toward the equator (Xie et al., 2010). While there is a high agreement across models on the mean state changes, the response of ENSO was found to be uncertain (Collins et al., 2010; Latif & Keenlyside, 2009; Taschetto et al., 2014) due to changes in the underlying feedback processes that tend to compensate one another (Kim & Jin, 2011) or decadal variability (Kim et al., 2014). Further studies, however, argued that there is in fact a detectable change in ENSO, not through the conventional measures of SSTs, but through its expression in rainfall (Cai, Santoso, et al., 2014; Power et al., 2013) and the zonal phase propagation of SST anomalies (Santoso et al., 2013)—physical variables that characterize the observed extreme El Niño, but only in models that can simulate such properties. Cai, Wang, et al. (2015) also found increased frequency of extreme La Niña in models that can simulate extreme ENSO. However, with the limited observational record, one basic question remains: What are ENSO extremes?

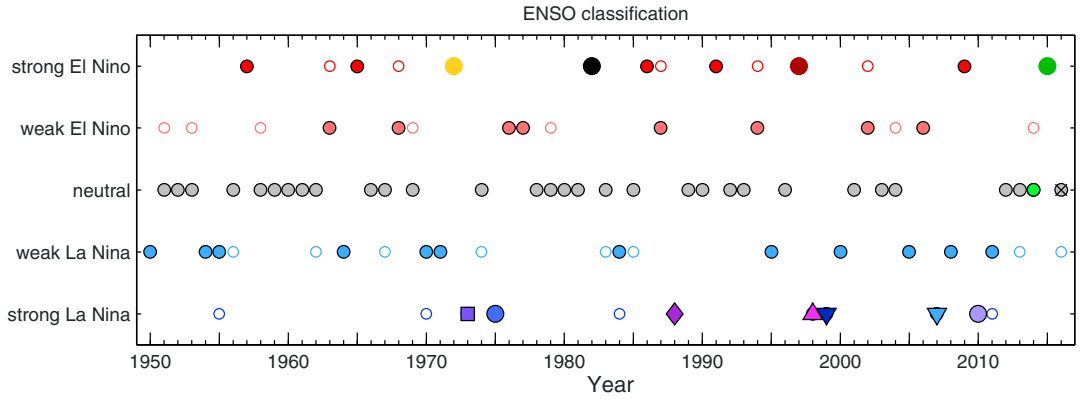

Figure 3. Classification of years as neutral, weak, or strong ENSO year. See section 3 for method. Empty circles denote years that could be marginally assigned into the stronger class (e.g., 1983/1984 and 2016/2017 neutral conditions could be marginally weak La Niña, and 2014/2015 could be a weak El Niño). The colors and marker types are consistently used throughout the paper.

3. Data Sets and ENSO Years

To aid the rest of the discussions, we first categorize ENSO events based on their strength which is typically measured by the Niño3.4 index in the boreal winter (Figure 3). For this purpose, it is of interest to utilize a long record, going as far back in time as possible to obtain sufficient samples for each different class of events. Even though data from the late 19th century are available, we choose to examine the 1950 to present (mid-2017) period when observations are more abundant, while still bearing in mind observational uncertainty pre-1970s (Kennedy, 2014). We use reanalysis products for smooth spatial and temporal coverage to reveal variability structures that have dynamical implications; these are the NOAA Extended Reconstructed SST version 4 (ERSSTv4) (Huang et al., 2015) and its recently updated version 5 (ERSSTv5) (Huang et al., 2017), the Hadley Centre SST (HadISST) (Rayner et al., 2003), and the Centennial In Situ Observation-Based Estimates (COBE) SST (Ishii et al., 2005). These products differ in various aspects such as the choice of observations, statistical and data assimilation methods, and resolution. Some intercomparisons across these four products are provided by Huang et al. (2017). As will be seen throughout the analysis below, these products are generally consistent across different metrics. They are also broadly consistent with one another in their long-term trends in the post 1950 period (Figure 8). This may not be necessarily the case if we consider trend from 1900, due to inconsistency in the estimate of ENSO events (Solomon & Newman, 2012), which could be amplified prior to 1950 (see Figure 30 and corresponding remarks in section 5).

We use multiple SST products not to construct observational error bars per se to attach on every metric. We do this primarily to construct a more generalized event classification that is less sensitive to variations in the analysis period, because not all of the other variables to be analyzed here (e.g., precipitation and heat content) are available for the same record period as the SST. To enhance this step further, we also take into account slight variations in the ENSO peak season. While various studies have used the December-to-February (DJF) average to mark the peak of ENSO, coinciding with the actual winter season, the Niño3.4 standard deviation peaks in November–January (NDJ; Figure 2b). Thus, we consider whether the strength of the Niño3.4 anomaly averaged over NDJ or DJF for any of the four SST reanalysis products exceeds 1 standard deviation for a strong ENSO year; between 0.5 and 1 standard deviation for a weak ENSO year; or falls below half of the standard deviation for a neutral year. If any of the years in the stronger class are also captured by the weaker class (via any of the products or seasons), then these years (denoted by empty circle in the stronger class; Figure 3) are assigned to the weaker class. Such years can also be considered as marginal events (e.g., 1983/1984, 2014/2015, 2016/2017 neutral conditions could be viewed as marginally weak ENSO events). Note that the Niño3.4 time series is first detrended over 1950–2016 to remove the long-term trend (Figure 8). This results in the following years to be robustly identified as the development phase of strong El Niño: 1957, 1965, 1972, 1982, 1991, 1997, 2009, and 2015; weak El Niño: 1963, 1968, 1976, 1977, 1987, 1994, 2002, and 2006; strong La Niña: 1973, 1975, 1988, 1998, 1999, 2007, and 2010; and weak La Niña: 1950, 1954, 1955,

1964, 1970, 1971, 1984, 1995, 2000, 2005, 2008, and 2011. These are assigned with unique colors and marker types which are consistently used throughout the paper.

Other than the 1982/1983, 1997/1998, and 2015/2016 El Niños, we also pay attention to the 1972/1973 event as it has been regarded as an extreme El Niño by previous studies (e.g., Chen et al., 2016; Hong et al., 2014). These four events are to be compared to the remaining five strong events. Shortening the analysis period to start from 1970 or 1980 would result in having only two other strong events to compare with (Figure A1), although there are also weaker events that could be considered as marginally strong (red empty circles). The classification is not very sensitive to variations in the analysis period or if the data are not detrended (Figure A1) and thus can be uniformly applied to mark the different years in all analysis with the different record periods. The sensitivity would be greater if we use only a single product and season, especially over the shorter period of which the products diverge more in the trends (Figures 8 and A2). Note that a few marginal events can be affected, such as the 2014/2015 warm event which is classified as a weak El Niño if the raw data are used or if detrended over 1980–2016 (Figure A1). Nonetheless, this does not influence our overarching discussions and conclusions about ENSO extremes. In certain plots, we also show the warm events that peak in the central Pacific, marked with a "plus" symbol. These are simply defined when the DJF average Niño4 index averaged across products is greater than 0.5°C and greater than Niño3, following Yeh et al. (2009), thus identifying the following years as CP El Niño: 1958, 1968, 1977, 1979, 1987, 1990, 1994, 2002, 2004, 2006, 2009, and 2014.

The generalized event classification is to be utilized in various analyses below that include empirical orthogonal function (EOF) and surface heat budget (section 4.1). To further illustrate observational uncertainty, three products for rainfall are also adopted: the standard and enhanced versions of the CPC Merged Analysis of Precipitation (CMAP) (Xie & Arkin, 1997), as well as the Global Precipitation Climatology Project (GPCP) version 2.3 (Adler et al., 2003), both are available from 1979. The rest of the data sets include the NCEP/NCAR Reanalysis (Kalnay et al., 1996) for sea level pressure (SLP) as well as monthly averaged zonal and meridional wind velocities at 850 hPa and daily data at the surface. While the Southern Oscillation Index (SOI) can be calculated from the NCEP reanalysis SLP, we chose to utilize SOI provided by the Australian Bureau of Meteorology. The average of ocean temperature above 300 m (T300) is used as a proxy for upper ocean heat content. Various indices of equatorial T300 are provided by the TAO Project Office of NOAA/PMEL (available from 1980). The Global Ocean Data Assimilation System (GODAS) reanalysis (Behringer, 2007), also available from 1980, is used for examining the T300 spatial pattern and to conduct heat budget analysis. To support the heat budget discussion, we also examine the output of the Estimating the Circulation and Climate of the Ocean—Phase II (ECCO2) reanalysis which is available from 1992 (Menemenlis et al., 2008). All of these products are continuously updated and made available to the public on regular basis.

Care should be taken in interpreting subsurface oceans in the equatorial Pacific prior to the mid-1980s when the establishment of TAO/TRITON array of moored buoys had just begun under the auspices of TOGA (Tropical Ocean-Global Atmosphere observing system) (McPhaden et al., 1998). This also applies to meteorological observations before TOGA and satellite era. For discussions on the complexity and historical development of ocean-atmosphere measurements, the readers can refer to articles by Woodruff et al. (2011), Abraham et al. (2013), Kennedy (2014), and Kent et al. (2017), among others. It is expected that differences in observational estimates produced by various reanalysis systems introduce uncertainties which are relevant for inter-event comparisons, but the divergence is unlikely to be large enough to alter the dynamical understanding that has been built through decades of reconciliation across theory, modeling, and observations. For example, modes of variability in different wind products are overall consistent with one another without introducing ambiguity about the basic understanding of the system (McGregor, Ramesh, et al., 2013). Nonetheless, observational uncertainties should be borne in mind in our discussions that follow, even when error bars are prescribed.

4. ENSO Extremes

Unlike moderate events, ENSO extremes are by nature a nonlinear phenomenon. The success of linear models in describing the general ENSO behavior (e.g., the recharge oscillator of Jin, 1997) gives an impression that ENSO is intrinsically a linear system with El Niño and La Niña being a mirror image to each other. This does at first appear to be the case as the distribution of the Niño3.4 index anomaly (detrended with seasonal cycle

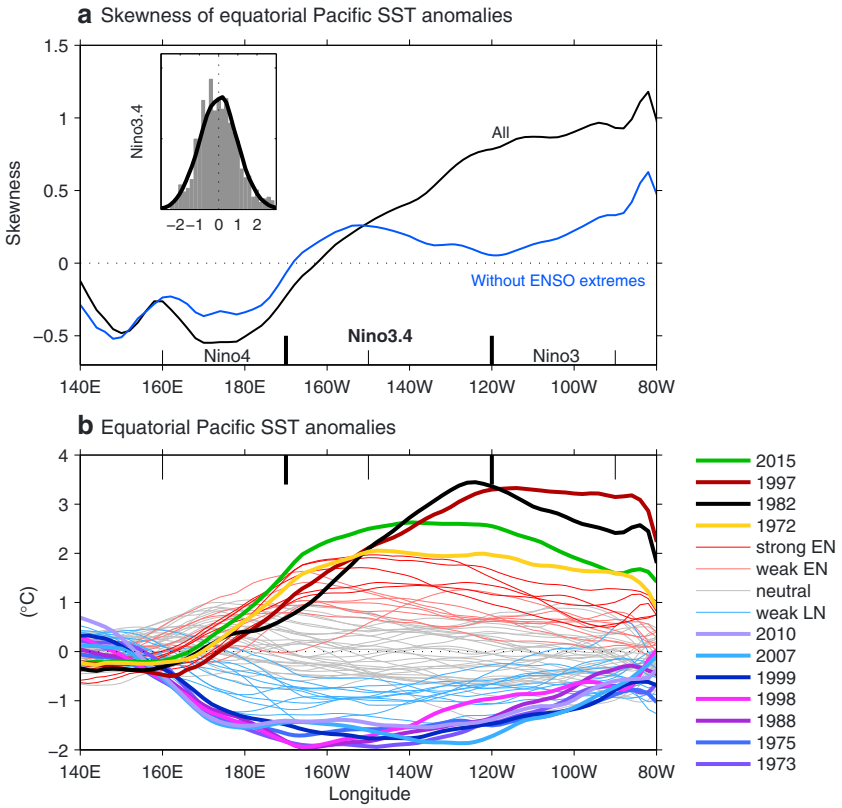

Figure 4. (a) Skewness of SST anomalies along the equatorial Pacific for all years from 1950 (black). The blue curve shows skewness calculated without the developing and decaying years of the strongest ENSO events: 1972/1973, 1982/1983, 1997/1998, 2015/2016 El Niño events, and 1973/1974, 1975/1976, 1988/1989, 1998/1999, 1999/2000, 2007/2008, 2010/2011 La Niña events. Inset shows histogram of standardized Niño3.4 anomalies (gray shading), with the overlaid black curve indicating histogram of 10,000 random numbers generated from a normal distribution. (b) SST anomalies along the equator averaged over December to the following February. The analysis is based on the ERSSTv5 reanalysis, with long-term trend removed.

removed) is approximately Gaussian (Figure 4a). However, this near normality, which is measured by skewness close to zero, does not hold everywhere across the equatorial Pacific (Burgers & Stephenson, 1999): the skewness of SST anomalies turns from slightly negative in the western central Pacific (e.g., the skewness of Niño4 index is about −0.5) to highly positive into the far eastern Pacific (e.g., skewness of Niño1+2 exceeds 1). This is clearly demonstrated in Figure 4a (black curve) showing the skewness along the equator, where it goes from negative in the west to highly positive in the east.

This nonnormal characteristic is primarily associated with strong ENSO events (Figure 4b), with exceptionally warm SST anomalies peaking toward the east notably during the 1972/1973, 1982/1983, 1997/1998, and 2015/2016 El Niño events, and cold SST anomalies peaking westward during 1973/1974, 1975/1976, 1988/1989, 1998/1999, 1999/2000, 2007/2008, and 2010/2011 La Niña events. The contribution of these strong events to the nonlinearity can be gauged by recalculating the skewness with these strong events removed. To illustrate this, we remove 12 months before and after their peak, resulting in severe weakening of the skewness (Figure 4a, blue curve). This demonstrates the nonlinear nature of strong ENSO events.

The nonlinearity in SSTs described above has been the motivating basis for active research into understanding the physics behind the asymmetry between El Niño and La Niña, such as in intensity, duration, pattern, and teleconnection (e.g., An & Jin, 2004; Boucharel et al., 2009; Cai, Santoso, et al., 2015; Capotondi et al., 2015; Choi et al., 2013; DiNezio & Deser, 2014; Dommenget et al., 2013; Frauen & Dommenget, 2010; Jin et al., 2003; Kang & Kug, 2002; Kessler, 2002; Kim et al., 2015; Levine et al., 2016; McGregor, Ramesh, et al., 2013; Monahan & Dai, 2004; Okumura & Deser, 2010; Santoso et al., 2013; Takahashi & Dewitte, 2016; Takahashi et al., 2011; Timmermann et al., 2003).

In this section, we explore the various processes underpinning ENSO, to further reveal the nonlinear nature of ENSO extremes, with the 2015/2016 El Niño event giving a useful perspective. We begin with an analysis of the surface ocean heat fluxes to get a sense of the rapidity of their evolution, followed by an examination of processes and the associated indices that capture the characteristics of these events.

4.1. Governing Ocean Heat Fluxes

A heat budget analysis of the ocean mixed layer has been generally used to examine the underlying processes behind ENSO (e.g., An & Jin, 2004; Jin et al., 2003; Kim et al., 2015; Su et al., 2010). The analysis decomposes heating rate, which shapes the SST anomalies, into its different components:

$$\int_{-H_m}^{0} T_t = \int_{-H_m}^{0} \left\{ Q' - \left[\left(u' T'_x + \bar{u}\, T'_x + u' \overline{T}_x \right) + \left(v' T'_y + \bar{v}\, T'_y + v' \overline{T}_y \right) + \left(w' T'_z + \overline{w} T'_z + w' \overline{T}_z \right) \right] \right\} + \text{Res}, \quad (1)$$

where Q is net air sea heat flux; u, v, and w correspond to zonal, meridional, and vertical current velocities; T is potential temperature. The subscripts x, y, and z denote derivative operators in the zonal, meridional, and vertical direction, respectively, and prime indicates anomaly from the climatological state denoted by the overbar. Each of the bracketed components correspond to zonal, meridional, and vertical advection (or transport) of heat, which can be further decomposed into nonlinear advection, advection of temperature anomaly by the climatological current, and advection of mean temperature by anomalous current. The current and temperature anomalies are linked to anomalous wind fields and thermocline depth variations. These collective terms are integrated across the surface mixed layer of depth H_m, commonly taken as 50 m, and any unresolved processes like turbulent mixing are typically contained in the residual term, Res. The heat budget analysis, which benefits from the increasing availability and improvements of ocean reanalysis products, allows a determination of the dominant terms and thus the important underlying processes that contribute to the changes in SST.

Examining the mixed-layer heat flux components in the eastern equatorial Pacific about the peak of ENSO events, Jin et al. (2003) and An & Jin (2004) found, using NCEP Ocean Data Assimilation System (ODAS) and the Simple Ocean Data Assimilation (SODA) beta 7 version, the nonlinear terms to be key in giving rise to the amplitude asymmetry. The horizontal and vertical nonlinear ocean advections were found to amplify warm SST anomalies but damp cold anomalies. However, with the more recent versions of the reanalysis products (SODA versions 2.0.2 and 1.4.2, and GODAS), Su et al. (2010) found that the nonlinear vertical advection instead damps the El Niño amplitude. They attributed these inconsistencies to biases in the vertical velocity derived from the previous reanalysis products. In further contrast to the earlier studies, using the latest version of SODA (version 2.2.4), Kim et al. (2015) found that the linear advection of mean temperature by zonal current anomaly ($u' \overline{T}_x$), that is, associated with the zonal advective feedback, becomes the major contributor, instead of the nonlinear terms that play a secondary role. Our analysis below based on the GODAS and ECCO2 data sets supports the important role of zonal advective feedback as concluded by Kim et al. (2015).

Figure 5 shows the various heat flux components in Niño4, Niño3.4, Niño3, and Niño1+2 regions, averaged over March to November (Period I; left column) and September to May the following year (Period II; right column) for each ENSO year from 1980 to present as covered by GODAS. The periods are chosen so as to capture the primary development and the peak to decay phases of ENSO evolution (see also Figure 6). The latter corresponds to the similar averaging period used by An and Jin (2004). The analysis is repeated using the ECCO2 data sets, which are available from 1992, and some of the results are shown in Figure 6. There are a number of interesting features underlining the nature of ENSO extremes that can be deduced from the GODAS analysis, which are broadly consistent with the ECCO2 results over the overlapping period. These are synthesized below:

1. *Increasing role of vertical advection eastward*. It can be seen that the prominence of the thermocline feedback (associated with the $\overline{w} T'_z$ term) and Ekman pumping feedback ($w' \overline{T}_z$) increase toward the eastern equatorial Pacific (Niño3, Niño1+2), while the relative importance of the zonal advective feedback ($u' \overline{T}_x$) increases toward central Pacific (Niño4). This highlights the fact that the thermocline depth shoals eastward, making it easier for changes in subsurface temperature to influence SSTs in the far eastern Pacific than in the central Pacific. It is noted however that the $\overline{w} T'_z$ term is comparable with or even smaller than $u' \overline{T}_x$ in the Niño3 region. This may at first appear at odds with prevailing ENSO theory

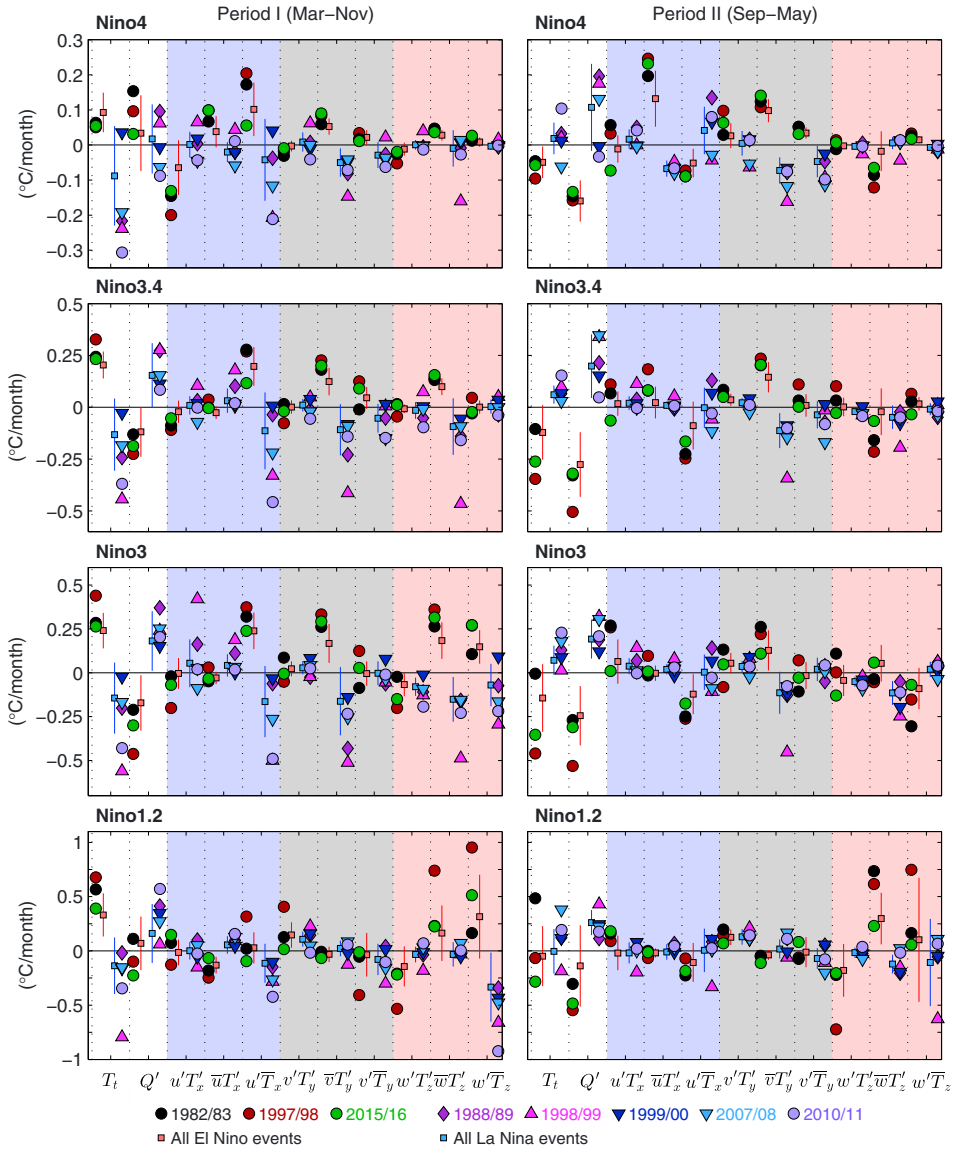

Figure 5. Main ocean heat flux components in the top 50 m as laid out in equation (1), (left column) averaged over March to November (Period I) and (right column) September to May in the following year (Period II) over the indicated regions. The values are shown for the different years as indicated by the different marker types. Red and blue markers with error bars are for the average of all El Niño and La Niña years, respectively. Error bars are 1 standard deviation unit above and below the means. The analysis is based on detrended data of GODAS reanalysis which covers 1980 to present. All terms shown have been averaged over 50 m, and the negative sign attached to all advection terms in equation (1) has been absorbed into each of the terms shown.

(e.g., Jin et al., 2006; Neelin et al., 1998) and many modeling studies (e.g., Borlace et al., 2013; Fedorov et al., 2015; Huang et al., 2012; Kim et al., 2014) that emphasize the dominance of the thermocline feedback in the eastern Pacific—although the relative dominance can substantially vary decadally and across different models. GODAS might have stronger bias in its velocity fields than ECCO2, as heat, momentum, and salt are conserved in ECCO2 but not in GODAS (e.g., Halpern et al., 2015; Huang et al., 2010). However, $\overline{w}T'_z$ is even smaller than $u'\overline{T}_x$ in ECCO2. It turns out that the discrepancy is not so much related to biases in the reanalysis products, but rather due to how the "thermocline feedback" is expressed in the heat budget equation. First note, $\overline{w}T'_z \approx \overline{w}\left(T'_0 - T'_{\mathrm{sub}}/H_m\right)$, where T'_0 is SST anomaly and T'_{sub} is subsurface anomaly below the mixed layer. In theoretical studies, the thermocline feedback is typically prescribed to $\overline{w}T'_{\mathrm{sub}}$ component so that T'_{sub} can then be expressed in terms of wind stress and SST anomaly as to formulate a conceptual model (e.g., Jin et al., 2006). The $\overline{w}T'_0$ component is, on the other hand, considered as part

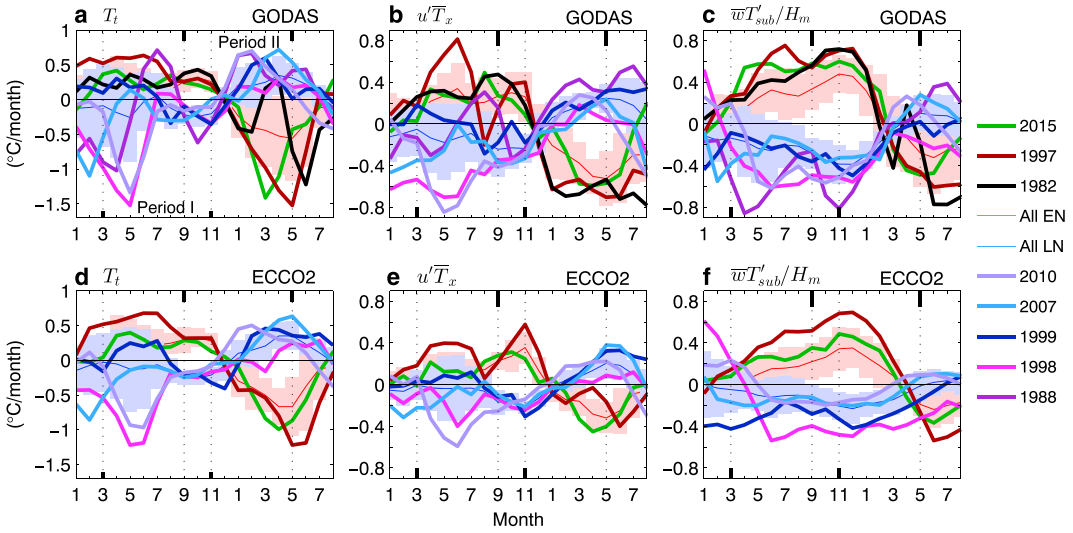

Figure 6. (a) Temperature tendency, (b) zonal advective feedback term, and (c) the subsurface component of the anomalous vertical advection by mean upwelling in the GODAS reanalysis. (d–f) As in Figures 6a–6c but for the ECCO2 reanalysis. Light red and blue shadings indicate 1 standard deviation unit above and below the mean for all El Niño and La Niña years, respectively.

of a damping term by the mean currents. Studies that adopt such framework will tend to report stronger dominance of the thermocline feedback (e.g., Boucharel et al., 2015; Ren & Jin, 2013). Figure 6 shows that the $\overline{w}T'_{sub}$ component is clearly larger than $u'\overline{T}_x$ in both GODAS and ECCO2. Also notable in Figure 6 is how the thermocline feedback defined as $\overline{w}T'_{sub}$ shows clearer role in maintaining SST anomalies a few months beyond the event peak. In either case, the relative dominance of the thermocline feedback increases toward eastern equatorial Pacific.

2. *Importance of zonal advective feedback*. The relative dominance of the zonal advective feedback ($u'\overline{T}_x$) increases westward. Even though $u'\overline{T}_x$ is the largest term in the central Pacific, it is still an important factor for the development of both warm and cold anomalies in the Niño3 region where the SST skewness is high (Figure 4a). The respective ensemble averages of all El Niño and La Niña years (red and blue square markers with error bars) during Period I display notable asymmetry between El Niño and La Niña in that the associated heating rate is robustly positive for El Niño, as also reflected in the total heating rate. Other important terms include $\overline{v}\,T'_y$, $\overline{w}T'_z$, and $w'\overline{T}_z$, which also display asymmetry between the opposite ENSO phases.
3. *Role of nonlinear terms*. The zonal and vertical nonlinear terms in the Niño3 largely reveal a damping on La Niña and El Niño, respectively , in agreement with Kim et al. (2015) and Su et al. (2010). The nonlinear terms become larger in the later period (Period II), acting to prolong the 1982/1983 and 1997/1998 El Niño SST anomalies, together with the large vertical advection terms in Niño1+2.
4. *Extreme heating/cooling rates*. Once the strongest ENSO events are revealed, rather than just examining the composites, two events emerge as the most extreme in the total heating/cooling rate (T_t) over the development period (Period I) in the eastern equatorial Pacific (Niño3.4, Niño3, Niño1+2). These are the 1997/1998 El Niño (dark red circle) and the subsequent 1998/1999 La Niña (upward triangle). In fact, the magnitude of T_t tends to be larger for the 1998/1999 La Niña than for the 1997/1998 El Niño across the equatorial Pacific.
5. *Relevance of initial conditions*. The stronger cooling rate for the 1998/1999 La Niña than the extreme heating rate of the 1997/1998 El Niño is understandable for the central Pacific where SST skewness is negative but is counterintuitive for the positively skewed SST in the eastern Pacific (Figure 4). Furthermore, the subsequent 1999/2000 La Niña (downward dark triangle; Figure 5) does not require much cooling rate to achieve its large negative SST anomalies. The cooling rate is even positive in the Niño4 region. These counterintuitive features emphasize the relevance of initial condition. Simply, the 1998/1999 La Niña starts off from an extremely warm condition associated with the 1997/1998 El Niño, and thus requires extremely large cooling to materialize as a strong La Niña. Then, the 1999/2000 La Niña does not

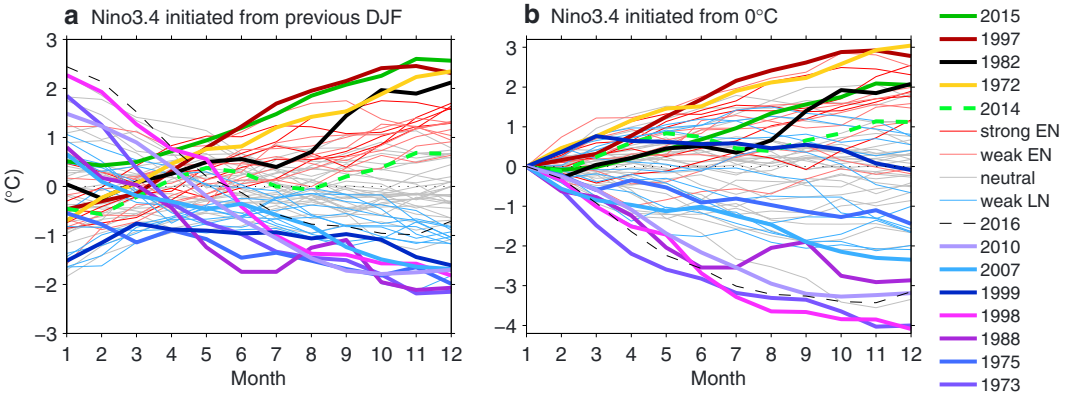

Figure 7. The relevance of initial condition. (a) Monthly Niño3.4 SST anomalies constructed by integrating the monthly SST tendency for each year forward from the previous December–February average value as initial condition. (b) The same as Figure 7a but taking 0°C anomaly as initial condition. The resulting SST anomalies at the end of the integration in December show skewness of 0.21 in Figure 7a and −0.46 in Figure 7b. The analysis is based on ERSSTv5 from 1950 onward.

require further cooling. The importance of initial condition is illustrated in Figure 7 which shows integrated Niño3.4 T_t forward from either an initial condition of December–February average anomaly (Figure 7a) or zero anomaly (Figure 7b) into the following December. The former results in a skewness of 0.21 in December and the latter results in skewness of −0.46, with strong La Niña amplitude being greater than El Niño. However, it is important to note that the initial condition does not only serve as a baseline but also determines the subsequent coupled feedback processes that determine the strength of the resulting event (e.g., Fedorov et al., 2015).

6. *The 2015/2016 El Niño*. The most striking distinction between the 2015/2016 El Niño and the 1982/1983 and 1997/1998 El Niños appears in the notably larger thermocline feedback-associated term ($\overline{w}T_z^{'}$) in the Niño1+2 region over Period II which acts to prolong the 1982/1983 and 1997/1998 El Niño. The zonal advective feedback in the Niño4 region is also larger in the past two strong El Niños than the 2015/2016 event. The total heating rates for the most recent El Niño are comparable with the 1982/1983 event, but notably weaker than the 1997/1998 event. However, note that the 1982/1983 event developed late as indicated by the more positive (or less negative) heating rates in Period II than other events. Despite the weaker heating rate than the 1997/1998 event, the magnitude of the 2015/2016 SST anomalies in Niño4 and Niño3.4 is comparable to the 1997/1998 El Niño. This highlights the role of the 2014/2015 warm condition (see also Abellán, McGregor, England, et al., 2017). Without the warm initial condition, the 2015/2016 El Niño would turn out weaker than the 1997/1998 El Niño (Figure 7).

The nonlinearity noted above manifests in asymmetric properties between El Niño and La Niña, in pattern, intensity, and evolution of the SST anomaly, rainfall, winds, upper ocean heat content, and many others. This will be revealed and discussed next to further understand the nature of this nonlinear phenomenon.

4.2. Extreme Characteristics

4.2.1. Sea Surface Temperature Anomalies

ENSO events are often characterized through their SST anomaly patterns at their peak in boreal winter, typically taken as the December-to-February (DJF) average. To reveal ENSO pattern, it is necessary to first have the data detrended, to remove the apparent long-term warming in the background climate from 1950 (Figure 8). Without detrending, the 2015/2016 pattern is overwhelmed by the background warming signal (Figure 9), making it difficult to compare against past ENSO events whose patterns differ little with or without detrending. The background long-term warming makes the 2015 Niño3.4 the warmest since at least 1950 (Figure 10), leading the event to be hailed as a record-breaking El Niño. Once the warming trend is removed, the 2015/2016 Niño3.4 is comparable with the 1997/1998 El Niño. This comparative analysis exploits small variations in the seasonal peak of ENSO (November–January and December–February) and possible variations across different reanalysis products (ERSSTv4, ERSSTv5, HadISST, and COBE) to provide an estimate of uncertainty for statistical significance test (see Figure 10 caption). Further, the background warming also contributes in making the 2015/2016 peak warm SST anomaly over the central Pacific (Niño4 region) to be record

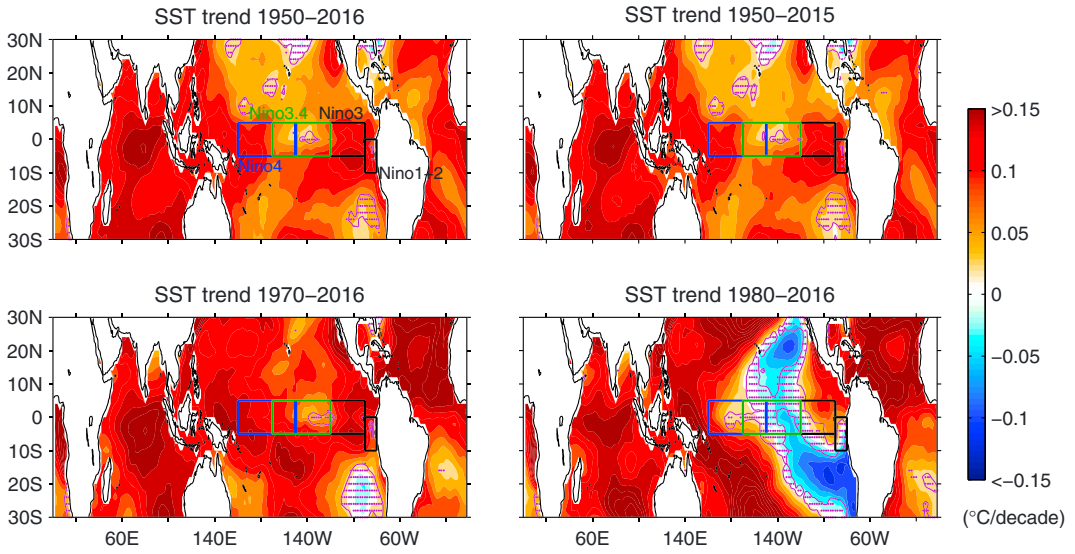

Figure 8. SST trends (°C/decade) averaged across the four SST reanalysis products across different periods. Stippled regions indicate any disagreement in the sign of the trend across the products. The corresponding trends for each product are shown in Figure A2.

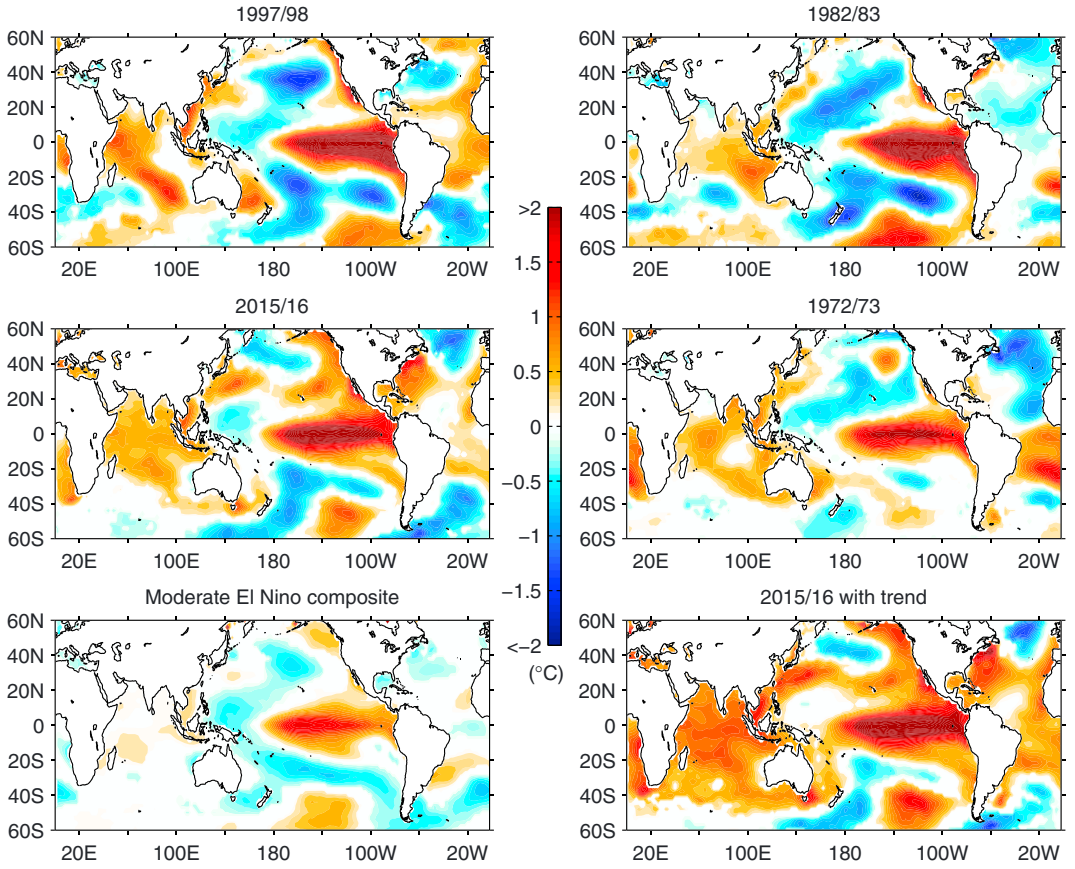

Figure 9. (top and middle rows) SST anomalies at the mature phase of four strongest El Niño events since 1950. Data are based on detrended December–February (DJF) average SST anomalies referenced to the 1950–2016 climatology averaged across ERSSTv4, ERSSTv5, HadISST, and COBE reanalysis products. (bottom left) Composite pattern for El Niño events of 1957/1958, 1965/1966, 1986/1987, 1991/1992, and 2009/2010. (bottom right) The raw 2015/2016 anomaly pattern. Statistically not significant anomalies have been set to 0 (P value $>$ 0.1 based on two-sided t test).

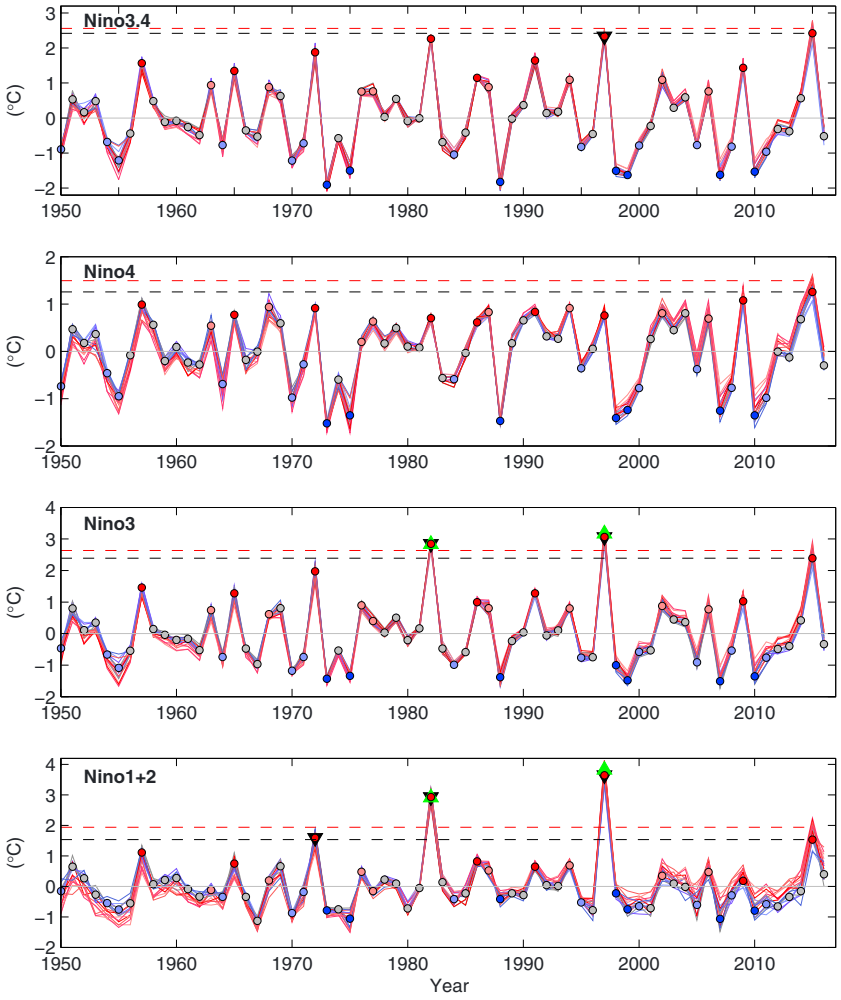

Figure 10. Time series of ENSO indices averaged over November–January (NDJ) and December–February (DJF) across the four reanalysis products. The raw and detrended time series are displayed in red and blue, respectively. The dashed horizontal lines indicate the corresponding 2015 values to provide a comparative gauge with past events. Any past events showing either not significantly different or significantly stronger warm anomalies than the 2015/2016 value are indicated with black downward triangle for the detrended time series and green upward triangle for the raw time series. Statistical significance is evaluated using a one-sided Student's *t* test at 99% confidence level based on the difference between the value at each year and the 2015 value, each having eight samples (NDJ and DJF values across the four products). Strong El Niño and strong La Niña events are marked with red and blue filled circles, respectively (lighter color for weak events); neutral years with gray circles.

breaking. Farther east, however, such as in the Niño3 region and Niño1+2 off the coast of Peru, the warm SST anomaly for the 2015/2016 El Niño is far weaker than in the 1982/1983 and 1997/1998 El Niños, regardless whether or not the data are detrended.

The ability for the far eastern equatorial Pacific (e.g., Niño3 and Niño1+2) to achieve unusually large warm anomaly underscores ENSO as a nonlinear system (see also section 4.1). Such nonlinearity renders SST skewness in the far eastern equatorial Pacific to be extraordinarily positive (Figure 4a), in fact the strongest in the tropical oceans (Figure 11a). The nonlinearity is largely attributed to the 1982/1983 and 1997/1998 events (Figure 11b). This becomes more apparent in the Niño3.4 versus Niño1+2 space (Figure 11c). As the Niño3.4 gradually warms toward a large value (e.g., above 2 standard deviation), there is a sharp increase in the Niño1+2 warming, attributed to the 1982/1983 and 1997/1998 El Niños. However, the 2015/2016 event appears to defy this nonlinear tendency, since, while its Niño3.4 anomaly is of similar magnitude to the 1982/1983 and 1997/1998 (above 2 standard deviation), the increase in the Niño1+2 remains incremental rather than abrupt. In the presence of background warming, the 2015/2016 Niño1+2 is pushed toward the

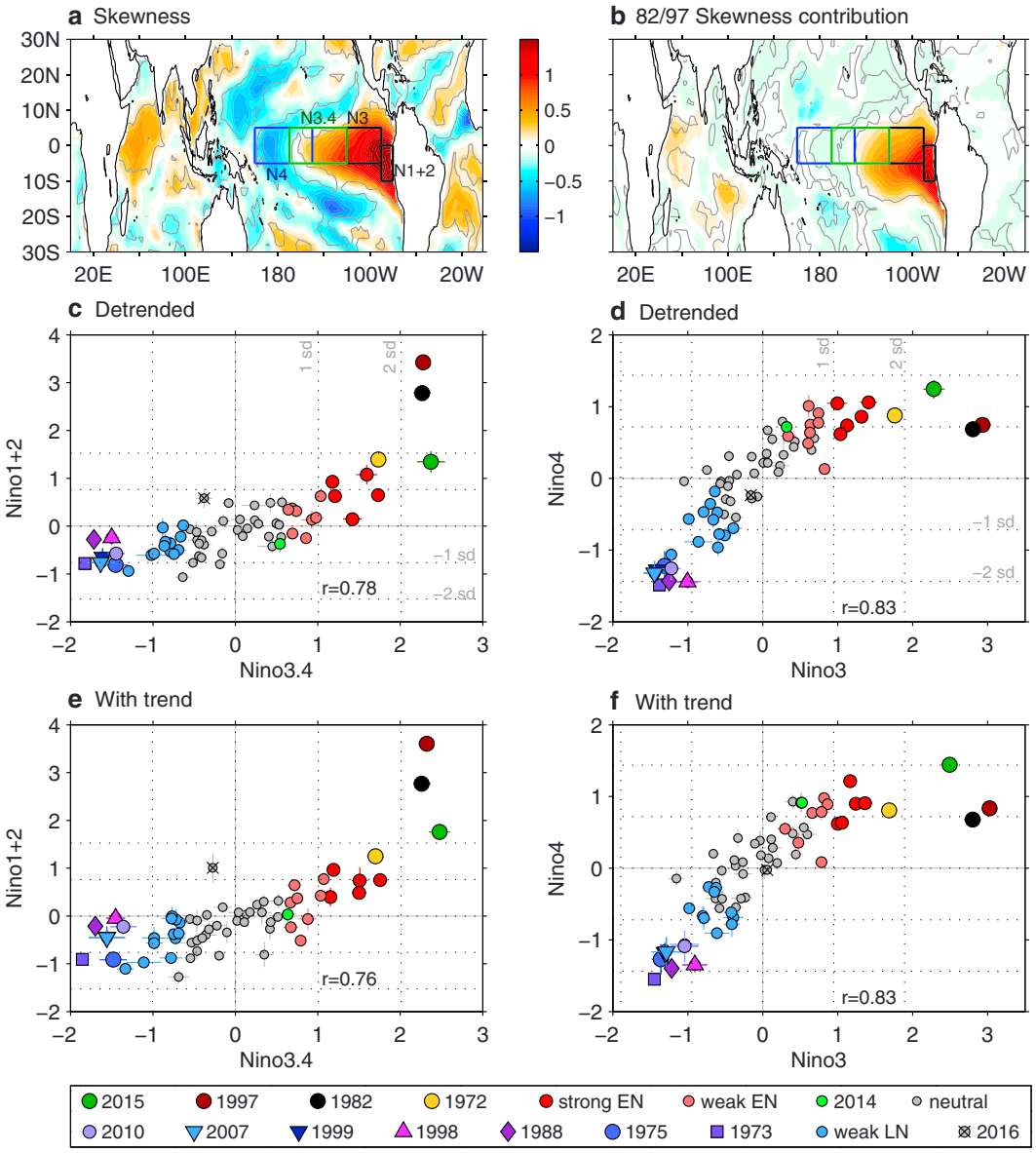

Figure 11. (a) Skewness of DJF average SST at each grid point. (b) The difference in skewness of SST for all years and with the 1982/1983 and 1997/1998 values removed, thus revealing the contribution of the 1982/1983 and 1997/1998 events to the skewness. (c) Niño1+2 against Niño3.4 averaged over DJF and detrended. (d) As in Figure 11c but for Niño4 against Niño3. (e, f), As in Figures 11c and 11d, respectively, but for the raw data. Vertical and horizontal dotted lines indicate 1 and 2 standard deviation units from 0 for each of the detrended variables. Correlation coefficient between the variables is displayed in each panel. The analysis is based on ensemble means of the four SST reanalysis products. Error bars are shown in Figures 11c–11f as 1 standard deviation unit above and below the ensemble means.

1982/1983 and 1997/1998 level (Figure 11e). Yet while the Niño3.4 is now larger than the 1982/1983 and 1997/1998 counterparts, the Niño1+2 still increases in a linear fashion.

Nonlinearity is also seen in Niño4, although this is less obvious than Niño1+2. As the eastern equatorial Pacific warms (Niño3 increases to large positive values), the increase in the Niño4 warm anomaly is curtailed—a nonlinear behavior again attributed to the 1982/1983 and 1997/1998 El Niño events (Figure 11d). The occurrence of the 2015/2016 El Niño, however, apparently undermines this nonlinear tendency as the amplitude of the Niño4 anomaly almost linearly tracks its large Niño3 anomaly, as well as in the presence of background warming (Figure 11f). Thus, the 2015/2016 El Niño displays somewhat a peculiar characteristic which will be put in perspective further below.

While the 1982/1983 and 1997/1998 El Niño events signify ENSO nonlinearity, strong La Niña events also play some role. Particularly, in contrast to the El Niño case, the Niño1+2 cold anomalies remain small as the Niño3.4 cold anomalies amplify further. On the other hand, the Niño4 cold anomalies almost linearly increase with the Niño3, unlike the more muted change during the 1982/1983 and 1997/1998 El Niño. Nonetheless, it is important to stress that there is still a strong degree of linearity in these relationships, as underscored by the high linear correlation coefficients (Figures 11c–11f). That is, despite the spatial irregularity, SSTs increase and decrease throughout central to eastern equatorial Pacific during El Niño and La Niña, respectively. It is the ENSO extremes that bring out the spatial irregularity.

The difference between Niño1+2 and Niño4 (each index in the form of anomaly and normalized), referred to as the "Trans-Niño index" (TNI) (Trenberth & Stepaniak, 2001), is an indication of the tendency for an ENSO event to peak in the eastern equatorial Pacific or in central Pacific. Trenberth & Stepaniak (2001) postulated that more than one index, other than the Niño3.4, is required to characterize ENSO. The use of TNI and Niño3.4 or Niño3 is instructive as they are approximately orthogonal to each other (Figure 12c), that is, the correlation is not statistically significant at zero lag ($r < 0.2$ for Niño3.4 and $r < 0.1$ for Niño3). This near orthogonality implies that the Niño3 and the TNI can be used to approximately represent the first and second leading modes of EOF decomposition of the tropical Pacific SSTs (10°S–10°N, 120°E–70°W), which, on the other hand, are perfectly orthogonal by construction. Their corresponding correlations with the principal components (PC) are near unity ($r > 0.95$).

The spatial patterns associated with the Niño3 and TNI (or analogously PC1 and PC2) are shown in Figures 12a and 12b. Since more positive TNI means warmer Niño1+2 relative to Niño4, an eastward amplification pattern associated with that of the 1982/1983 and 1997/1998 events can be obtained by superimposing the positive Niño3 and TNI patterns (Figures 12a and 12b). To obtain a pattern associated with typical El Niño events with core warming toward central Pacific, a negative TNI pattern is to be superimposed on a positive Niño3 pattern. Such combinations are shown in Figures 12e and 12f, represented by the "*E*" and "*C*" patterns via

$$E = (\mathrm{PC1} + \mathrm{PC2})/\sqrt{2} \tag{2}$$

$$C = (\mathrm{PC1} - \mathrm{PC2})/\sqrt{2}, \tag{3}$$

(Dommenget et al., 2013; Takahashi et al., 2011); that is, the *E*-*C* space (Figure 12g) is a rotation of the Niño3-TNI about the origin (Figure 12c). In Figure 12c, it can be seen that the 1982/1983 and 1997/1998 extreme events have a large positive Niño3 and TNI, thus a large *E* index but small and even negative *C* index (Figure 12g), indicating the tendency to peak toward eastern Pacific. As the Niño3 becomes less positive, that is, weaker El Niño and neutral events, the TNI tends to be negative, thus smaller *E* index but larger *C* index. This depiction captures the central Pacific El Niño which also includes the 2014/2015 warm event. Strong La Niña events also tend to peak over central Pacific, as shown by more positive TNI coinciding with more negative Niño3, thus large *C* index, but small *E* index (Figure 12g). These measures reveal that the 2015/2016 El Niño, as well as the 1972/1973 event, falls in between these two regimes (Figures 12c and 12g). Interestingly, in the presence of background warming, there is a tendency for the 2015/2016 event to appear more like an eastern Pacific event (Figure 12h). The relationships across these various SST indices are summarized in Table 1.

The evolution of the TNI with respect to Niño3 (Figure 13a) infers the direction of zonal phase propagation of SST anomalies along the equator which has dynamical significance, as also emphasized by Aiken et al. (2013) via a linear inverse model approach, and so it may further provide insight on the nature of the 2015/2016 El Niño and ENSO extremes. Theoretical studies (e.g., Jin & Neelin, 1993; Neelin et al., 1998) showed that the propagation direction arises from competing positive feedback processes: westward if the zonal advective and Ekman pumping feedbacks dominate; eastward if the thermocline feedback dominates. However, this linear theory would imply that both El Niño and La Niña propagate eastward and is not consistent with observations (Figure 12e; McPhaden & Zhang, 2009). In reality, it is only the 1982/1983 and 1997/1998 El Niños that exhibit prominent eastward propagation signature, which is linked to strongly nonlinear processes (Kim et al., 2015; Lengaigne & Vecchi, 2010; Santoso et al., 2013).

A switch from positive (negative) to negative (positive) TNI over a warm (cold) Niño3 indicates a westward propagation, as this indicates that the warm (cold) anomaly first strengthens in the far eastern Pacific and

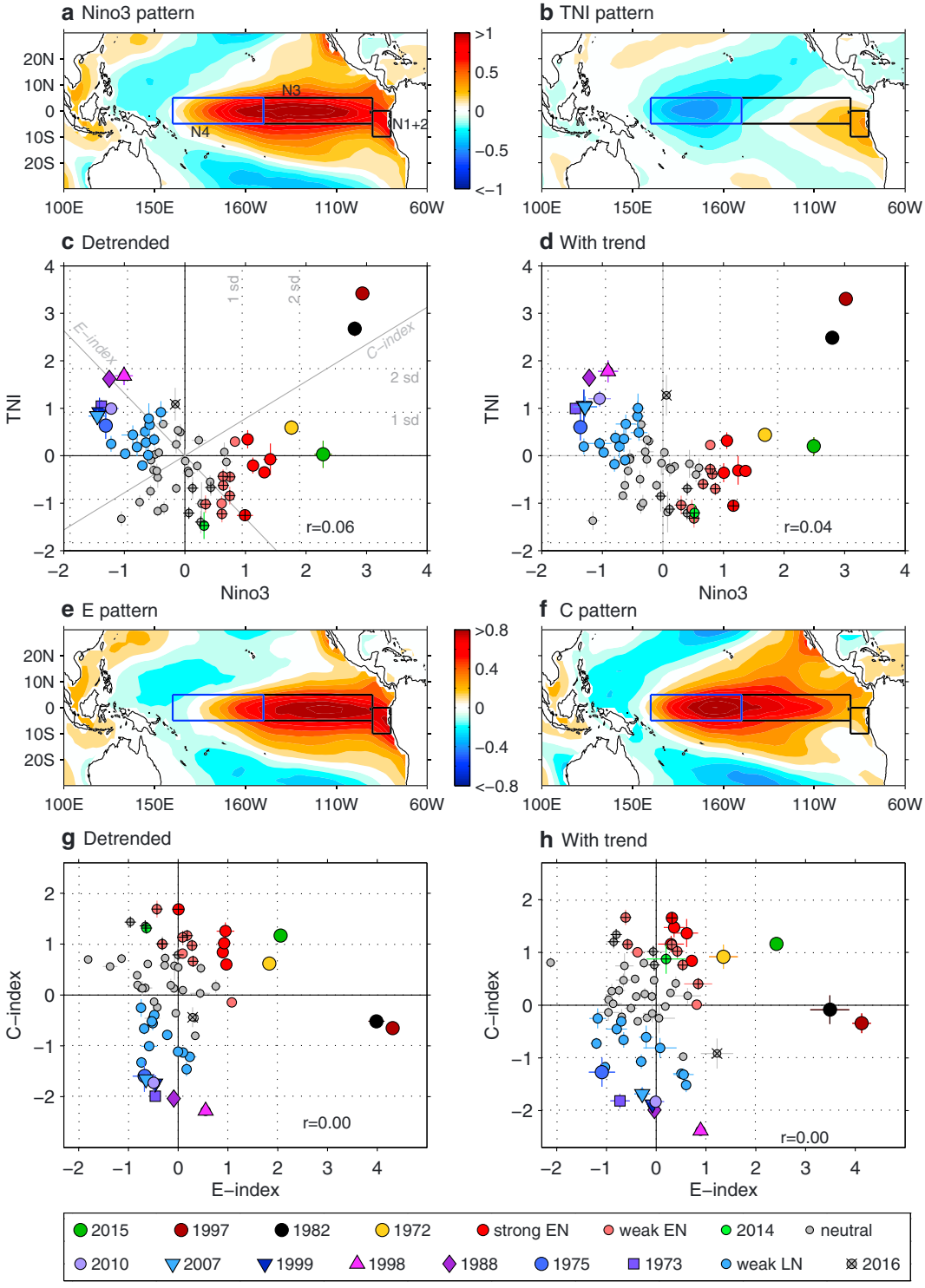

Figure 12. (a, b) Grid point SST regressed onto detrended Niño3 and the Trans-Niño index (TNI), respectively, representing the first and second EOF modes. The EOF modes account for about 90% of the total variance in the domain (10°S–10°N, 120°E–70°W). The analysis is based on DJF, the typical ENSO peak season. (c, d) TNI against Niño3 for the detrended and raw data, respectively. Vertical and horizontal dotted lines indicate 1 and 2 standard deviation units from 0 for each of the detrended variables. In Figure 12c, the E index and C index axes (gray) approximately represent a rotation of the Niño3-TNI axes about the origin, and each value of E and C indices is a linear combination of Niño3 and TNI. (e, f) Grid point SST regressed onto the E index and C index, respectively. (g, h) As in Figures 12c and 12d but for the C index against E index. Central Pacific El Niño events defined using the detrended data are indicated with "plus" marker. The analysis is based on four SST reanalysis products with ensemble mean shown. Error bars are shown as 1 standard deviation unit above and below the ensemble means.

Table 1
Correlations Between Various SST Indices (See Section 4.2.1 for Details)

	EOF1	EOF2	*E* mode	*C* mode	Skewness
Niño4	**0.91**	**−0.41**	0.36	**0.93**	*−0.43*
Niño3.4	**0.99**	−0.07	**0.65**	**0.75**	*0.37*
Niño3	**0.98**	0.16	**0.81**	**0.58**	*0.94*
Niño1+2	**0.83**	**0.48**	**0.93**	0.25	*2.18*
TNI	−0.09	**0.96**	**0.61**	**−0.74**	*1.03*
Skewness	*0.39*	*0.99*	*2.17*	*−0.40*	

Note. Correlation values greater than 0.4 are significant well above the 95% confidence level and shown in bold. The analysis is conducted using ensemble mean time series across the four SST reanalysis products.

then peaks over central Pacific. Such relationship between Niño3 and TNI is prevalent prior to the 1970s and after the 1990s (Figure 13b), with a switch to the opposite relationship in between these periods indicating the prominence of eastward propagation, which is mostly attributed to the 1982/1983 and 1997/1998 events (Figure 13e). These switches in propagation direction appear to be in phase with the IPO, with the most recent period corresponding to the negative phase of the IPO. This linkage supports earlier studies (e.g., An & Jin, 2000; Fedorov & Philander, 2000; Wang & An, 2002) which suggested a link between ENSO dynamics and changes in the background climate consistent with the IPO phases.

Plotting the month-to-month changes in TNI (dTNI/d*t*) averaged from May to the following April against the DJF average Niño3 (Figure 13c) reveals a change toward a more positive TNI (warmer in the east than west) with stronger El Niño and La Niña events. For El Niño (positive Niño3), a positive dTNI/d*t* indicates a tendency for an eastward propagation. For La Niña (negative Niño3), a positive dTNI/d*t* indicates a tendency for a westward propagation. This contrasting tendency between El Niño and La Niña is illustrated in Figure 13d in terms of the time-longitude gradient of the SST anomalies (Figure 13e), also referred to as the "zonal phase-transition slope" (Santoso et al., 2013). The zonal phase-transition slope is essentially a measure for the speed of SST anomaly peak propagating in the east-west direction. This analysis shows that 2015/2016 El Niño does not exhibit a clear zonal phase propagation, in contrast to the 1982/1983 and 1997/1998 events. As shown in Figure 13d, with the exception of the 1982/1983 and 1997/1998 El Niño events, most ENSO events are either westward propagating (nearly all La Niña and weak El Niño events) or non-propagating (e.g., 2015/2016 and 1972/1973 El Niños). Sustained eastward reversal of the equatorial Pacific surface currents over the latter half of the year is a key factor in giving rise to the prominent eastward propagation characteristic of the 1982/1983 and 1997/1998 events (Santoso et al., 2013). The total currents are westward during other events and particularly strongly westward during La Niña events. Ocean Surface Current Analysis Real-time (OSCAR) data available from 1992 (Figure 14) do not show a clear eastward surface current reversal in 2015, thus is consistent with its lack of an eastward propagation characteristic.

4.2.2. Rainfall

A pertinent indicator for El Niño extremity is rainfall over the eastern equatorial Pacific, as the warm SST anomalies tend to induce atmospheric convection and thus heavy precipitation over this climatologically cold and dry region (Cai, Santoso, et al., 2014; Chung et al., 2014; Lengaigne & Vecchi, 2010; Power et al., 2013). Rainfall anomaly at the height of the 1982/1983 and 1997/1998 El Niño events expands into the Niño3 and Niño1+2 regions (Figure 15a) where their SST anomalies peak (section 4.2.1). Such intrusion is less apparent in the 2015/2016 El Niño (Figure 15b) and completely absent in moderate events (Figure 15c), which, on the other hand, exhibit notably weaker far-eastern Pacific warming. The along-equator profile of rainfall anomaly clearly shows that unlike the 1982/1983 and 1997/1998 El Niños whose rainfall anomaly peaks eastward, all other events including the 2015/2016 El Niño, and especially strong La Niña events, tend to peak towards central western Pacific (Figure 15d). These inter-event differences illustrate the link between rainfall and the underlying SST anomaly pattern, through shifts in convective zones. This linkage is depicted in Table 2, showing high statistically significant correlations between various SST and rainfall indices and, in particular, strongest response to SSTs just to the east. For instance, Niño4 rainfall is most correlated with Niño3.4 SSTs; Niño3.4 rainfall with Niño3 SSTs; and Niño3 rainfall with Niño1+2 SSTs (Figures 15e–15g). One notable feature is that the nonlinearity in the rainfall is considerably stronger than that of SST, highlighting the nonlinear nature of atmospheric convection. The skewness for rainfall is highly positive toward the east (Table 3), much greater than the positive skewness of the SST anomaly (Table 1).

The ENSO rainfall response can be further understood through EOF decomposition. For this purpose, the EOF analysis is applied to detrended DJF average rainfall anomalies over central to eastern tropical Pacific (30°S–30°N, 160°E–80°W), capturing the SPCZ and ITCZ. The leading mode depicts anomalously high rainfall along the southern and northern flank of the climatological ITCZ and SPCZ, respectively, peaking in the central Pacific (Niño4), and anomalously low rainfall extending from the Maritime Continent to the south of the climatological SPCZ (Figure 16a). Such anomalous pattern is to be expected in a typical El Niño, acting to shift the convective zones eastward and equatorward, and the reverse occurs in a La Niña. As such, the principal

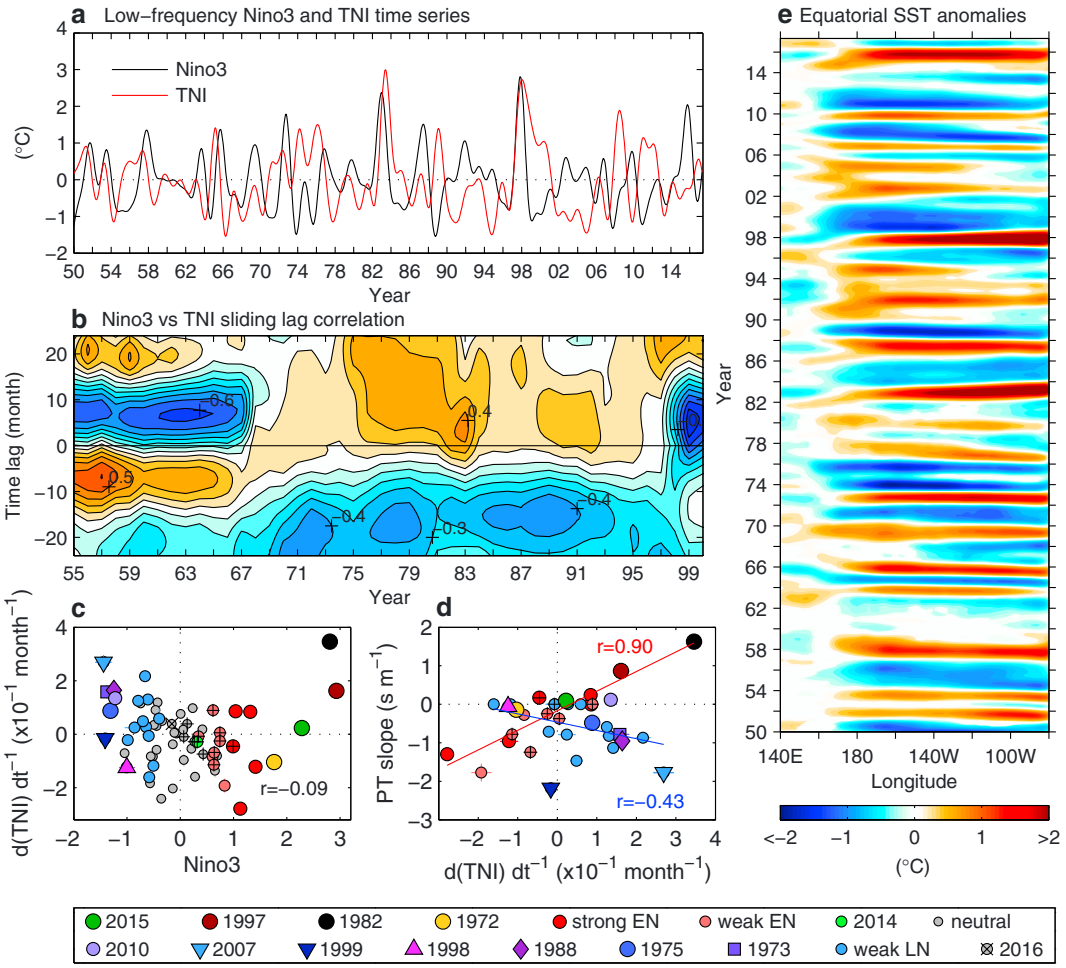

Figure 13. (a) Time series of Niño3 and TNI which have been detrended and low-pass filtered to remove signals with period shorter than 18 months. The filtering is to bring out the zonal propagation feature which is an interannual signal and is also applied in the analysis in the other panels. (b) Lead-lag correlation between Niño3 and TNI over 16 year sliding window as an indicator of zonal propagation direction. X ticks mark January of the indicated year as the start of the sliding window. Positive (negative) time lags in month indicate Niño3 leading (lagging) TNI. As such, positive and negative correlations at negative and positive time lags, respectively, indicate eastward propagating SST anomalies (e.g., in the post-1970 period). (c) Average of the month-to-month change in TNI from May to the following year April (dTNI/d*t*) against the DJF average Niño3. (d) The phase transition slopes against dTNI/d*t*. Positive (negative) slope indicates eastward (westward) propagation. The correlation coefficients between the two variables for only El Niño events and only La Niña events are displayed. (e) Hövmöller diagram of equatorial Pacific SST anomalies (5°S–5°N) from January 1950 to May 2017. The analysis in all panels is conducted for each of the four SST reanalysis products and shown as the ensemble mean with error bars shown as 1 standard deviation unit above and below ensemble mean. In Figure 13e, any statistically nonsignificant anomalies across the four products have been set to zero. The phase transition slope in Figure 13d corresponds to the time-longitude slope of the peak SST anomaly in Figure 13e for the ENSO years, calculated for each reanalysis product.

component time series is strongly correlated with the central to eastern Pacific SST indices, especially the Niño3.4 index (r = 0.95; Table 2). Simply, the EOF1-related rainfall anomalies tend to amplify with stronger ENSO events. The second EOF (Figure 16b), on the other hand, is not associated with central to eastern SSTs anomalies, but with the far eastern SSTs in Niño1+2 (r = 0.57). The correlation is even stronger with the TNI (r = 0.87), as opposed to EOF1, which is not at all correlated with the TNI. Thus, the link between EOF1 and EOF2 rainfall (Figure 16c) is very similar to the nonlinear relationship between Niño3 and the TNI (Figure 12c), indicating the tight link between SST pattern and rainfall.

The EOF2 rainfall pattern depicts an eastward shift of the EOF1; the positive anomaly now occupies the entire eastern equatorial Pacific regions, including the Niño1+2 region. Thus, superimposing positive

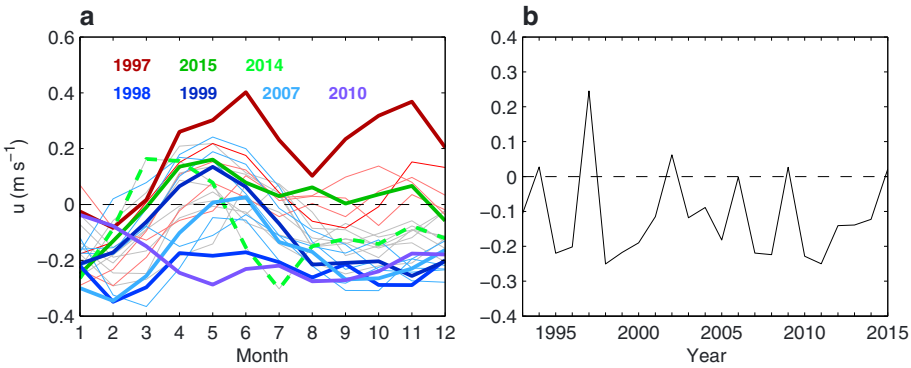

Figure 14. Ocean surface zonal current velocity over central-eastern equatorial Pacific (5°S–5°N, 160°E–90°W) from 1993 to 2015 based on Ocean Surface Currents Analysis Real-time (OSCAR) observations (Bonjean & Lagerloef, 2002). (a) Monthly evolution during the developing year of the various events. Dashed green line marks 2014 values. Light-colored lines indicate weaker events with gray for neutral events. (b) Time series of August-to-December average surface current velocity.

EOF2 pattern onto positive EOF1 would result in an even stronger eastward and equatorward shift of the ITCZ and the SPCZ. Among the El Niño events, there are only four that exhibit both positive EOF1 and EOF2: 1982/1983, 1997/1998, 1991/1992, and the recent 2015/2016 El Niño. An event with both positive EOF1 and EOF2 not only tends to correspond with large eastern equatorial Pacific rainfall but also coincides with an extreme phenomenon referred to as the "zonal SPCZ" wherein the usually southward oriented convective zone assumes a zonal position toward the equator (Cai et al., 2012). A particularly extreme zonal SPCZ, marked by extraordinarily positive EOF2 (well above 2 standard deviation), occurred during the 1982/1983 and 1997/1998 El Niño events in which the SPCZ appears much less defined than that seen during weak El Niño events (Figures 15a and 15c). The 2015/2016 El Niño is marked by a weak positive EOF2 (below 1 standard deviation; Figure 16c) but a particularly large EOF1 (above 2 standard deviation) even exceeding the 1982/1983 and 1997/1998 level, thus indicating that the 2015/2016 El Niño also exhibits a zonal SPCZ (Figure 15b). For La Niña and weaker El Niño events, the EOF1 and EOF2 combination is such that the anomalous rainfall (dry anomaly for La Niña; wet for El Niño) tends to peak toward the western Pacific. This is especially so for strong La Niña events which would also see stronger poleward migration of the SPCZ and ITCZ.

The nature of this interplay can also be examined from the perspective of "*E*" and "*C*" mode as done for the SST patterns (Figure 12), revealing more eastward shifted rainfall pattern for the *E* mode than the *C* mode (Figures 16d and 16e). The event scatter in the E-C space paints a consistent picture as the SST counterpart in that the 1982/1983 and 1997/1998 El Niño events are of the same type (a strongly eastern Pacific El Niño), and the 2015/2016 El Niño is of a mixed EP and CP type of event. It also becomes clear from this perspective that a zonal SPCZ event tends to require substantial warming of the eastern equatorial Pacific: the Central Pacific events (marked with "plus" in Figures 16c and 16f) corresponding with small E index in the SST (Figure 12g), shows notably weaker E index than C index in rainfall, and thus are not exhibiting a zonal SPCZ characteristic. This is in agreement to the conclusion of Borlace et al. (2014) who used perturbed physics ensemble experiments to show that zonal SPCZ events tend to not occur with purely CP El Niño. The 2015/2016 zonal SPCZ event coinciding with an EP-CP mixed El Niño reaffirms this argument. It is also clear from this analysis that, opposite to extreme El Niño, extreme La Niña tends to exhibit suppressed rainfall peaking toward the Maritime Continent, thus corroborating the fact that extreme La Niña events are in fact CP events.

Thus, there is an inherent nonlinearity in the equatorial Pacific climate system that produces rainfall asymmetry (e.g., Chung et al., 2014; Chung & Power, 2014; Hoerling et al., 2001), manifesting in *E* mode rainfall that reveals a high positive skewness and *C* mode with a small skewness (Table 3). This largely stems from EOF2-related process, marked by a positive skewness that is almost 4 times larger than the skewness of EOF1 (Table 3). This also translates to high positive skewness seen in the total equatorial rainfall (Table 3). EOF2 is a nonlinear process related to the east-west SST contrast as described by the TNI ($r = 0.87$ between EOF2 rainfall and TNI; Table 2) which underpins ENSO extremes (section 4.2.1), involving dramatic shifts in convective zones.

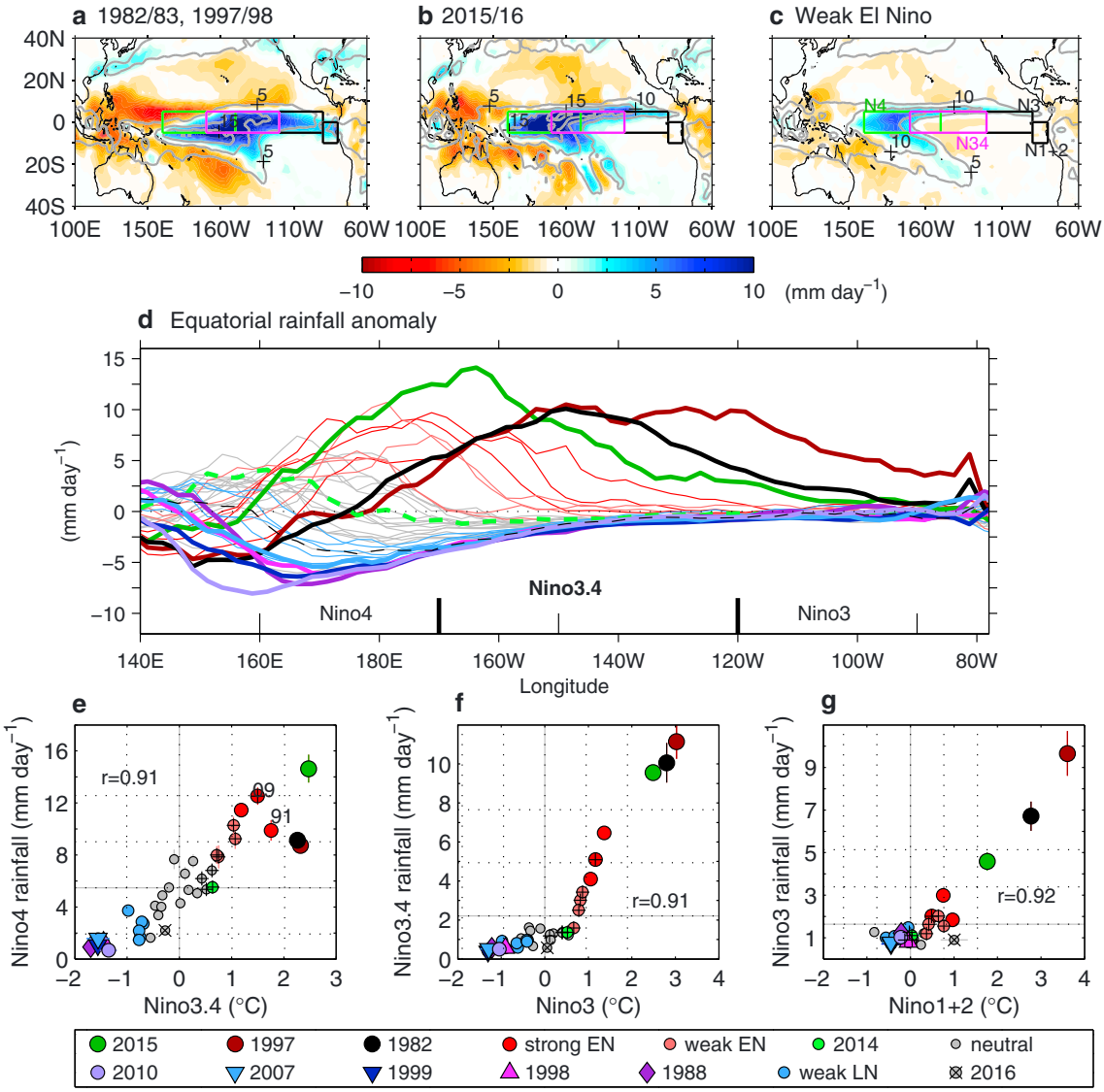

Figure 15. DJF rainfall anomalies (color shading) for (a) the average of 1982/1983 and 1997/1998 El Niño, (b) 2015/2016 El Niño, and (c) the average of weak El Niño events. The corresponding total rainfall contours are shown in gray (5 mm/d interval). (d) Equatorial profile of detrended DJF average rainfall anomalies (5°S–5°N). (e–g) Relationship between SST and rainfall anomalies over the specified regions. Dotted lines in Figures 15e–15g are 1 and 2 standard deviation units from the mean. Central Pacific El Niño events are indicated with "plus" marker. The analysis is based on three rainfall reanalysis products with ensemble means shown. Error bars are shown in Figures 15e–15g, corresponding to 1 standard deviation unit above and below the ensemble means.

Table 2
December–February Average Rainfall Versus December–February Average SST Indices

	Niño4	Niño3.4	Niño3	Niño1+2	TNI	*E* mode	*C* mode
Niño4 rainfall	**0.89**	**0.91**	**0.82**	**0.57**	−0.26	**0.43**	**0.75**
Niño3.4 rainfall	**0.57**	**0.84**	**0.91**	**0.90**	0.38	**0.88**	0.24
Niño3 rainfall	0.38	**0.68**	**0.81**	**0.92**	**0.59**	**0.92**	0.01
Niño1+2 rainfall	0.01	0.30	**0.47**	**0.75**	**0.77**	**0.76**	−0.31
EOF1 rainfall	**0.88**	**0.95**	**0.90**	**0.70**	−0.12	**0.57**	**0.69**
EOF2 rainfall	−0.29	0.06	0.27	**0.57**	**0.87**	**0.71**	**−0.60**
E Mode rainfall	**0.41**	**0.72**	**0.83**	**0.90**	**0.53**	**0.90**	0.06
C Mode rainfall	**0.83**	**0.63**	**0.45**	0.10	**−0.70**	−0.10	**0.91**

Note. All correlations are based on detrended data, with values greater than 0.4 significant well above the 95% confidence level and shown in bold. The correlations are computed using ensemble mean of the three rainfall products and four SST products.

Table 3
Correlations Between Rainfall Averaged Over the Specific Regions and the Rainfall Orthogonal Modes (See Section 4.2.2)

	EOF1 rainfall	EOF2 rainfall	*E* mode rainfall	*C* mode rainfall	Skewness
Niño4 rainfall	**0.97**	−0.19	**0.55**	**0.82**	*0.66*
Niño3.4 rainfall	**0.83**	**0.53**	**0.96**	0.22	*2.22*
Niño3 rainfall	**0.64**	**0.72**	**0.96**	−0.06	*3.37*
Niño1+2 rainfall	0.25	**0.78**	**0.73**	−0.37	*4.03*
Skewness	*0.61*	*1.68*	*2.67*	*−0.01*	

Note. To provide an indication of nonlinearity in rainfall, the corresponding skewness is presented. The analysis is conducted using ensemble mean of the three rainfall products.

The 2015/2016 El Niño involves weaker shifts in ITCZ and SPCZ, as indicated by considerably weaker EOF2 (Figure 16c) and TNI (Figure 12c), than the 1982/1983 and 1997/1998 counterparts. As such, it is expected that rainfall in the eastern equatorial Pacific would be lower than in 1982/1983 and 1997/1998 El Niños. While this is true for the Niño3 rainfall (Figure 15g), the 2015/2016 Niño3.4 rainfall is of comparable intensity as the 1982/1983 and 1997/1998 events. This is related to the record high Niño4 rainfall (Figure 15e), apparently due to the fact that the 2015/2016 El Niño is also a central Pacific event with a record-breaking Niño4 warming (Figure 10). Nonetheless, based on the total rainfall metrics alone (Figures 15e–15g), the 2015/2016 El Niño appears like an extraordinary El Niño.

Cai, Borlace, et al. (2014) used an arbitrarily selected threshold of 5 mm/d in Niño3 total rainfall to characterize extreme El Niño. With an ensemble mean of 4.6 mm/d, the 2015/2016 Niño3 rainfall is just shy of that threshold. Considering observational uncertainties (e.g., 4.3 mm/d for CMAP, 5.1 mm/d for GPCP), the 2015/2016

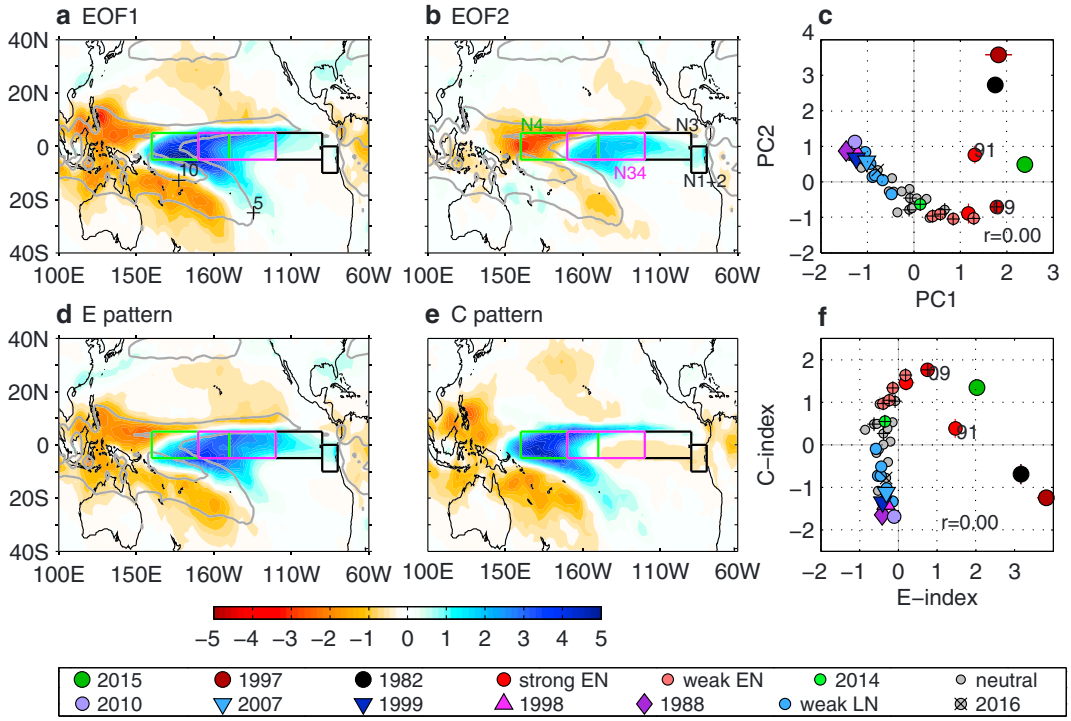

Figure 16. The (a) first and (b) second leading mode of rainfall variability, presented as regression of the standardized EOF principal time series onto grid point DJF average rainfall (1979–2016). The EOF decomposition is applied on detrended rainfall over 30°S–30°N, 160°E–80°W. (c) Scatterplot for the corresponding first and second principal components (PC1 and PC2). (d–f) The same as Figures 16a–16c but for the *E* and *C* modes. Gray contours on the spatial maps denote the long-term mean rainfall shown on 5 mm/d interval. Dashed lines in Figures 16c and 16f are 1 and 2 standard deviation units from the mean (horizontal and vertical lines). Central Pacific El Niño events are indicated with '+' marker. The analysis is based on three rainfall products with ensemble means presented. Error bars in Figures 16c and 16f correspond to 1 standard deviation unit above and below the mean.

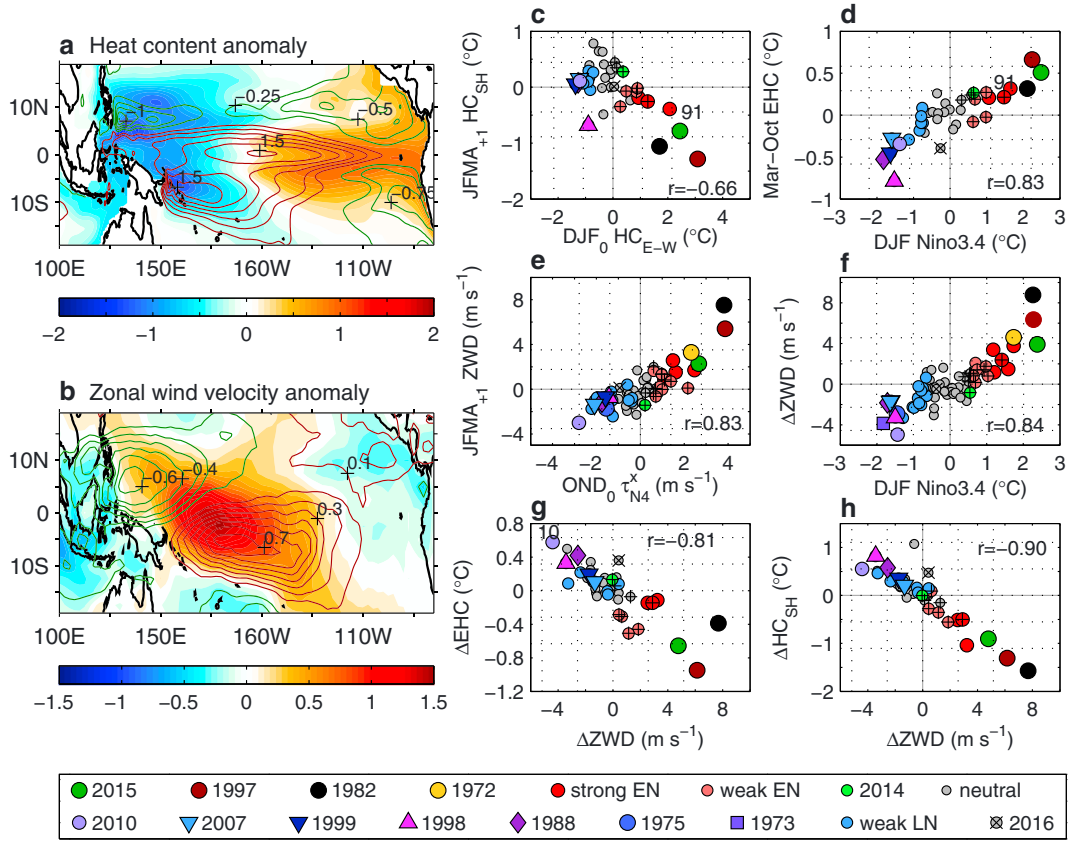

Figure 17. (a) Patterns of the first (color shading) and second (contours) leading modes of heat content (HC) variability presented as regression of the upper 300 m ocean temperature (T300) onto $HC_{E\text{-}W}$ and HC_{SH}, respectively. $HC_{E\text{-}W}$ is the difference in T300 between the east (5°S–5°N, 155°W–80°W) and western (5°S–5°N, 120°E–155°W) regions. HC_{SH} is T300 averaged over 10°S–3°N, 140°E–130°W. These respective indices are representative of the first (42.6%) and second (15.1%) principal component time series in an EOF analysis of T300 over 20°S–20°N, 120°E–80°W. (b) As in Figure 17a but for zonal wind velocity, with ZW_{N4} and ZWD indices representing the first (25.6%) and second (11.8%) EOF, respectively. ZW_{N4} is zonal wind velocity averaged over the Niño4 region. ZWD is the difference in zonal wind velocity between southern core (10°S–2°S, 180°–130°W) and northern core (2°N–10°N, 120°E–170°E) regions. (c) HC_{SH} averaged over the following January–April against DJF average $HC_{E\text{-}W}$. (d) March–October average EHC (T300 over 5°S–5°N, 120°E–80°W) against DJF Niño3.4. (e) ZWD averaged over the following year January–April against ZW_{N4} over October–December. (f) Change in ZWD from June–September to the following January–April (ΔZWD) against DJF Niño3.4. (g) Change in EHC from August–November to the following January–April (ΔEHC) against ΔZWD. (h) The change in HC_{SH} from August–November to the following January–April (ΔHC_{SH}) against ΔZWD. All data are detrended according to the common period between the variables in each panel. Dashed lines in Figures 17c–17h are 1 and 2 standard deviation units from the mean computed using the detrended indices.

Niño3 rainfall is about the 5 mm/d extreme El Niño threshold. The 2015/2016 event is clearly larger than all events other than the 1982/1983 and 1997/1998 El Niños. Prior to 2015, even reducing this threshold to 4 mm/d would still have excluded events other than the 1982/1983 and 1997/1998 events. Thus, the 2015/2016 El Niño should be regarded as an extreme El Niño based on the Niño3 rainfall metric alone.

4.2.3. Upper Ocean Heat Content and Zonal Wind Evolution

Underpinning ENSO is changes in upper ocean heat content and winds across the equatorial Pacific as a consequence of the Bjerknes coupled air-sea feedback. The westward blowing Trade Winds deepen the oceanic thermocline toward the Maritime Continent and forces Ekman upwelling and equatorward Sverdrup transport. A series of eastward propagating Kelvin waves act to distribute the accumulated heat across the equatorial Pacific in a state of "recharge," leading to a deepened thermocline in the east and an increase in SSTs. The increased SSTs then reinforce westerly wind anomalies which further deepen the thermocline, again increasing the SST and so forth in a positive feedback loop leading to the emergence of an El Niño. At the peak of El Niño, the westerly wind anomaly elevates thermocline in the west and through upwelling Kelvin

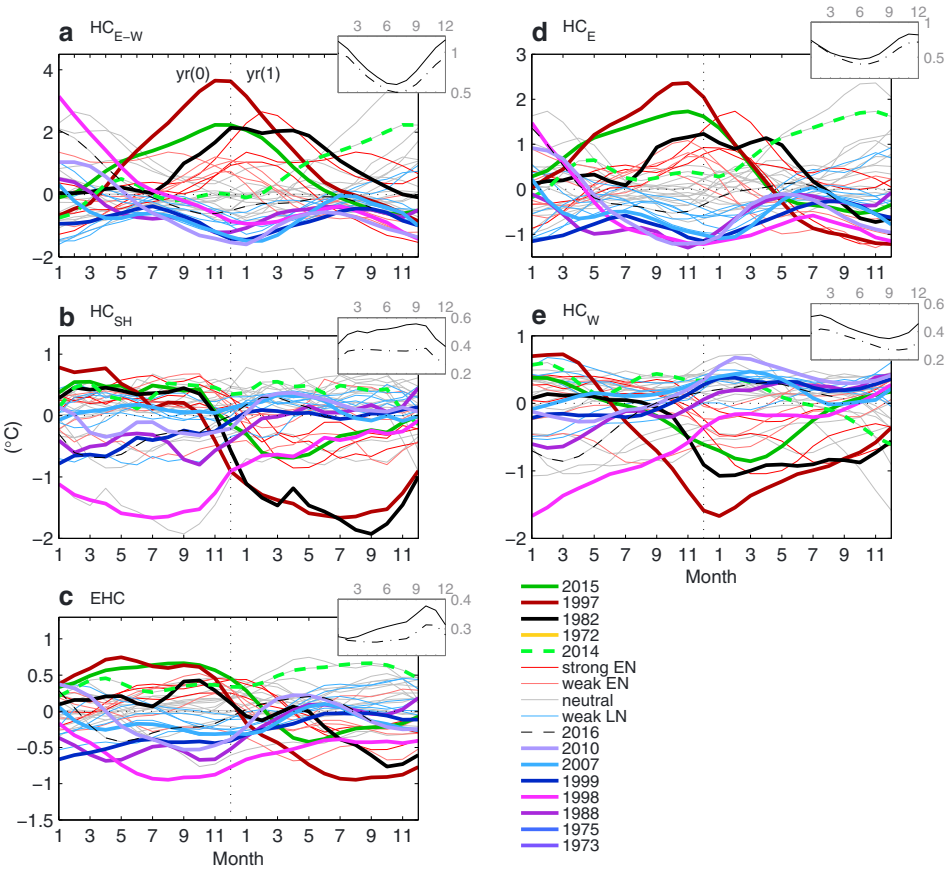

Figure 18. Temporal evolution of heat content (T300) anomalies for each event from January of the current year to December of the following year. (a) East (5°S–5°N, 155°W–80°W) minus west (5°S–5°N, 120°E–155°W) equatorial heat content (HC_{E-W}). (b) Southern Hemisphere focused (10°S–3°N, 140°E–130°W) heat content anomaly (HC_{SH}). (c) Equatorial heat content (EHC, or "warm water volume"; 5°S–5°N, 120°E–80°W). (d) Eastern equatorial Pacific heat content (5°S–5°N, 155°W–80°W). (e) Western equatorial Pacific heat content (5°S–5°N, 120°E–155°W). Insets show the corresponding monthly standard deviation with (solid line) and without (dash-dotted line) the years enveloping the 1982/1983 and 1997/1998 El Niño events (i.e., excluding January 1982 to December 1983 and January 1997 to December 1998).

waves and subsurface poleward Sverdrup transport, this leads to an equatorial state of "discharge," which is conducive for a La Niña to occur. This suite of processes occurs in a quasi-oscillatory manner and is the basis for the ENSO recharge oscillator theory (Jin, 1997) that underpins ENSO predictability.

The coupled dynamics described above can be disentangled using EOF decomposition (Figure 17). EOF analysis conducted on detrended monthly average of top 300 m ocean temperature (T300), as a proxy for upper ocean heat content (HC), within the tropical Pacific (20°S–20°N, 120°E–80°W) reveals two dominant modes. EOF1, often referred to as the "tilt mode," depicts a flattening of the equatorial Pacific thermocline during an El Niño (the converse in a La Niña; color shading in Figure 17a), peaking in boreal winter (Figure 18a, inset) just like the ENSO SSTs. The temporal evolution is overall captured by the time series of east-minus-west HC anomaly (HC_{E-W}), underscored by a high correlation of 0.95 between HC_{E-W} and the principal component time series and is highly correlated with Niño3.4 SST (r = 0.90; Figure 19).

EOF2, known as the "recharge mode," depicts anomalously high HC across the equatorial Pacific, with a secondary anomaly peak in the vicinity of the SPCZ (Figure 17a, contours). It is found that EOF2 can be best represented by a Southern Hemisphere-skewed HC index (HC_{SH}), which is an average over 10°S–3°N, 140°E–130°W encompassing the two core regions (PC2 and HC_{SH} are highly correlated with r = 0.98). PC2 is less strongly correlated (r = 0.71) with the more commonly used equatorial heat content metric (an average over 5°S–5°N, 120°E–80°W; referred hereafter as EHC). EHC is closely related to the volume of water above 20°C isotherm within that region, widely known as "warm water volume" (WWV) (Meinen & McPhaden, 2000).

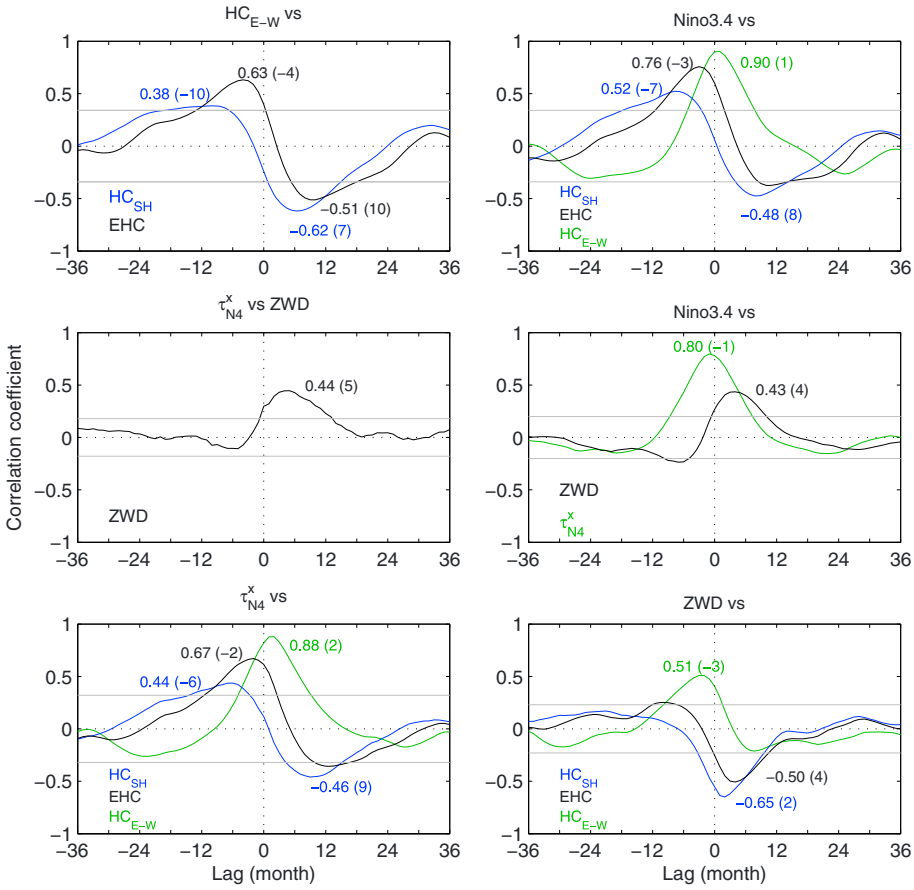

Figure 19. Lead-lag correlations between various processes illustrating the essence of the recharge oscillator theory. Positive (negative) months indicate the variable in the panel title leading (lagging) the other variables. (top left) East-minus-west equatorial heat content ($HC_{E\text{-}W}$) versus Southern Hemisphere focused (10°S–3°N, 140°E–130°W) heat content anomaly (HC_{SH}) and equatorial heat content (EHC, or "warm water volume"; 5°S–5°N, 120°E–80°W). (top right) Niño3.4 index versus the variables in Figure 19 (top left). (middle left) Zonal wind velocity averaged over the Niño4 region (ZW_{N4}) versus the difference in zonal wind velocity between southern core (10°S–°S, 180°–130°W) and northern core (2°N–10°N, 120°E–170°E) regions (ZWD). (middle right) Niño3.4 index versus the variables in Figure 19 (middle left). (bottom left) ZW_{N4} versus the variables in Figure 19 (top left). (bottom right), ZWD versus the variables in Figure 19 (top left). Peak correlation coefficients are labeled with the corresponding time lag (month) in bracket. All data are detrended prior to correlation.

Nonetheless, both HC_{SH} and EHC depict a recharge state three seasons prior to the peak of most El Niño before switching to a discharge in the following year (Figure 19). For La Niña though the switch to a recharge state is not as apparent. In fact, the three extreme La Niña events either lead to no recharge (1988/1989, 1999/2000) or to an ensuing discharge (1998/1999). The discharge following the 1982/1983 and 1997/1998 El Niño events is more prominent relative to other events in HC_{SH} than EHC, contributing to a high negative skewness in HC, especially HC_{SH} (Table 4). Excluding the 1982/1983 and 1997/1998 events reduces the HC_{SH} skewness by 60%. Lag-correlation analysis (Figure 19) shows that EHC is a more accurate predictor for Niño3.4 than HC_{SH}. While HC_{SH} is less accurate, it provides a longer lead time and is better correlated with Niño3.4 after the peak of ENSO.

Table 4
Skewness and Trends of the Various Heat Content and Zonal Wind Variables (See Section 4.2.3 and Figure 17)

	Skewness	Trend (1950–2015)	Trend (1980–2015)
$HC_{E\text{-}W}$	1.09	N/A	−0.23°C/decade
HC_{SH}	−0.96	N/A	0.02°C/decade
EHC	−0.77	N/A	0.08°C/decade
ΔEHC	−0.82	N/A	−0.02°C/decade
ΔHC_{SH}	−0.97	N/A	−0.02°C/decade
ZW_{N4}	0.58	0.07 m/s/decade	−0.38 m/s/decade
ZWD	1.70	0.11 m/s/decade	−0.59 m/s/decade
ΔZWD	1.07	−0.12 m/s/decade	−0.71 m/s/decade

For zonal winds (ZW), EOF1 (Figure 17) can be simply represented by zonal wind anomalies in the Niño4 region (ZW_{N4}; $r = 0.97$). ZW_{N4} describes the typical ENSO wind anomalies, peaking in boreal winter (Figure 20), though the peak season apparently shifts to boreal fall in the 1982/1983, 1997/1998, and 2015/2016 El Niño events. EOF2, on the other hand,

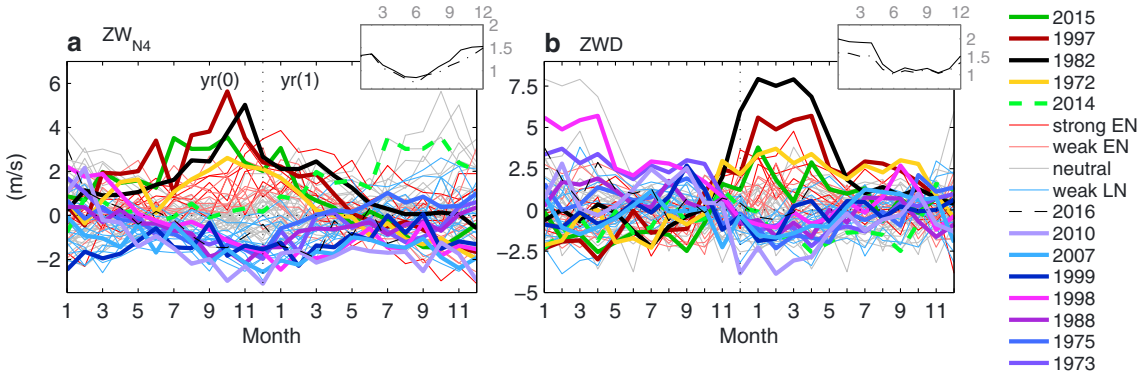

Figure 20. (a) The 24 month evolution of Niño4 zonal wind anomaly (ZW_{N4}). The inset shows standard deviation of year-to-year Niño4 wind anomaly as a function of month (solid line), and without the 24 month evolution of the 1982/1983 and 1997/1998 El Niño events (dashed line). (b) As in Figure 20a but for the zonal wind difference (ZWD) index. The ZWD index is defined as τ^x in southern box (10°S–2°S, 180°–130°W) minus τ^x in northern box (2°N–10°N, 120°E–170°E). Insets show the corresponding monthly standard deviation with (solid line) and without (dash-dotted line) the years enveloping the 1982/1983 and 1997/1998 El Niño events (i.e., excluding January 1982 to December 1983, and January 1997 to December 1998).

depicts a dipole anomaly pattern alternating in sign between the south central Pacific (10°S–2°S, 180°–130°W) and the northwestern Pacific near the Philippines (2°N–10°N, 120°E–170°E). It can be effectively represented as the difference of zonal winds between the southern and northern core regions, referred to hereafter as ZWD (r = 0.91). ZWD switches from negative during El Niño development phase to positive following the peak of El Niño (the converse for La Niña). Superimposing the ZWD anomaly pattern onto that of ZW_{N4} (Figure 17b) results in a northward shifted pattern of ZW_{N4} during El Niño development and a southward shift following El Niño peak (Harrison, 1987; McGregor et al., 2012). The ZWD process is a nonlinear process, with a high positive skewness, associated with the 1982/1983 and 1997/1998 extreme El Niños.

The interactions between the heat content and zonal wind variables and with Niño3.4 SST are summarized in the lag-correlation analysis shown in Figure 19, verifying the linear recharge oscillator theory described earlier in this section. As noted above, these variables do however exhibit a certain degree of nonlinearity as indicated by a nonzero skewness (Table 4). While the root of the nonlinearity is extreme ENSO events (Figures 17c–17h), in some of the variables, however, the separation between extreme ENSO and moderate events is not clear. For instance, the discharge of heat content following the peak of El Niño events (HC_{SH} averaged over the following January–April) is exceptionally strong in the 1982/1983 and 1997/1998 events (Figure 17c). The 2015 event discharge is weaker than the 1982/1983 and 1997/1998 events but is stronger than other El Niño events since 1980. However, in terms of the east-west heat content difference ($HC_{E\text{-}W}$) in the typical ENSO peak season (DJF), the 2015/2016 event comes second after the 1997 (above 2 standard deviation), whereas the 1982 extreme El Niño is weaker than the 1991 event, which is not even considered as an extreme El Niño according to the SST and rainfall properties. Note that the EHC does not show the 1982/1983 event to exhibit an unusually strong discharge (Figure 18c). In terms of recharge/discharge leading up to El Niño/La Niña peak (EHC averaged over March–October; Figure 17d), there is only a weak distinction in extreme El Niño and extreme La Niña from moderate events. Again, the 1982/1983 event appears weaker than 2015/2016 and 1997/1998 events. However, it should be noted that the 1982/1983 event occurred in pre-TOGA observing period which started in mid-1980s (section 3), so observational uncertainty needs to be borne in mind. Nonetheless, the negative skewness of EHC (Table 4) is contributed by the development of the 1998/1999 extreme La Niña event following a strong discharge induced by the 1997/1998 extreme El Niño. It is worth noting also that the level of the EHC leading up to the 2016/2017 marginally weak La Niña is comparable to that of strong La Niña events (Figure 17d), thus highlighting the discharge effect of the 2015/2016 El Niño.

For zonal wind anomalies, a clear distinction is seen in the southward wind shift following the peak of 1982/1983 and 1997/1998 El Niño (ZWD averaged over the following year January–April; Figure 17e). The notably large separation from other events is unlikely to be within observational uncertainty. On the other hand, the 2015/2016 event is comparable to the 1972/1973 and moderate El Niño events. The 1982/1983 and 1997/1998 events are also categorically distinct in terms of the intensity of the westerly wind

anomaly (Niño4 averaged over October–December). Zonal wind anomalies are not distinctive across cold events, and only the strong 2010/2011 La Niña emerges as a slight outlier.

The extent of the wind movement, that is, the shift from the northernmost to southernmost position from ENSO growth to decay seasons (change in ZWD from June–September to the following year January–April) is closely related to the magnitude of the ENSO SST anomalies (Figure 17f). More intense Niño3.4 SSTs correspond with larger wind shift which in turn leads to larger extent of recharge-discharge either side of the ENSO peak (change in EHC or HC_{SH} from August–November to the following year January–April; Figures 17g and 17h). The 1982/1983 and 1997/1998 El Niño events emerge as the strongest in the southward wind shift and heat content discharge measured using HC_{SH}. The 2015/2016 El Niño event is more comparable to other strong events and only appears extreme in terms of southward wind shift post 1980, as well as EHC discharge (Figure 17g). However, when the raw data are examined (not shown), the southward wind shift does not appear as strong in the 2015/2016 event, but the recharge and discharge become more comparable with the 1982/1983 and 1997/1998 events. This discrepancy is due to a long-term trend toward northward wind shift in the post-1980 (negative ZWD) and a trend toward a high equatorial heat content (Table 4), consistent with the enhanced Trade Wind trend (negative ZW_{N4}) associated with the ensuing negative phase of the IPO (L'Heureux et al., 2013).

4.2.4. Stochastic Wind Surges

Daily occurrences of westerly winds exist over the western half of the equatorial Pacific (Figure 21), in the backdrop of predominantly easterly winds across the equatorial Pacific. Partly associated with synoptic-scale phenomena, such as tropical cyclones and the Madden-Julian oscillation (Puy et al., 2016), heightened occurrences of westerly wind bursts (WWB) are seen during El Niño years (e.g., Chen et al., 2015). They facilitate warming in the central eastern equatorial Pacific by driving surface convergence and subsequent downwelling Kelvin waves that deepen the thermocline in the east (Lengaigne et al., 2004). While WWB can be viewed as a source of stochastic forcing for ENSO, recent research has led to a realization that WWB occurrences are not entirely random, but there is a certain degree of dependency upon the prevailing climatic state (e.g., Eisenman et al., 2005; Gebbie et al., 2007). This carries an implication in that there is a tighter association between WWB activities and El Niño intensity. For instance, WWB was unusually active during the extreme El Niño development in1997 (McPhaden, 1999). There are likely some factors that can enhance WWB activities, such as cold southerly wind surges during boreal summer and autumn which also tend to be more intense during extreme El Niños (Hong et al., 2014). Thus, it is also of interest to view ENSO extremes and the 2015/2016 El Niño from the perspective of these zonal and meridional wind surges.

Previous studies have diagnosed WWBs by imposing thresholds on magnitude, duration, and zonal extent of the wind fetch at different regions (e.g., see Table 1 of Puy et al., 2016), often resulting in different numbers of individual WWB diagnosed across studies. Here we diagnose WWB activities by taking the spatial average of surface zonal wind velocities over equatorial Western Pacific (WP; 5°S–5°N, 130°E–180°), that is, spanning the WWB active "W" and "C" regions of Harrison and Vecchi (1997). Approaching the peak of El Niño events at the end of the year, WP westerly winds progressively extend to the central Pacific (CP; 155°E–150°W; Figures 21d and 21f), spanning the "C" and "E" regions of Harrison and Vecchi (1997). This index is considerably easier to compute than that of Puy et al. (2016), while providing a broad indication of heightened or reduced level of WWB activities. There is a clear tendency for more days in WP winds blowing eastward during stronger El Niño events (Figure 21f), than in neutral years or central Pacific El Niño, and even in boreal summer when the climatological easterly winds are strongest. Relative to seasonal cycle, the wind reversal corresponds to velocity anomalies in excess of 2 m s^{-1} (Figure 21g). Over CP, eastward blowing winds are limited, as the climatology is predominantly easterly (Figure 21h). In this region, westerly winds occur in boreal fall during stronger El Niño events, requiring much larger anomaly in excess of 4 m s^{-1} than in WP, to reverse the climatologically stronger CP easterly winds (Figure 21i).

The WWBs are determined based on the number of days the WP and CP zonal winds exceeding 0.5 m s^{-1} and 0 m s^{-1}, respectively. Using higher thresholds tend to further isolate the strongest El Niño events (Figure 22). We focus on boreal summer (JJA) for WP winds and fall (SON) for CP winds, in particular, since during these seasons cold southerly wind surges also contribute to WWBs (Hong et al., 2014). Easterly wind bursts (EWB) are also examined, which are, on the other hand, associated with La Niña development (Chiodi & Harrison, 2015). In this case, we simply take the counterparts of the WP and CP winds with the corresponding threshold

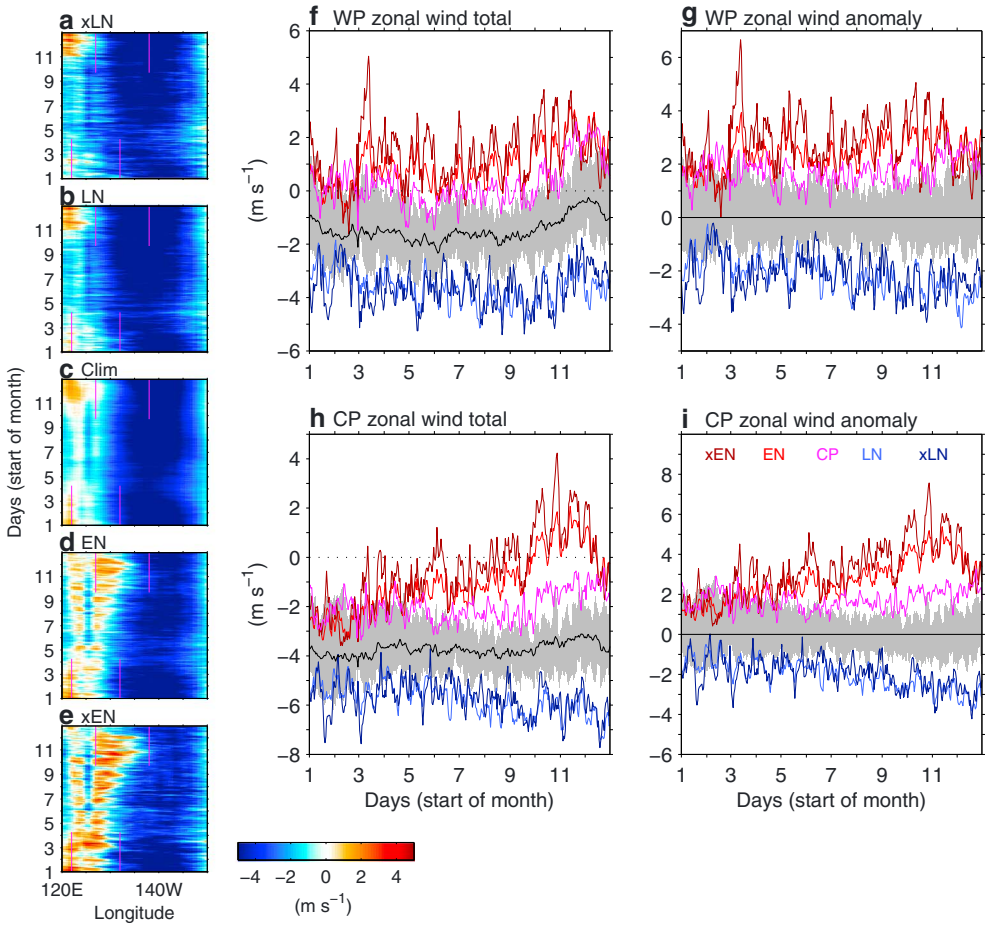

Figure 21. Daily occurrences of westerly and easterly wind bursts along the equatorial Pacific Ocean. Daily surface zonal wind velocity averaged over 5°S–5°N averaged across (a) extreme La Niña years (1973/1974, 1988/1989, and 1998/1999), (b) all strong La Niña, (c) all years, (d) all strong El Niño, (e) extreme El Niño (1972/1973, 1982/1983, 1997/1998, and 2015/2016). (f) Daily surface zonal wind velocity averaged over the western equatorial Pacific (5°S–5°N, 130°E–180°) at 1 standard deviation above the mean for extreme El Niño years (dark red), all strong El Niño (red), Central Pacific/Modoki El Niño (magenta), and below the mean for extreme La Niña years (dark blue) and strong La Niña (blue). Gray-shaded region corresponds to 1 standard deviation above and below the mean for neutral years. The climatological average is indicated by the black line. (g) As in Figure 21f but in the form of anomaly. (h, i) As in Figures 21f and 21g, respectively, but for central Pacific (5°S–5°N, 155°E–150°W). The zonal extents for the regions are shown in Figures 21a–21e.

of -2 m s^{-1} and -4 m s^{-1} (figure not shown), which sufficiently separate La Niña events from normal conditions (see also Figure 21).

Higher occurrences of WWB in boreal summer are associated with Southern Oscillation pattern in sea level pressure (SLP), with anomalously high pressure over Australia and low pressure over much of the Pacific Ocean, intensifying in the Southern Hemisphere midlatitude (Figure 23a). Associated with this SLP anomaly pattern is an anticyclonic atmospheric circulation over South Australia (e.g., Stephens et al., 2007), which meanders equatorward before diverting eastward at the equator. Similar patterns but of opposite sign can be seen for higher occurrences of EWB (Figure 23b).

The characteristics of these cold southerly surges are described by the "Southern Hemisphere booster" (SHB) index (Hong et al., 2014), which is the average of meridional wind velocity over the eastern board of Australia (30°S–10°S, 140°E–170°E; Figure 23a, black box). The notion that SHB is conducive for WWBs is reflected by significant positive correlations between SHB index and westerly wind days in WP and CP (Figures 23c and 23d). At about 0.5–0.6, the correlation strength is considered moderate, but is expected given that the SHB is not the only factor affecting WWB. There is considerable overlap across different events in terms of SHB

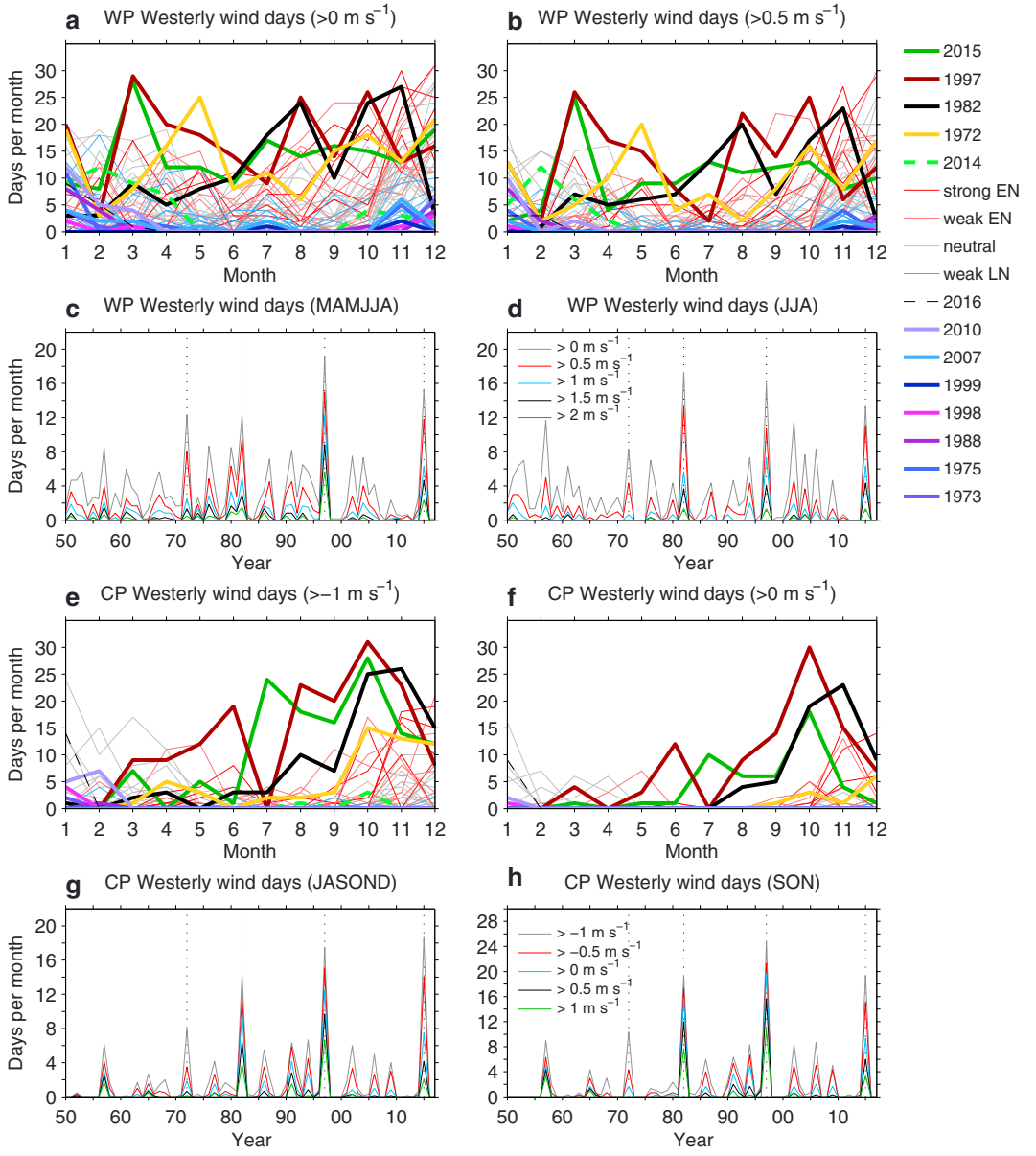

Figure 22. Number of wind burst days per month exceeding a threshold. (a) Westerly wind days with zonal velocity greater than 0 m s^{-1} in the western equatorial Pacific (see Figure 23a for the region) for various ENSO events. (b) As in Figure 22a but exceeding 0.5 m s^{-1}. (c) Westerly wind days in the western equatorial Pacific averaged from March to August exceeding various thresholds (see Figure 22d). (d) As in Figure 22c but for June to August average. (e, f) As in Figures 22a and 22b but for central equatorial Pacific exceeding the indicated thresholds. (g, h) As in Figures 22c and 22d but for July to December and September to November average, respectively, exceeding the various thresholds indicated in Figure 22h.

and WWB. The 1972/1973 strong El Niño, for instance, had the largest SHB among events other than the 1982/1983, 1997/1998, and 2015/2016 El Niños, but in terms of WWB activities, the 1972/1973 event appears only moderate. The 1982/1983 and 1997/1998 El Niños are the only events that exhibit the most active WWB during boreal summer to fall, consistently with the strongest SHB on record. The 2015/2016 El Niño is comparable to the 1982/1983 and 1997/1998 events in terms of WWB activity in JJA, but with only a moderate SHB. In SON, WWB activities are maintained in the 2015/2016 event as the SHB picks up. Nonetheless, overall, the 2015/2016 can be seen as somewhat comparable to the 1982/1983 and 1997/1998 events in terms of these wind surges and is clearly larger than the less extreme events on the available record.

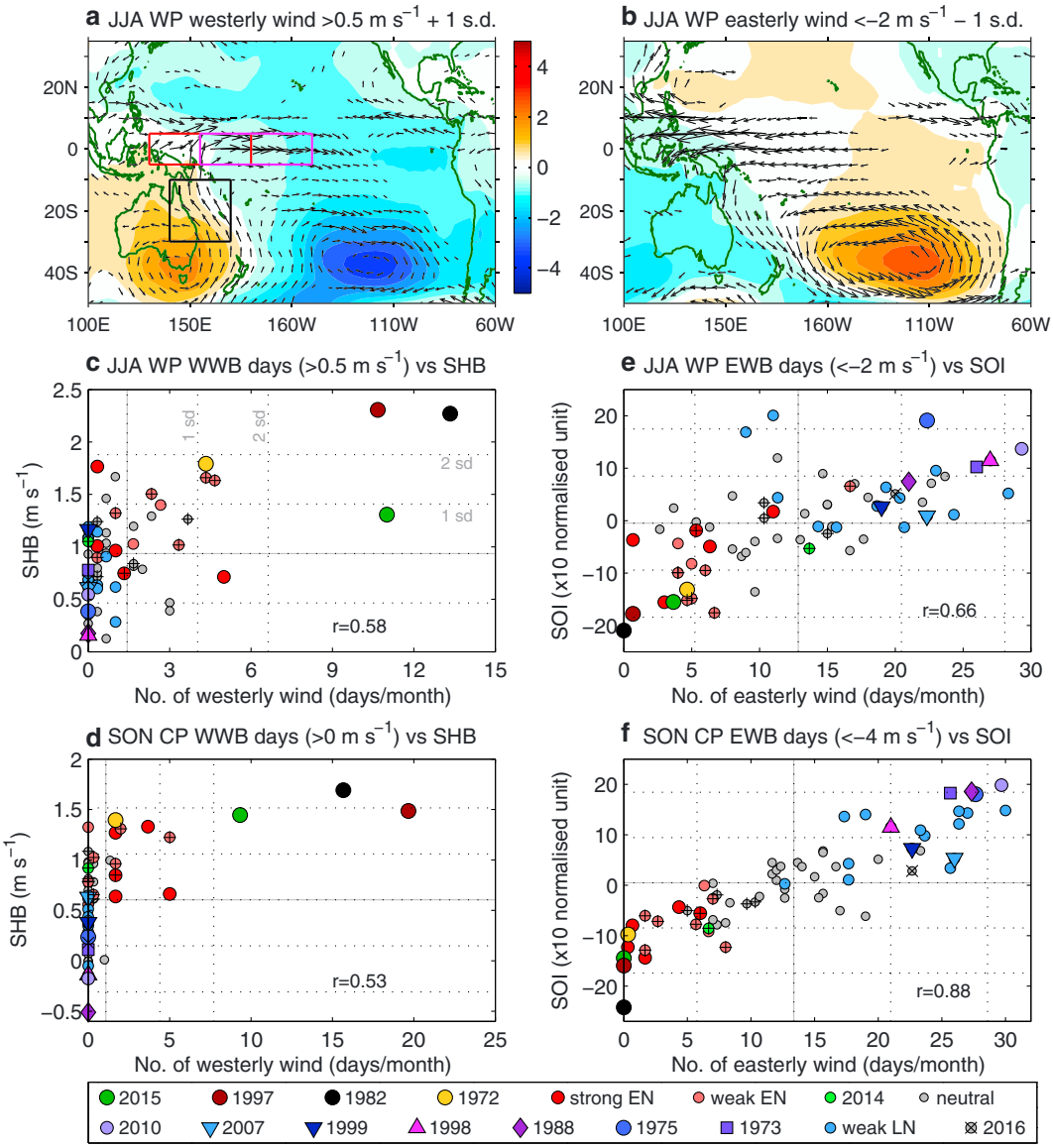

Figure 23. (a) Composites of SLP anomaly (color shading) and zonal and meridional wind velocity at 850 hPa (vectors) for years when the JJA average number of days in which westerly winds with zonal velocity at surface level, averaged over Western Pacific (WP; 5°S–5°N, 130°E–180°E; red box), exceeding 0.5 m s^{-1} is greater than 1 standard deviation above the mean. Only velocity vectors with speed greater than 0.5 m s^{-1} are shown. (b) As in Figure 23a but for easterly winds with velocity exceeding −2 m s^{-1}. (c) JJA average Southern Hemisphere booster (SHB) index against JJA average number of days of WP westerly winds exceeding 0.5 m s^{-1}. The SHB index is meridional wind velocity at 850 hPa averaged over 30°S–10°S, 140°E–170°E (black box in Figure 23a). (d) SON average SHB index against SON average number of westerly winds over Central Pacific (CP; 5S–5N, 155E–150 W; magenta box in Figure 23a) exceeding 0 m s^{-1}. (e) JJA average Southern Oscillation index (SOI) against JJA average number of WP easterly winds exceeding −2 m s^{-1}. (f) SON average SOI against SON average number of CP easterly winds exceeding −4 m s^{-1}. Raw data are used in Figures 23c–23f, and the correlation coefficient between the variables indicated in each panel is significant above the 95% confidence level (similar correlation coefficients are obtained when detrended). Mean values are indicated by solid gray lines, and standard deviations at 1 unit interval from the mean are indicated by dotted lines. Central Pacific El Niño events are indicated with "plus" marker.

One feature worth noting is that by boreal fall, WWB activities in central Pacific are absent during all La Niña and most neutral years, as well as most central Pacific El Niño years, except those CP El Niños that also involve significant warming in the eastern Pacific (Figure 23d). This signifies the role of eastern Pacific warming for generating CP WWB.

Just like WWB, EWB are also significantly correlated to SHB ($r = -0.50$ and -0.75 for WP and CP EWB in JJA and SON, respectively). The relationship between equatorial wind bursts and southerly surges is established through the hemispheric-scale east-west SLP see-saw in the Southern Oscillation (Figures 23a and 23b). The number of EWB and WWB days is highly correlated to the SOI at above 95% confidence level ($|r| > 0.5$). In terms of SOI and EWB (Figures 23e and 23f), extreme ENSO events do not appear to be strikingly distinct from other types of events. An exception to this is the large negative value of SOI in SON during the 1982/1983 El Niño. In short, unlike WWB and SHB, the SOI and the EWB do not provide a strong distinctive characterization for extreme events. Nonetheless, strong La Niña events tend to be preceded by above average EWBs, highlighting the important role of EWB in La Niña onset (Chiodi & Harrison, 2015). The role of the EWB is not only limited to La Niña development, but can also have an effect on El Niño. This is demonstrated by the above average EWB in 2014 in boreal summer (Figure 23e), which preconditions the 2015/2016 El Niño by preventing warm water volume discharge (Hu & Fedorov, 2017a; Levine & McPhaden, 2016), thus contributing to the high EHC seen in 2015 (Figure 17d). The relatively high occurrences of EWB in 2014, which coincided with the absence of WWBs (Figures 23c and 23d; Menkes et al., 2014), also contributed to the failed materialization of a strong El Niño in 2014 boreal winter through suppression of positive Bjerknes feedback that supports El Niño growth (Hu & Fedorov, 2016).

5. Summary and Discussions

Although the basic dynamics of ENSO implies that it can be viewed as a simple deterministic linear system independent of the annual cycle (section 2), in reality there is a strong degree of chaos, stochasticity, nonlinearity, and seasonality. Various studies to date have collectively conducted in-depth investigation on each of these aspects, yet there is still scope for further understanding given the short observational record. In this regard, the emergence of the strong 2015/2016 El Niño provides a great opportunity for a reflection.

5.1. Characteristics of ENSO Extremes

In section 4, we examined various observed variables that are relevant to ENSO genesis in order to characterize the 2015/2016 El Niño and put this in perspective of past events. This in turn further exposes the nonlinear nature of the system, which manifests in ENSO extremes.

The analysis reveals many similarities between the 1982/1983 and 1997/1998 extreme El Niño events, thus justifying them to be grouped together as a strongly nonlinear type of El Niño, but the latter still emerges as the strongest El Niño on record. The recent 2015/2016 El Niño is indeed extreme, marked by record-breaking warm anomaly in the central Pacific, but weaker in many measures than the two previous extreme El Niños. The 1982/1983 and 1997/1998 El Niños exhibit SST anomalies that peak toward the far eastern Pacific, resulting in exceptional warming in the Niño3 and Niño1+2 regions. This distinctive characteristic pattern and evolution also manifests in the 1982/1983 and 1997/1998 events having an apparent eastward propagation signature in their SST anomalies that is not seen in other events including the recent 2015/2016 El Niño (Figure 13). Strong La Niña events tend to exhibit westward propagation, such that the cold SST anomalies peak prominently in the Niño4 region.

The distinctive SST patterns are also reflected in the rainfall response (Figures 15 and 16). The 2015/2016 El Niño displays record breaking rainfall in the Niño4 region, whereas the 1982/1983 and 1997/1998 events exhibit exceptionally intense precipitation over the normally cold and dry eastern equatorial Pacific (Niño3 region). However, even if the Niño3 rainfall for 2015/2016 is notably weaker than the 1982/1983 and 1997/1998 events, it is still distinctively large relative to any other events. From this angle, the 2015/2016 event can still be considered as an extreme El Niño following the rainfall threshold-based definition of Cai, Borlace, et al. (2014).

The analysis of Climate Model Intercomparison Project (CMIP) models ensemble by Cai, Borlace, et al. (2014) and Cai, Santoso, et al. (2015) shows that the increasing Niño3 rainfall exceeding a certain threshold under greenhouse warming is an indicator for more frequent occurrences of an extreme El Niño. They argued that the use of rainfall to identify extreme El Niño events is not only physically meaningful but also relevant in terms of impact. In view of the latter aspect, they show that extreme El Niño events need not occur with eastward propagating SST anomalies, which are also projected to increase in frequency

under greenhouse warming (Santoso et al., 2013). Thus, in that sense, the 2015 event can be viewed as the first emergence of an extreme El Niño in the 21st century—one which satisfies the rainfall threshold definition, but not necessarily the eastward propagation characteristic. While these projections concern eastern Pacific El Niño, an earlier study by Yeh et al. (2009) projected an increase in central Pacific or Modoki El Niño frequency. The 2015/2016 El Niño does exhibit an exceptionally strong central Pacific warming, but it cannot be classified as a purely CP El Niño, since it exhibits eastern Pacific warming that is stronger than in the central Pacific (sections 3 and 4.2.1). In fact, it is the preceding weak 2014/2015 warm event that can be classified as a CP El Niño.

In many other metrics, such as wind variability, heat content, and wind surges, the 2015/2016 El Niño does register as an extreme, but still notably weaker than the 1982/1983 and 1997/1998 El Niños. The 1982/1983 and 1997/1998 El Niños exhibit abnormally large magnitude of westerly wind anomalies during their growth period and the southward shift of the wind anomalies following the event peak that leads to a strong heat content discharge (Figure 17). They also exhibit a spike in WWB activity (Figures 22 and 23), especially in boreal fall when the climatological winds are predominantly easterly, exceeding the level of any other ENSO events. The high WWB activity late in the year was linked to the development of very warm SSTs that expand eastward into the eastern equatorial Pacific, thus is more associated with more strongly eastern Pacific El Niño (Levine et al., 2016). The weaker level of the WWB activity in the 2015/2016 El Niño, which is shown here to be less of an eastern Pacific type of El Niño, verifies the nature of this state-dependent stochastic forcing.

There is a statistically significant positive correlation between WWB activity and cold southerly wind surges from the Southern Hemisphere (represented by the SHB index). The SHB for the 1982/1983 and 1997/1998 events remain the strongest, particularly during boreal summer, with the 2015/2016 and 1972/1973 events becoming comparable with the 1982/1983 and 1997/1998 events in boreal fall (Figure 23). The link between SHB and WWB stems from the underlying Southern Oscillation pattern in atmospheric pressure. However, despite a consistent tendency, the Southern Oscillation Index (SOI) during ENSO development phase does not show strong distinctive characteristic for extreme ENSO, especially extreme La Niña events. Easterly wind burst activity also cannot distinctively characterize extreme La Niña events. While the processes for extreme La Niña tend to be stronger than those of moderate events, the distinction is not as obvious as in the extreme El Niño case. Nonetheless, there are a few processes that do exhibit somewhat distinctive characteristics for extreme La Niña: cold central Pacific SST anomalies at the peak of the event and the equatorial heat content discharge during the development phase.

5.2. Distinctiveness and Detectability

The results above can be summarized in Figure 24 where we consider whether the range of a certain variable averaged over a 3 month sliding window for a given class of events intersects the range for weaker events including events of the opposite phase. Nonoverlapping range indicates a clear distinction, and so the mean between the minimum value of the stronger sample and the maximum value of the weaker sample is plotted. Given the limited observational record for extreme events, prescribing probability is challenging. As such, we simply use range instead of confidence interval. The classes of events are shown in the figure legend. Given the significant overlap in the various variables for strong La Niña events, we assign three events in 1973/1974, 1988/1989, and 1998/1999 as extreme La Niña, and the rationale for this can be found in Figure 25. This analysis can also address the question of when the earliest possible time is for a given class of events to be potentially detectable. By "detectable" we mean for the events to exhibit characteristics that are distinct from weaker events. However, note that even if the sample ranges do not overlap, we still cannot be 100% sure that the true characteristics across events are completely distinct. For instance, future observations can potentially weaken this distinction, as demonstrated by the 2015/2016 event in some of the variables discussed above. Here we have only used one observational product for each variable. The exercise can be certainly extended using multiple products to be more rigorous and to examine the impact of observational uncertainty.

One notable feature in Figure 24 is that in general the emergence of extreme ENSO event cannot be readily detected prior to boreal summer. There are few exceptions. The 1997/1998 El Niño emerges to be detectable very early in some of the variables including EHC and WWB activity in the Western Pacific. In most cases though, detectability for extreme El Niño occurs in boreal summer at the earliest

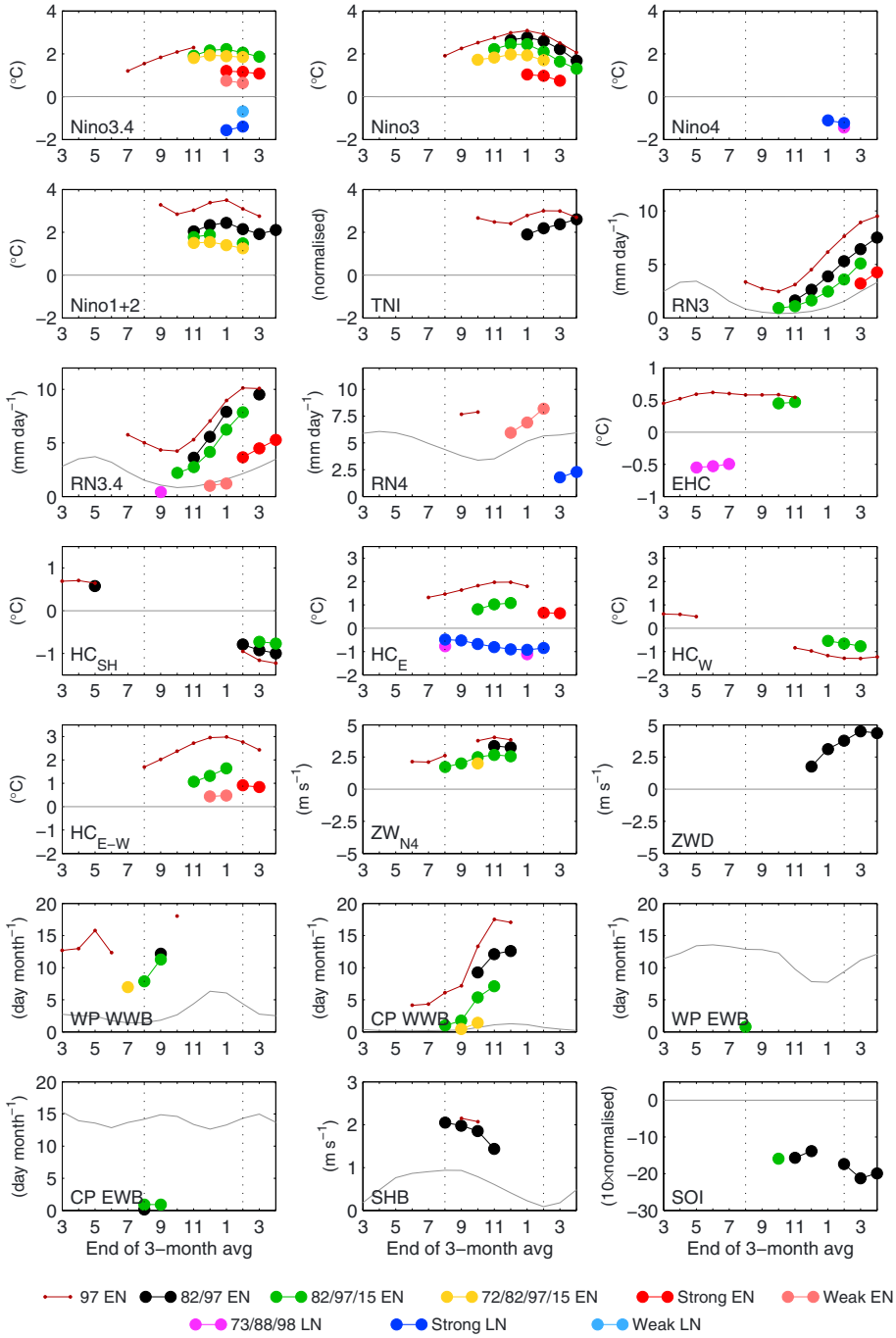

Figure 24. "Potential signal emergence" in the various variables for different classes of events. Values are shown only when the minimum (M1) of the 3 month averaged value of each event class (e.g., [1982/1983, 1997/1998], [1982/1983, 1997/1998, 2015/2016], etc.) is greater than the maximum (M2) of the 3 month averaged value of any weaker events, including neutral and the opposite phase. The values in each panel are the average of M1 and M2, plotted at the last month of the 3 month window. All data are first detrended over the available period for each variable. The SST and rainfall are based on ERSSTv5 and standard CMAP rainfall, respectively. The values for the strongest El Niño (1997/1998) are shown as a comparison. Vertical dotted lines indicate the month of August and the following February, spanning the development to mature phase of ENSO. The variables include the various SST indices (Niño3.4, Niño3, Niño4, Niño1+2, and TNI), rainfall averaged over Niño3.4, Niño3, and Niño4 regions (RN3.4, RN3, and RN4, respectively), heat content variables (EHC, HC_{SH}, HC_E, HC_W, and $HC_{E\text{-}W}$), zonal wind velocity anomalies (ZW_{N4} and ZWD), number of westerly and easterly wind bursts in the western and central Pacific (WWB_{WP}, WWB_{CP}, EWB_{WP}, and EWB_{CP}), the Southern Hemisphere Booster (SHB), and the Southern Oscillation Index (SOI). Gray lines indicate the mean climatological values.

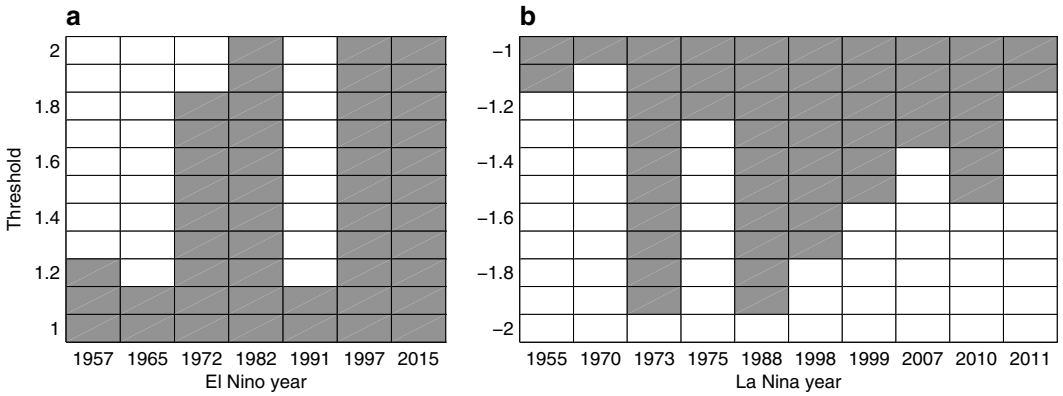

Figure 25. Sensitivity of extreme ENSO year identification to amplitude thresholds. (a) Extreme El Niño years identified using Niño3 anomaly averaged over November to January (NDJ) and December to February (DJF) both exceed *M* times the corresponding standard deviations, where the amplitude threshold, *M*, is varied from 1 to 2 on 0.1 interval. (b) As in Figure 25a but for extreme La Niña years identified using Niño4 anomaly more negative than *M* times its standard deviation, where *M* is varied from −2 to −1 on 0.1 interval. The years that satisfy the condition for all of the four SST reanalysis products (ERSSTv4, ERSSTv5, HadISST, and COBE) are shaded in gray. Thus, the ENSO definition would be less sensitive to the choice of observational product or peak season. The quoted years refer to the years of the ENSO development phase.

(e.g., SHB) and when the 2015/2016 or 1972/1973 event is considered as an extreme El Niño (e.g., WWB_{WP}, WWB_{CP}, and ZW_{N4}). While the number of variables for detecting an extreme La Niña is more limited, such events can also be potentially detected as early as boreal spring (March–May) using the equatorial heat content (EHC). This stems from the fact that EHC beats SST persistence in predicting SST anomalies in boreal winter (McPhaden, 2003) (see also Figure 26). Low heat content in

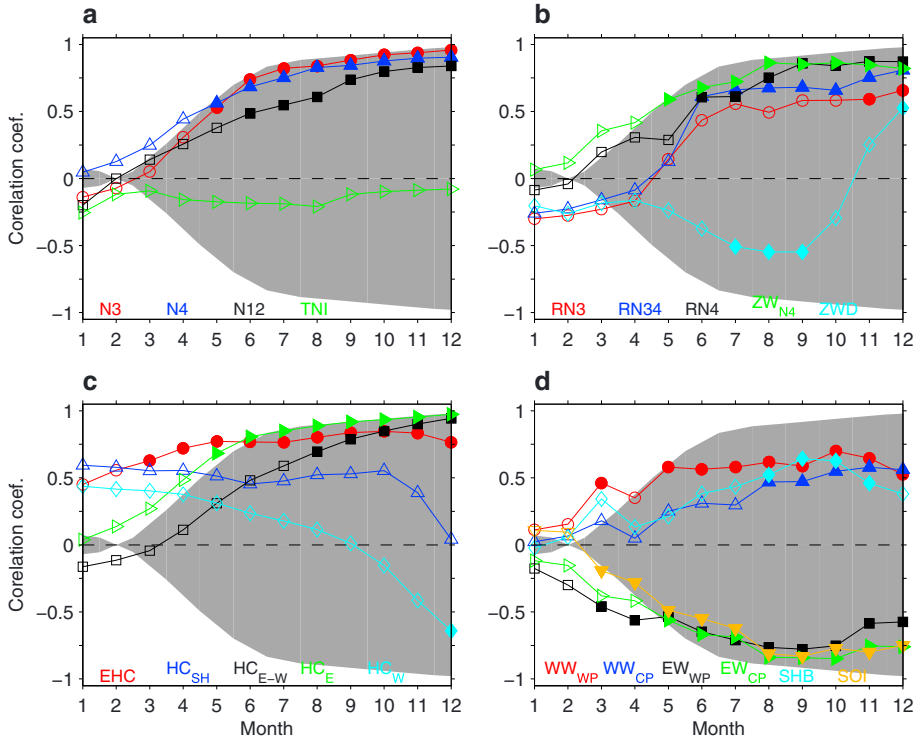

Figure 26. Correlation coefficient between various variables at each month against DJF average Niño3.4 index. The gray envelope is the correlation between Niño3.4 at each month against DJF Niño3.4 index. Statistically significant correlation above 95% confidence level is indicated by filled markers.

the eastern equatorial Pacific (HC_E) in boreal summer also appears as an indicator for a strong La Niña. In short, in general, we may need to wait until the end of boreal summer (August) to be sure about the extremity of ENSO events (as also suggested by Takahashi & Dewitte, 2016 for extreme El Niño) using different indices for different class of events. The conventional linear correlation analysis (Figure 26) is only useful for determining the phase of the events, but less so for the magnitude.

The analysis also shows that around the peak of ENSO events in boreal winter, extreme El Niño events are distinguishable from moderate events in terms of the various processes (Figure 24). For extreme La Niña, variables are much more limited (Niño3.4, Niño4, and HC_E), which exhibit distinctive characteristics. At present, there is no comprehensive evaluation of ENSO extremes in climate models, and so this information can be used for model validation purposes.

Thus, it is extreme El Niño that can be more immediately distinguished from other events. This stems from the strongly nonlinear processes in the eastern Pacific, giving rise to high skewness in many of the variables assessed here. This nonlinearity manifests in two regimes of strong and moderate events, distinguishable in SST patterns with the former exhibiting an "eastern Pacific" pattern and the latter a "central Pacific" pattern (Takahashi & Dewitte, 2016; Takahashi et al., 2011; Figure 12), as well as in rainfall as we have shown in Figure 16. Takahashi & Dewitte (2016) found that such regimes exist in a millennial-long run of the GFDL CM2.1 climate model, showing transitional events between regimes. In the limited observations, the strong regime is populated only by the 1982/1983 and 1997/1998 El Niño. The 2015/2016 El Niño appears as a transitional event, that is, a mixed EP and CP patterns, highlighting the continuum nature of the ENSO coupled system which is less apparent in the short observational record.

5.3. Future Research Directions and Closing Remarks

Future observations will eventually paint a complete picture of ENSO continuum, but in the interim it is crucial that more comprehensive analysis of climate models be conducted to better understand how and why models can simulate different ENSO regimes, or if they tend to be locked in one or the other. This would lead to further understanding of basic physical processes that impact ENSO simulation, for instance, how models handle atmospheric convection (e.g., Bellenger et al., 2014) or small-scale processes like tropical instability waves (An, 2008). It is also necessary to evaluate whether models that simulate such regimes can properly simulate the relevant seasonally phase-locked nonlinear processes like the southward wind shifts (Abellán, McGregor, & England, 2017; Stuecker et al., 2013). Improvements in ENSO simulation will continue to benefit from collective effort in evaluating future generations of climate models (e.g., Bellenger et al., 2014; Capotondi et al., 2006; Guilyardi et al., 2009, 2016; Taschetto et al., 2014). Such an effort will help unravel the complexities of nonlinear processes governing ENSO extremes, including the effects of remote forcing. Getting all these aspects right should lead to better prediction of ENSO extremes and diversity (e.g., Hendon et al., 2009).

As noted in section 2.2, ENSO is influenced by modes of climate variability sourced outside tropical Pacific. Despite several investigations in this area, how these remote forcings may contribute to ENSO extremes is still not clear. Part of the challenge is that the remote variability itself is not entirely independent of ENSO, owing to the pronounced global teleconnections of ENSO via the atmosphere and ocean (e.g., Alexander et al., 2002; Liu & Alexander, 2007). This makes it difficult to determine cause and effect. For instance, as the Pacific and Indian Oceans are linked through the atmospheric Walker Circulation, anomalous suppression and enhancement of atmospheric convection over the Western Pacific Warm Pool during El Niño and La Niña tend to result in cooccurrences with positive and negative phases of the Indian Ocean Dipole (IOD) during boreal autumn (Figure 27a). As such, there is a significant positive correlation between ENSO and IOD (Figure 27c; e.g., Meyers et al., 2007). Note that the correlation is not perfect, given that IODs can also be generated in the absence of ENSO (e.g., Behera et al., 2006; Kajtar et al., 2017). As pointed out by Zhang et al. (2015), and as can be gleaned in Figure 27c, the strength of the correlation is largely due to eastern Pacific El Niño events. We note that there is also asymmetry in which extreme El Niño events have occurred with notable positive IODs, including the 2015/2016 event, unlike extreme La Niñas, which were accompanied by neutral and weak IODs. Much stronger correlation exists between ENSO and Indian Ocean basin-wide mode (IOBM; Figures 27b and 27d)—a uniform warming and cooling across the tropical Indian Ocean that emerges in boreal winter, largely in

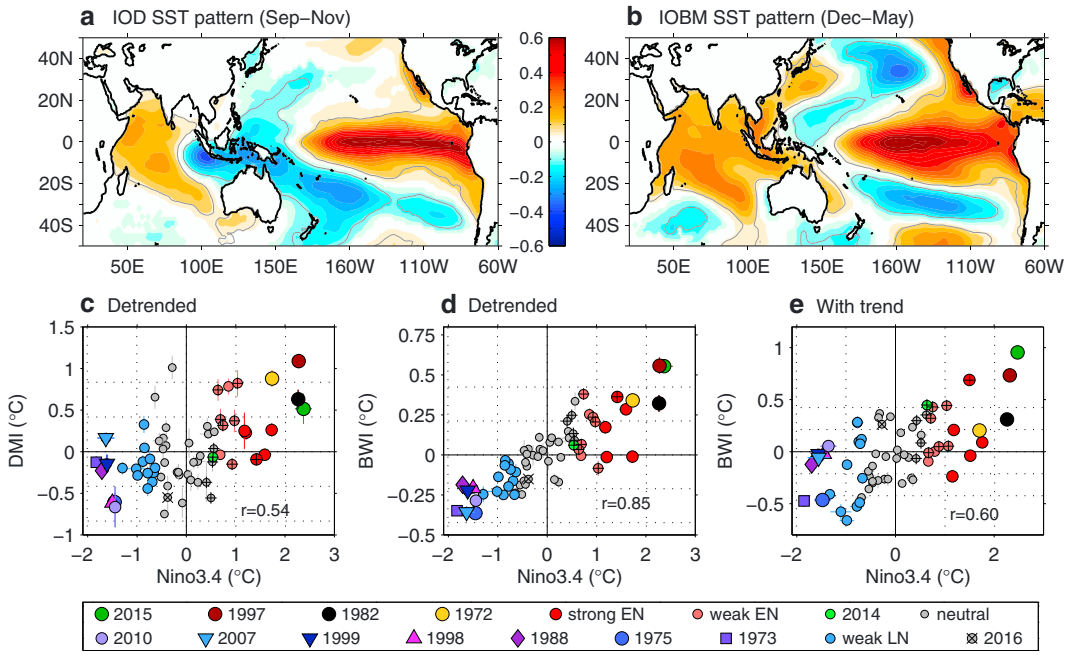

Figure 27. Dominant modes of SST variability in the Indian Ocean. (a) SST anomaly pattern associated with the Indian Ocean dipole (IOD) expressed as regression coefficients of the Dipole Mode Index (DMI) onto SSTs averaged over boreal fall (September–November; SON) when IOD peaks. (b) SST anomaly pattern associated with the Indian Ocean basin-wide mode (IOBM) expressed as regression coefficients of the basin-wide index (BWI) onto SSTs averaged over December to May (DJFMAM) when the IOBM is most prominent. (c) Detrended DJF average Niño3.4 index against the SON average DMI. (d) Detrended DJF average Niño3.4 index against the DJFMAM average BWI. (e) As in Figure 27d but for the raw data. The DMI is the difference between SST anomalies averaged over 10°S–10°N, 50°–70°E and 10°S–0°, 90°–110°E (Saji et al., 1999). BWI is SST anomalies averaged over 20°S–20°N, 40°–100°E (Saji et al., 2006). The analysis is based on ensemble means of the four SST reanalysis products. Error bars are shown in Figures 27c–27e as 1 standard deviation unit above and below the ensemble means.

response to air-sea heat fluxes induced by ENSO, lasting into the next summer (Du et al., 2009; Klein et al., 1999; Lau & Nath, 2003).

Thus, due to these strong relationships, previous studies have utilized climate models to artificially eliminate Indian Ocean variability and then examine the change in ENSO (e.g., Dommenget et al., 2006; Santoso et al., 2012; Terray et al., 2016; Wu & Kirtman, 2004). While the results may be model and experimental design dependent, the latest consensus is that the net effect of Indian Ocean SST variability is a damping on ENSO (Terray et al., 2016). The negative feedback appears to be associated with the effect of IOBM in promoting fast transition from El Niño to La Niña (Kug et al., 2006), providing further explanation for why La Niña tends to last longer than El Niño (Okumura & Deser, 2010), in addition to the nonlinear southward wind shift processes in the tropical Pacific (Stuecker et al., 2013).

The effect of IOD on ENSO is somewhat a more contentious issue. On the one hand, the IOD may have no influence on ensuing ENSO development due to destructive interference of atmospheric Kelvin waves arising from the opposite polarity of the east-west SST anomalies (Annamalai et al., 2005). On the other hand, the IOD could potentially initiate ENSO in the following year (Izumo et al., 2010), through the Indonesian throughflow (Yuan et al., 2011) and/or the atmospheric bridge aided by the IOBM that immediately follows the IOD (Izumo et al., 2016). Adding to the challenge in this research area is that current generation of climate models still exhibit significant bias in the Indian Ocean (e.g., too strong IOD amplitude; Cai & Cowan, 2013). The strength of interbasin interactions is also likely to vary across different background climates (Santoso et al., 2012; see their Figure 5b). Future research should take these issues into account, at the same time paying particular attention to individual IOD/IOBM events rather than making a generalization across all events as this tends to hide nonlinear features. These considerations, along with accounting for different initial conditions in the Pacific, may better identify the effect of IOD

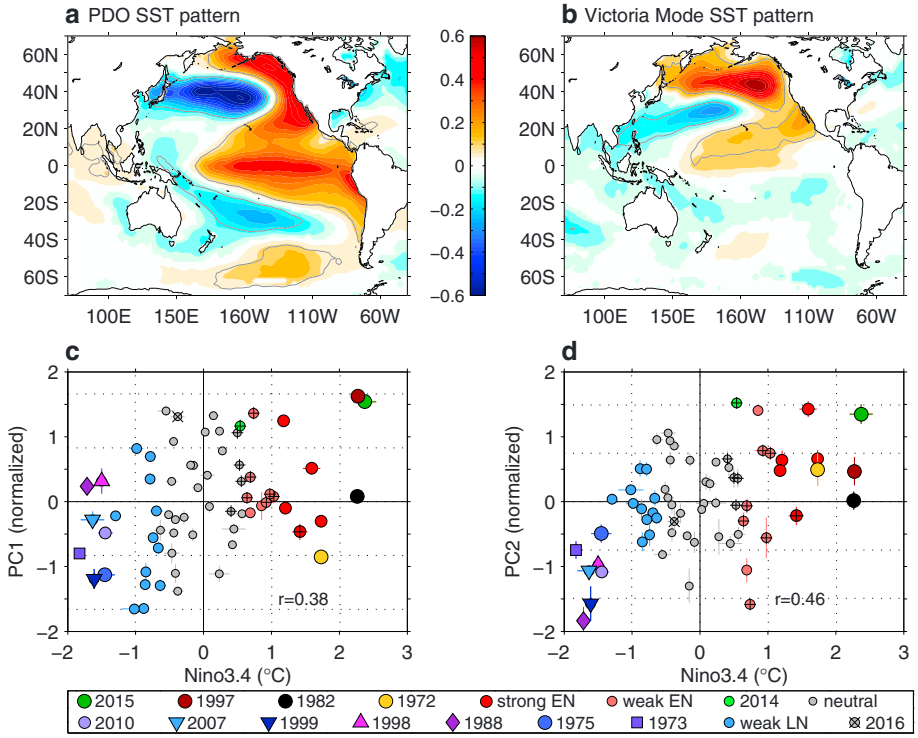

Figure 28. Dominant modes of SST variability in the North Pacific. (a) Pacific Decadal Oscillation (PDO) pattern expressed as the regression of SST onto the first principal component (PC1) time series of an EOF analysis of monthly SST anomaly over North Pacific (124°E–100°W, 20°N–65°N) after the monthly mean of global average SST anomaly removed from each grid point (explaining 23% of total variance), following the method of Bond et al. (2003). (b) SST pattern associated with Victoria Mode (VM) expressed as in Figure 28a but with PC2 (explaining 12% of total variance). (c) Detrended DJF average Niño3.4 index against January–December average PC1. (d) As in Figure 28c but for PC2. The analysis is based on ensemble means of the four SST reanalysis products. Error bars are shown in Figures 28c–28d as 1 standard deviation unit above and below the ensemble means.

on ENSO development toward eventual emergence of an extreme ENSO event (e.g., via the potential influence of IOD on WWB and SHB during boreal summer-autumn). In addition, these interbasin interactions may change under greenhouse warming, especially as significant changes to the IOD and IOBM are possible in a warmer future (Cai, Santoso, et al., 2014; Chu et al., 2014; Zheng et al., 2011). The steep Indian Ocean surface warming trend, which elevated the 2015/2016 IOBM to be the strongest on record (Figure 27e), is expected to influence the dynamics of ENSO and its extremes in ways that are not yet fully understood.

There are various other modes of variability that can influence ENSO, for example in the Atlantic basin (e.g., Kucharski et al., 2016), as well as extratropics (e.g., Boschat et al., 2013). The Pacific Meridional Mode or the Victoria Mode in the North Pacific (e.g., Di Lorenzo et al., 2015; Ding, Li, & Tseng, 2015; Furtado et al., 2012) and the South Pacific Meridional Mode (Zhang et al., 2014) may favor formation of Central Pacific and Eastern Pacific ENSO, respectively (Ding, Li, & Tseng, 2015; Paek et al., 2017; Vimont et al., 2014; Yu et al., 2010). Detailed discussions on ENSO remote forcings warrant a separate review paper, but it is worth noting here that the North Pacific extratropical forcing received much attention during the genesis of the 2015/2016 El Niño due to the presence of a persistent marine heatwave in the northeast Pacific that led to significant ecological disruptions and marine life mortality (Di Lorenzo & Mantua, 2016). This marine heatwave (popularly dubbed "The Blob" in the media) emerged in the fall of 2013 in response to the positive phase of the North Pacific Oscillation (NPO) driving atmospheric ridge over northeast Pacific (Bond et al., 2015).

The SST footprint of the NPO manifests in the Victoria Mode (VM; Figure 28b), which is independent of the PDO (Figure 28a), exhibiting northeast-southwest oriented SST dipole with warm anomalies

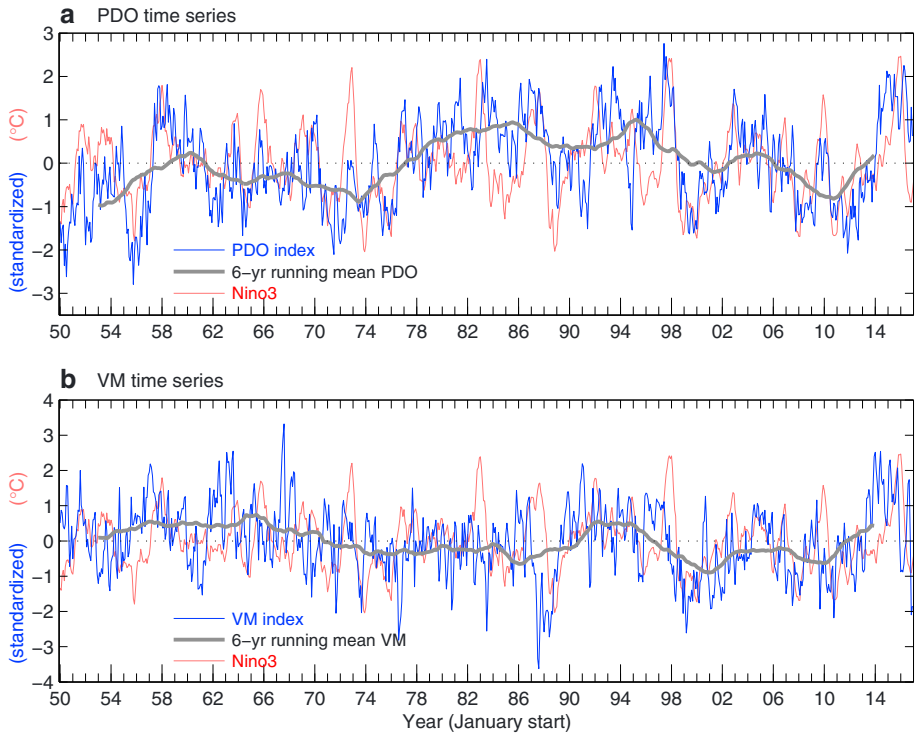

Figure 29. Time series of (a) the PDO index defined as PC1 in Figure 28, (b) the Victoria Mode (VM) index defined as PC2. The time series shown are ensemble average across four SST reanalysis products.

extending from off California northwestward across the extratropical Pacific. The VM, which is closely related to the North Pacific Gyre Oscillation (Di Lorenzo et al., 2008), has been suggested to trigger ENSO events through alterations of air-sea coupling in the tropical Pacific and subsurface ocean heat anomalies leading to surface warming in the central Pacific (Ding, Li, Tseng, et al., 2015). Tseng et al. (2017) suggested that the Blob is part of VM evolution leading to the emergence of the 2015/2016 El Niño. Figure 28d shows that the VM positive phase during 2015 was particularly strong, following another strong positive state in 2014, before turning weakly negative in 2016. While the 2015 VM is not distinct from some of the previous moderate El Niños, it is clearly much stronger than in the 1982/1983 and 1997/1998 extreme El Niños. This further highlights the distinction of the 2015/2016 El Niño from the 1982/1983 and 1997/1998 events in terms of the forcing hemisphere (see also Paek et al., 2017). The 2014–2015 marine heatwave may have an anthropogenic footprint (Wang et al., 2014; Weller et al., 2015). With continued increase in greenhouse gas emission, the implications for ENSO and its extremes need to be investigated, while keeping in mind model imperfections in simulating modes of extratropical Pacific (Lin et al., 2015).

While we have examined many key processes in this review paper, there are several other measures, such as wind power and available potential energy (Brown & Fedorov, 2010) that can provide further insight on the nature of ENSO extremes. In addition, the analysis presented here has not considered the influence of decadal variability, such as the IPO or PDO (Figure 28a). Nonetheless, it is possible that the 2015/2016 El Niño marks a transition from a negative to a positive IPO (Meehl et al., 2016) and ends the recent global warming hiatus (Hu & Fedorov, 2017b). In fact the PDO index for 2016 is positive (Figure 28c), thus making the decadal phase switch more likely (Figure 29a). In this regard, it is intriguing to ask when the next major El Niño will be of the same class as the 1982/1983 and 1997/1998 events, as both events occurred in a positive phase of the decadal oscillation. Is there still a possibility for such an event to exceed the magnitude of the 1997/1998 El Niño?

The 2015/2016 El Niño magnitude was partly boosted by the already warm equatorial Pacific in 2014 (section 4.1), as opposed to the previous strong events that were initiated from a cooler condition.

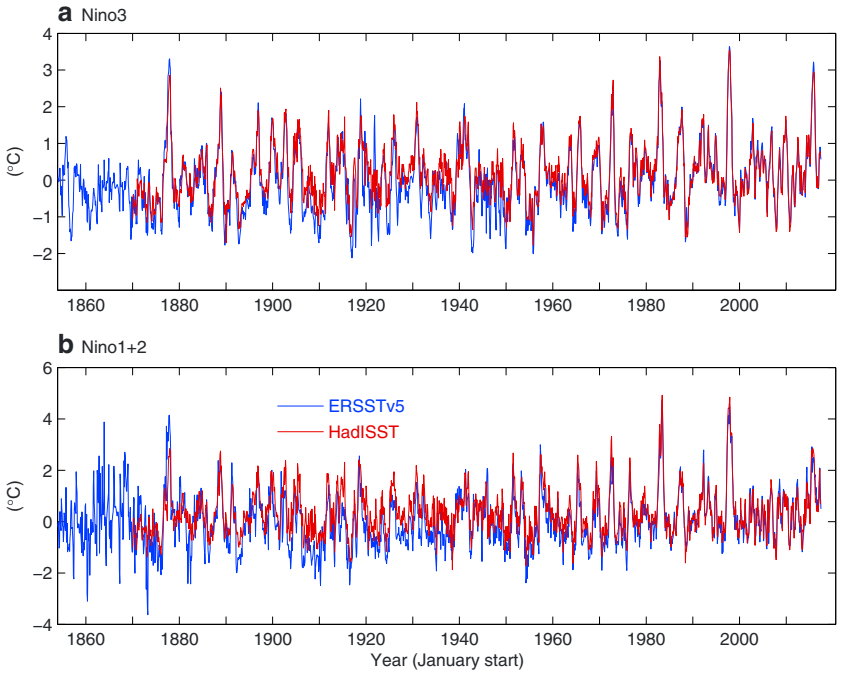

Figure 30. Time series of (a) Niño3 index, (b) Niño1+2 index from 1854 in ERSSTv5 (blue) and 1870 in HadISST (red), with seasonal mean over 1870–2016 removed.

Thus, there is still a possibility that a future 1982/1983 or 1997/1998 type of extremes has a potential to break records. The warming background climate due to unabated greenhouse gas forcing may have the capacity to influence such preconditioning. In an ensemble of CMIP3 and CMIP5 climate models that can simulate the eastward propagation characteristic of 1982/1983 and 1997/1998 events, Santoso et al. (2013; their Figure 4) showed that there is a potential for El Niño events in the 21st century to achieve Niño3 anomaly (with respect to long-term trend) that is about 30% higher than in the 20th century under a moderate greenhouse gas emission scenario (SRES A1B, RCP4.5; Meehl et al., 2007; Taylor et al., 2012). This and the potential for increased occurrences of events similar to the 1997/1+98 El Niño highlight the need to reduce emissions (e.g., via the Paris Agreement). However, even if global warming is halted, the risk associated with increased frequency of extreme El Niño events may still continue for several decades (Power et al., 2017; Wang et al., 2017). Despite these projections, it is not yet clear to what extent they are affected by climate model biases. There is some indication that the "cold tongue bias" (too cold equatorial Pacific) (e.g., Luo et al., 2005) could affect the projection of ENSO amplitude statistics (Kim et al., 2014). Further research is required to examine this issue along with climate model evaluation that focuses on a comprehensive set of processes associated with both phases of ENSO extremes. There is hope nonetheless for more reliable future projections as models continue to advance, as demonstrated by some improvements in ENSO simulation in CMIP5 from CMIP3 models, albeit modest (e.g., Bellenger et al., 2014; Kim & Yu, 2012).

To anticipate what the future may bring, it is instructive to enhance past record reconstructions to narrow uncertainties. SST reanalysis products shown in Figure 30 suggest an extreme El Niño occurring in 1876–1878 with potentially comparable strength to the extreme Niño of recent decades (see also Giese & Ray, 2011). However, it is clear that observational uncertainties are particularly notable before 1950 as also demonstrated by the stronger divergence between ERSSTv5 and HadISST pre-1950 (Figure 30). Nonetheless, with a long instrumental record (Figure 30) we can gauge how extreme El Niño occurrences seem to have become more frequent in recent decades, as emphasized by the occurrence of the 2015/2016 El Niño. It is intriguing to think whether such occurrences are unique in modern times due to anthropogenic greenhouse forcing.

Paleo-ENSO studies have suggested there were epochs of strong and weak ENSO activity in the distant past (e.g., Cobb et al., 2013; Tudhope et al., 2001), with a possibility that the late-twentieth-century ENSO activity is anomalously high for over at least the past few centuries, thus indicating the potential influence of anthropogenic greenhouse warming. (Li et al., 2013; McGregor, Timmermann, et al., 2013). As mentioned in section 1, paleo data can be used to provide useful information about the gross ENSO statistics, but less so for the characteristics of individual events, including their spatial patterns (see, e.g., Gagan, 2009; Rosenthal & Broccoli, 2004 for challenges in paleo reconstructions). As highlighted in this review paper, ENSO extremes exhibit diverse characteristics in spatial pattern and evolution. To extract such information from the past, it would require sustained collective effort among paleo-climatologists, climate dynamicists, and modelers, with climate models used to guide paleo data and vice versa. In addition, because modern observations are used to train paleo proxy records, ocean reanalysis systems need to be continuously improved to increase data reliability. Our existing ocean observing systems certainly must be sustained and enhanced to gather new data with high accuracy. This is needed not just for guiding paleo reconstructions and models but also for monitoring and predicting emerging climate events like the 2015/2016 extreme El Niño.

These various possibilities provide a rich opportunity for future research on ENSO and its extremes.

Appendix A

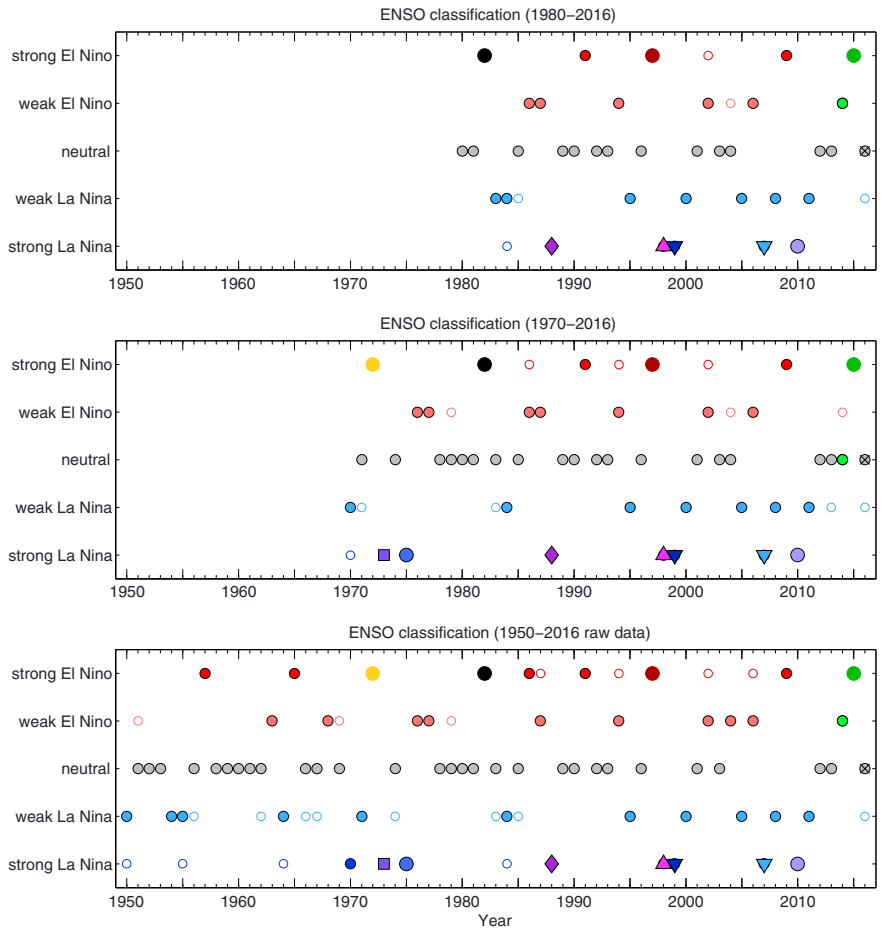

Figure A1. Sensitivity of classification of years into neutral, weak, or strong ENSO to different period of analysis: (top) Based on detrended Niño3.4 over 1980–2016, (middle) based on detrended Niño3.4 over 1970–2016, and (bottom) raw Niño3.4 over 1950–2016. See section 3 for classification method. Empty circles denote years that can be marginally assigned into the stronger class (e.g., 1983/1984 and 2016/2017 neutral conditions could be marginally weak La Niña, and 2014/2015 could be a weak El Niño). To be compared with Figure 3.

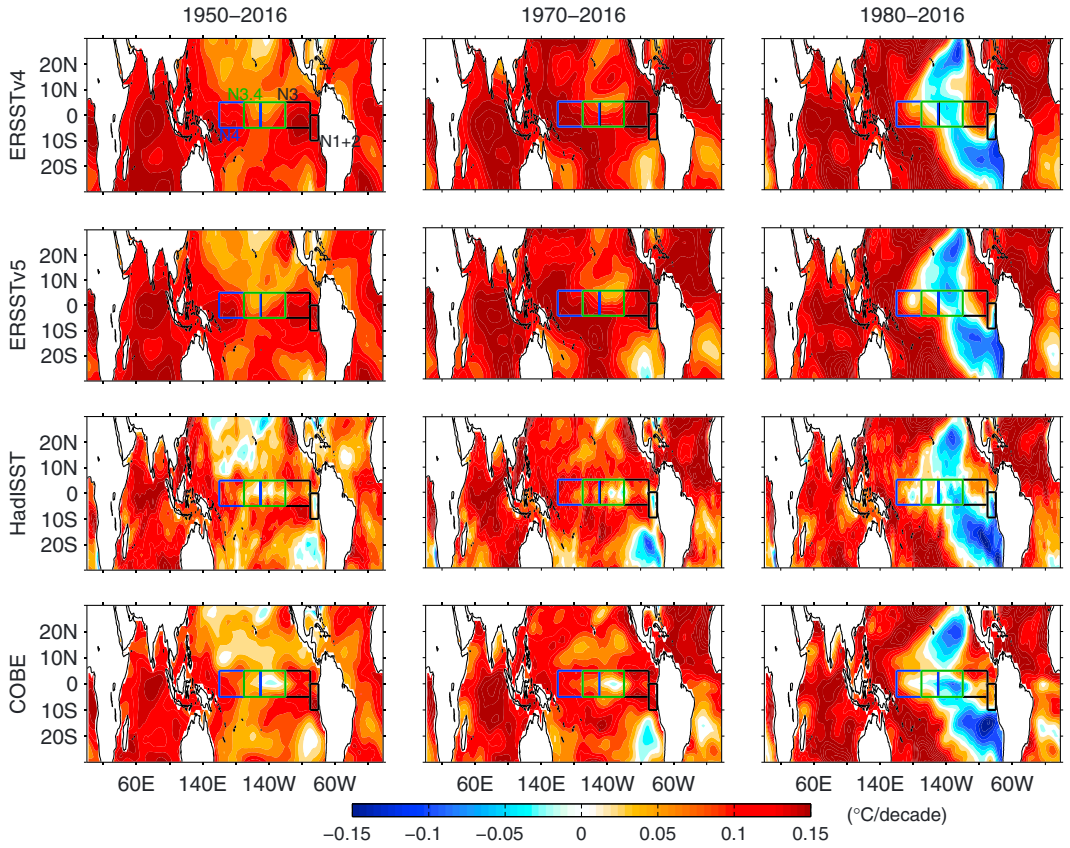

Figure A2. SST trends across different reanalysis products over (left column) 1950–2016, (middle column) 1970–2016, and (right column) 1980–2016.

Acknowledgments

The equatorial heat content variables (T300) are provided by TAO Project Office of NOAA/PMEL (www.pmel.noaa.gov/tao/wwv/data/). NOAA_ERSST_V4 and V5, COBE SST, CMAP and GPCP Precipitation, NCEP Reanalysis, and GODAS data are provided by the NOAA/OAR/ESRL PSD, Boulder, Colorado, USA, from their Web site at http://www.esrl.noaa.gov/psd/. The HadISST data were downloaded from http://www.metoffice.gov.uk/hadobs/hadisst/, and the SOI from http://www.bom.gov.au/climate/current/soihtm1.shtml. The ECCO2 data set (ecco2.jpl.nasa.gov) and OSCAR were downloaded from http://apdrc.soest.hawaii.edu/dods/public_data/. The motivation for the research stemmed from ENSO workshop Sydney February 2015 (https://www.climatescience.org.au/content/806-enso-workshop-australia-2015) and was first presented at the CLIVAR Pacific Region Panel meeting in Santiago (October 2015) and subsequently in 2016 in Qingdao. The authors thank CLIVAR Pacific Panel members for their comments and suggestions, as well as Alexey Fedorov, an anonymous reviewer, and the *Reviews of Geophysics* Editor in Chief, for their feedback that significantly improved the paper. This work is supported by Centre for Southern Hemisphere Ocean Research (CSHOR). A. S. is supported by the Australian Research Council and the Earth Science and Climate Change Hub of the Australian Government's National Environmental Science Programme (NESP). W. C. is supported by the Earth Science and Climate Change Hub of NESP and a CSIRO Office of Chief Executive Science Leader award. M. J. M. is supported by NOAA. This is PMEL contribution 4701.

References

Abellán, E., McGregor, S., & England, M. (2017). Analysis of the southward wind shift of ENSO in CMIP5 models. *Journal of Climate*, *30*(7), 2415–2435. https://doi.org/10.1175/JCLI-D-16-0326.1

Abellán, E., McGregor, S., England, M. H., & Santoso, A. (2017). Distinctive role of ocean advection anomalies in the development of the extreme 2015–16 El Niño. *Climate Dynamics*. https://doi.org/10.1007/s00382-017-4007-0

Abraham, J. P., Baringer, M., Bindoff, N. L., Boyer, T., Cheng, L. J., Church, J. A., … Domingues, C. M. (2013). A review of global ocean temperature observations: Implications for ocean heat content estimates and climate change. *Reviews of Geophysics*, *51*, 450–483. https://doi.org/10.1002/rog.20022

Adams, R. M., Chen, C.-C., McCarl, B. A., & Weiher, R. F. (1999). The economic consequences of ENSO events for agriculture. *Climate Research*, *13*, 165–172. https://doi.org/10.3354/cr013165

Adler, R. F., Huffman, G. J., Chang, A., Ferraro, R., Xie, P.-P., Janowiak, J., … Schneider, U. (2003). The version 2 global precipitation climatology project (GPCP) monthly precipitation analysis (1979–present). *Journal of Hydrometeorology*, *4*(6), 1147–1167. https://doi.org/10.1175/1525-7541(2003)004%3C1147:TVGPCP%3E2.0.CO;2

Aiken, C. M., Santoso, A., McGregor, S., & England, M. H. (2013). The 1970's shift in ENSO dynamics: A linear inverse model perspective. *Geophysical Research Letters*, *40*, 1612–1617. https://doi.org/10.1002/grl.50264

Aiken, C. M., Santoso, A., McGregor, S., & England, M. H. (2015). Optimal forcing of ENSO either side of the 1970's climate shift and its implications for predictability. *Climate Dynamics*, *45*(1-2), 47–65. https://doi.org/10.1007/s00382-014-2300-8

Alexander, M. A., Bladé, I., Newman, M., Lanzante, J. R., Lau, N.-C., & Scott, J. D. (2002). The atmospheric bridge: The influence of ENSO teleconnections on air–sea interaction over the global oceans. *Journal of Climate*, *15*(16), 2205–2231. https://doi.org/10.1175/1520-0442(2002)015%3C2205:TABTIO%3E2.0.CO;2

An, S.-I. (2008). Interannual variations of the tropical ocean instability wave and ENSO. *Journal of Climate*, *21*(15), 3680–3686. https://doi.org/10.1175/2008JCLI1701.1

An, S.-I., & Jin, F.-F. (2000). An eigen analysis of the interdecadal changes in the structure and frequency of ENSO mode. *Geophysical Research Letters*, *27*(16), 2573–2576. https://doi.org/10.1029/1999GL011090

An, S.-I., & Jin, F.-F. (2004). Nonlinearity and asymmetry of ENSO. *Journal of Climate*, *17*(12), 2399–2412. https://doi.org/10.1175/1520-0442(2004)017%3C2399:NAAOE%3E2.0.CO;2

An, S.-I., & Wang, B. (2000). Interdecadal change of the structure of the ENSO mode and its impact on the ENSO frequency. *Journal of Climate*, *13*(12), 2044–2055. https://doi.org/10.1175/1520-0442(2000)013%3C2044:ICOTSO%3E2.0.CO;2

An, S.-I., & Wang, B. (2001). Mechanisms of locking of the El Niño and La Niña mature phases to boreal winter. *Journal of Climate*, *14*(9), 2164–2176. https://doi.org/10.1175/1520-0442(2001)014%3C2164:MOLOTE%3E2.0.CO;2

Annamalai, H., Xie, S. P., McCreary, J. P., & Murtugudde, R. (2005). Impact of Indian Ocean sea surface temperature on developing El Niño. *Journal of Climate*, *18*, 302–319. https://doi.org/10.1175/JCLI-3268.1

Aronson, R. B., Precht, W. F., Macintyre, I. G., & Murdoch, T. J. T. (2000). Ecosystems: Coral bleach-out in Belize. *Nature*, *405*(6782), 36. https://doi.org/10.1038/35011132

Ashok, K., Behera, S. K., Rao, S. A., Weng, H., & Yamagata, T. (2007). El Niño Modoki and its possible teleconnection. *Journal of Geophysical Research*, *112*, C11007. https://doi.org/10.1029/2006JC003798

Balmaseda, M. A., Davey, M. K., & Anderson, D. L. T. (1995). Decadal and seasonal dependence of ENSO prediction skill. *Journal of Climate*, *8*(11), 2705–2715. https://doi.org/10.1175/1520-0442(1995)008%3C2705:DASDOE%3E2.0.CO;2

Barnard, P. L., Short, A. D., Harley, M. D., Splinter, K. D., Vitousek, S., Turner, I. L., … Banno, M. (2015). Coastal vulnerability across the Pacific dominated by El Niño/Southern Oscillation. *Nature Geoscience*, *8*(10), 801–807. https://doi.org/10.1038/ngeo2539

Barnston, A. G., Tippett, M. K., L'Heureux, M. L., Li, S., & DeWitt, D. G. (2012). Skill of real-time seasonal ENSO model predictions during 2002–11: Is our capability increasing? *Bulletin of the American Meteorological Society*, *93*(5), 631–651. https://doi.org/10.1175/BAMS-D-11-00111.1

Battisti, D. S., & Hirst, A. C. (1989). Interannual variability in a tropical atmosphere–ocean model: Influence of the basic state, ocean geometry and nonlinearity. *Journal of the Atmospheric Sciences*, *46*(12), 1687–1712. https://doi.org/10.1175/1520-0469(1989)046%3C1687:IVIATA%3E2.0.CO;2

Behera, S. K., Luo, J. J., Masson, S., Rao, S. A., Sakuma, H., & Yamagata, T. (2006). A CGCM study on the interaction between IOD and ENSO. *Journal of Climate*, *19*(9), 1688–1705. https://doi.org/10.1175/JCLI3797.1

Behringer, D. W. (2007). The Global Ocean Data Assimilation System at NCEP. In *11th Symp. On 'Integrated Observing and Assimilation Systems for Atmosphere, Oceans, and Land Surface', AMS 87th Annual Meeting* (pp. 1–12). San Antonio, TX: Henry B. Gonzales Convention Center.

Bell, G. D., & Chelliah, M. (2006). Leading tropical modes associated with interannual and multidecadal fluctuations in North Atlantic hurricane activity. *Journal of Climate*, *19*(4), 590–612. https://doi.org/10.1175/JCLI3659.1

Bell, G. D., Halpert, M. S., Kousky, V. E., Gelman, M. E., Ropelewski, C. F., Douglas, A. V., & Schnell, R. C. (1999). Climate assessment for 1998. *Bulletin of the American Meteorological Society*, *80*(5), 1040–1040. https://doi.org/10.1175/1520-0477(1999)080%3C1040:CAF%3E2.0.CO;2

Bellenger, H., Guilyardi, E., Leloup, J., Lengaigne, M., & Vialard, J. (2014). ENSO representation in climate models: From CMIP3 to CMIP5. *Climate Dynamics*, *42*(7-8), 1999–2018. https://doi.org/10.1007/s00382-013-1783-z

Bjerknes, J. (1966). A possible response of the atmospheric Hadley circulation to equatorial anomalies of ocean temperature. *Tellus*, *18*(4), 820–829. https://doi.org/10.1111/j.2153-3490.1966.tb00303.x

Blanke, B., Neelin, J. D., & Gutzler, D. (1997). Estimating the effect of stochastic wind stress forcing on ENSO irregularity. *Journal of Climate*, *10*(7), 1473–1486. https://doi.org/10.1175/1520-0442(1997)010%3C1473:ETEOSW%3E2.0.CO;2

Blunden, J., & Arndt, D. S. (Eds.) (2016). State of the climate in 2015. *Bulletin of the American Meteorological Society*, *97*(8), S1–S275.

Bond, N. A., Cronin, M. F., Freeland, H., & Mantua, N. (2015). Causes and impacts of the 2014 warm anomaly in the NE Pacific. *Geophysical Research Letters*, *42*, 3414–3420. https://doi.org/10.1002/2015GL063306

Bond, N. A., Overland, J. E., Spillane, M., & Stabeno, P. (2003). Recent shifts in the state of the North Pacific. *Geophysical Research Letters*, *30*(23). 2183. https://doi.org/10.1029/2003GL018597

Bonjean, F., & Lagerloef, G. S. (2002). Diagnostic model and analysis of the surface currents in the tropical Pacific Ocean. *Journal of Physical Oceanography*, *32*(10), 2938–2954. https://doi.org/10.1175/1520-0485(2002)032<2938:DMAAOT>2.0.CO;2

Borlace, S., Cai, W., & Santoso, A. (2013). Multidecadal ENSO amplitude variability in a 1000-yr simulation of a coupled global climate model: Implications for observed ENSO variability. *Journal of Climate*, *26*(23), 9399–9407. https://doi.org/10.1175/JCU-D-13-00281.1

Borlace, S., Santoso, A., Cai, W., & Collins, M. (2014). Extreme swings of the South Pacific convergence zone and the different types of el Niño events. *Geophysical Research Letters*, *41*, 4695–4703. https://doi.org/10.1002/2014GL060551

Boschat, G., Terray, P., & Masson, S. (2013). Extratropical forcing of ENSO. *Geophysical Research Letters*, *40*, 1605–1611. https://doi.org/10.1002/grl.50229

Boucharel, J., Dewitte, B., Garel, B., & du Penhoat, Y. (2009). ENSO's non-stationary and non-Gaussian character: The role of climate shifts. *Nonlinear Processes in Geophysics*, *16*(4), 453–473. https://doi.org/10.5194/npg-16-453-2009

Boucharel, J., Timmermann, A., Santoso, A., England, M. H., Jin, F.-F., & Balmaseda, M. (2015). A surface layer variance heat budget for ENSO. *Geophysical Research Letters*, *42*, 3529–3537. https://doi.org/10.1002/2015GL063843

Braconnot, P., Luan, Y., Brewer, S., & Zheng, W. (2012). Impact of Earth's orbit and freshwater fluxes on Holocene climate mean seasonal cycle and ENSO characteristics. *Climate Dynamics*, *38*(5-6), 1081–1092. https://doi.org/10.1007/s00382-011-1029-x

Brown, J. N., & Fedorov, A. V. (2010). How much energy is transferred from the winds to the thermocline on ENSO time scales? *Journal of Climate*, *23*(6), 1563–1580. https://doi.org/10.1175/2009JCLI2914.1

Burgers, G., & Stephenson, D. B. (1999). The "normality" of El Niño. *Geophysical Research Letters*, *26*(8), 1027–1030. https://doi.org/10.1029/1999GL900161

Cai, W., Borlace, S., Lengaigne, M., van Rensch, P., Collins, M., Vecchi, G., … Jin, F.-F. (2014). Increasing frequency of extreme El Niño events due to greenhouse warming. *Nature Climate Change*, *4*(2), 111–116. https://doi.org/10.1038/nclimate2100

Cai, W., & Cowan, T. (2013). Why is the amplitude of the Indian Ocean dipole overly large in CMIP3 and CMIP5 climate models? *Geophysical Research Letters*, *40*, 1200–1205. https://doi.org/10.1002/grl.50208

Cai, W., Lengaigne, M., Borlace, S., Collins, M., Cowan, T., McPhaden, M. J., … Widlansky, M. J. (2012). More extreme swings of the South Pacific convergence zone due to greenhouse warming. *Nature*, *488*(7411), 365–369. https://doi.org/10.1038/nature11358

Cai, W., Santoso, A., Wang, G., Weller, E., Wu, L., K. A., … Yamagata, T. (2014). Increased frequency of extreme Indian Ocean dipole events due to greenhouse warming. *Nature*, *510*(7504), 254–258. https://doi.org/10.1038/nature13327

Cai, W., Santoso, A., Wang, G., Yeh, S.-W., An, S.-I., Cobb, K. M., … Wu, L. (2015). ENSO and greenhouse warming. *Nature Climate Change*, *5*(9), 849–859. https://doi.org/10.1038/nclimate2743

Cai, W., Wang, G., Santoso, A., McPhaden, M. J., Wu, L., Jin, F.-F., … Guilyardi, E. (2015). Increased frequency of extreme La Niña events under greenhouse warming. *Nature Climate Change*, *5*(2), 132–137. https://doi.org/10.1038/nclimate2492

Cane, M. A. (2005). The evolution of El Niño, past and future. *Earth and Planetary Science Letters*, *230*(3-4), 227–240. https://doi.org/10.1016/j.epsl.2004.12.003

Cane, M., & Zebiak, S. E. (1985). A theory for El Niño and the southern oscillation. *Science*, *228*(4703), 1085–1087. https://doi.org/10.1126/science.228.4703.1085

Capotondi, A., & Sardeshmukh, P. D. (2017). Is El Niño really changing? *Geophysical Research Letters*, *44*, 8548–8556. https://doi.org/10.1002/2017GL074515

Capotondi, A., Wittenberg, A. T., & Masina, S. (2006). Spatial and temporal structure of tropical Pacific interannual variability in 20th century coupled simulations. *Ocean Modelling*, *15*(3–4), 274–298. https://doi.org/10.1016/j.ocemod.2006.02.004

Capotondi, A., Wittenberg, A. T., Newman, M., Di Lorenzo, E., Yu, J.-Y., Braconnot, P., … Dewitte, B. (2015). Understanding ENSO diversity. *Bulletin of the American Meteorological Society*, *96*(6), 921–938. https://doi.org/10.1175/BAMS-D-13-00117.1
Cashin, P., Mohaddes, K., & Raissi, M. (2015). Fair weather or foul? The macroeconomic effects of el Niño, IMF Working Papers, 15/89, 30 pp.
Changnon, S. A. (Ed.) (2001). *El Niño 1997–1998: The climate event of the century* (p. 215). New York: Oxford University Press.
Chen, D., & Cane, M. (2008). El Niño prediction and predictability. *Journal of Computational Physics*, *227*(7), 3625–3640. https://doi.org/10.1016/j.jcp.2007.05.014
Chen, L., Li, T., Behera, S. K., & Doi, T. (2016). Distinctive precursory air-sea signals between regular and super El Niños. *Advances in Atmospheric Sciences*, *33*(8), 996–1004. https://doi.org/10.1007/s00376-016-5250-8
Chen, D., Lian, T., Fu, C., Cane, M. A., Tang, Y., & Murtugudde, R. (2015). Strong influence of westerly wind bursts on el Niño diversity. *Nature Geoscience*, *8*(5), 339–345. https://doi.org/10.1038/ngeo2399
Chiodi, A., & Harrison, D. (2015). Equatorial Pacific easterly wind surges and the onset of La Niña events. *Journal of Climate*, *28*(2), 776–792. https://doi.org/10.1175/JCLI-D-14-00227.1
Choi, J., An, S.-I., Kug, J.-S., & Yeh, S.-W. (2011). The role of mean state on changes in El Niño's flavor. *Climate Dynamics*, *37*(5-6), 1205–1215. https://doi.org/10.1007/s00382-010-0912-1
Choi, K., Vecchi, G. A., & Wittenberg, A. T. (2013). ENSO transition, duration, and amplitude asymmetries: Role of the nonlinear wind stress coupling in a conceptual model. *Journal of Climate*, *26*(23), 9462–9476. https://doi.org/10.1175/JCLI-D-13-00045.1
Chu, J.-E., Ha, K.-J., Lee, J.-Y., Wang, B., Kim, B.-H., & Chung, C. E. (2014). Future change of the Indian Ocean basin-wide and dipole modes in the CMIP5. *Climate Dynamics*, *43*(1-2), 535–551. https://doi.org/10.1007/s00382-013-2002-7
Chung, C. T. Y., & Power, S. B. (2014). Precipitation response to La Niña and global warming in the Indo-Pacific. *Climate Dynamics*, *43*(12), 3293–3307. https://doi.org/10.1007/s00382-014-2105-9
Chung, C. T. Y., Power, S. B., Arblaster, J. M., Rashid, H., & Roff, G. L. (2014). Nonlinear precipitation response to El Niño and global warming in the Indo-Pacific. *Climate Dynamics*, *42*(7-8), 1837–1856. https://doi.org/10.1007/s00382-013-1892-8
Clement, A. C., Seager, R., & Cane, M. A. (1999). Orbital controls on the El Niño/Southern Oscillation and the tropical climate. *Paleoceanography*, *14*(4), 441–456. https://doi.org/10.1029/1999PA900013
Cobb, K. M., Charles, C. D., Cheng, H., & Edwards, R. L. (2003). El Niño/Southern Oscillation and tropical Pacific climate during the last millennium. *Nature*, *424*(6946), 271–276. https://doi.org/10.1038/nature01779
Cobb, K. M., Westphal, N., Sayani, H. R., Watson, J. T., Di Lorenzo, E., Cheng, H., … Charles, C. D. (2013). Highly variable El Niño–Southern Oscillation throughout the Holocene. *Science*, *339*(6115), 67–70. https://doi.org/10.1126/science.1228246
Cole, J. E., Overpeck, J. T., & Cook, E. R. (2002). Multiyear La Niña events and persistent drought in the contiguous United States. *Geophysical Research Letters*, *29*(13), 1647. https://doi.org/10.1029/2001GL013561
Collins, M., An, S.-I., Cai, W., Ganachaud, A., Guilyardi, E., Jin, F.-F., … Lengaigne, M. (2010). The impact of global warming on the tropical Pacific Ocean and El Niño. *Nature Geoscience*, *3*(6), 391–397. https://doi.org/10.1038/ngeo868
Del Ninno, C., & Dorosh, P. A. (2001). Averting a food crisis: Private imports and public targeted distribution in Bangladesh after the 1998 flood. *Agricultural Economics*, *25*(2-3), 337–346. https://doi.org/10.1016/S0169-5150(01)00090-1
Di Lorenzo, E., Liguori, G., Schneider, N., Furtado, J., Anderson, B. T., & Alexander, M. (2015). ENSO and meridional modes: A null hypothesis for Pacific climate variability. *Geophysical Research Letters*, *42*, 9440–9448. https://doi.org/10.1002/2015GL066281
Di Lorenzo, E., & Mantua, N. (2016). Multi-year persistence of the 2014/15 North Pacific marine heatwave. *Nature Climate Change*, *6*(11), 1042–1047. https://doi.org/10.1038/nclimate3082
Di Lorenzo, E., Schneider, N., Cobb, K. M., Franks, P. J. S., Chhak, K., Miller, A. J., … Bograd, S. J. (2008). North Pacific gyre oscillation links ocean climate and ecosystem change. *Geophysical Research Letters*, *35*, L08607. https://doi.org/10.1029/2007GL032838
DiNezio, P. N., Clement, A. C., Vecchi, G. A., Soden, B. J., Kirtman, B. P., & Lee, S. K. (2009). Climate response of the equatorial pacific to global warming. *Journal of Climate*, *22*(18), 4873–4892. https://doi.org/10.1175/2009JCLI2982.1
DiNezio, P. N., & Deser, C. (2014). Nonlinear controls on the persistence of la Niña. *Journal of Climate*, *27*(19), 7335–7355. https://doi.org/10.1175/JCLI-D-14-00033.1
Ding, R., Li, J., & Tseng, Y.-H. (2015). The impact of South Pacific extratropical forcing on ENSO and comparisons with the North Pacific. *Climate Dynamics*, *44*(7–8), 2017–2034. https://doi.org/10.1007/s00382-014-2303-5
Ding, R., Li, J., Tseng, Y.-H., Sun, C., & Guo, Y. (2015). The Victoria mode in the North Pacific linking extratropical sea level pressure variations to ENSO. *Journal of Geophysical Research: Atmospheres*, *120*, 27–45. https://doi.org/10.1002/2014JD022221
Dommenget, D., Bayr, T., & Frauen, C. (2013). Analysis of the non-linearity in the pattern and time evolution of El Niño Southern Oscillation. *Climate Dynamics*, *40*(11-12), 2825–2847. https://doi.org/10.1007/s00382-012-1475-0
Dommenget, D., Semenov, V., & Latif, M. (2006). Impacts of the tropical Indian and Atlantic Oceans on ENSO. *Geophysical Research Letters*, *33*, L11701. https://doi.org/10.1029/2006GL025871
Dommenget, D., & Yu, Y. (2016). The seasonally changing cloud feedbacks contribution to the ENSO seasonal phase-locking. *Climate Dynamics*, *47*(12), 3661–3672. https://doi.org/10.1007/s00382-016-3034-6
Du, Y., Xie, S.-P., Huang, G., & Hu, K. (2009). Role of air–sea interaction in the long persistence of El Niño-induced North Indian Ocean warming. *Journal of Climate*, *22*(8), 2023–2038. https://doi.org/10.1175/2008JCLI2590.1
Eckert, C., & Latif, M. (1997). Predictability of a stochastically forced hybrid coupled model of el Niño. *Journal of Climate*, *10*(7), 1488–1504. https://doi.org/10.1175/1520-0442(1997)010%3C1488:POASFH%3E2.0.CO;2
Eisenman, I., Yu, L., & Tziperman, E. (2005). Westerly wind bursts: ENSO's tail rather than the dog? *Journal of Climate*, *18*(24), 5224–5238. https://doi.org/10.1175/JCLI3588.1
England, M. H., McGregor, S., Spence, P., Meehl, G. A., Timmermann, A., Cai, W., … McPhaden, M. J. (2014). Recent intensification of wind-driven circulation in the Pacific and the ongoing warming hiatus. *Nature Climate Change*, *4*(3), 222–227. https://doi.org/10.1038/nclimate2106
Fedorov, A. V. (2002). The response of the coupled tropical ocean-atmosphere to westerly wind bursts. *Quarterly Journal of the Royal Meteorological Society*, *128*(579), 1–23. https://doi.org/10.1002/qj.200212857901
Fedorov, A. V. (2010). Ocean response to wind variations, warm water volume, and simple models of ENSO in the low-frequency approximation. *Journal of Climate*, *23*(14), 3855–3873. https://doi.org/10.1175/2010JCLI3044.1
Fedorov, A. V., Harper, S. L., Philander, S. G., Winter, B., & Wittenberg, A. (2003). How predictable is El Niño? *Bulletin of the American Meteorological Society*, *84*(7), 911–919. https://doi.org/10.1175/BAMS-84-7-911
Fedorov, A. V., Hu, S., Lengaigne, M., & Guilyardi, E. (2015). The impact of westerly wind bursts and ocean initial state on the development, and diversity of El Niño events. *Climate Dynamics*, *44*(5-6), 1381–1401. https://doi.org/10.1007/s00382-014-2126-4
Fedorov, A. V., & Philander, S. G. (2000). Is El Niño changing? *Science*, *288*(5473), 1997–2002. https://doi.org/10.1126/science.288.5473.1997

Fedorov, A. V., & Philander, S. G. (2001). A stability analysis of tropical ocean-atmosphere interactions: Bridging measurements and theory for El Niño. *Journal of Climate*, *14*(14), 3086–3101. https://doi.org/10.1175/1520-0442(2001)014%3C3086:ASAOTO%3E2.0.CO;2

Flügel, M., & Chang, P. (1998). Does the predictability of ENSO depend on the seasonal cycle? *Journal of the Atmospheric Sciences*, *55*(21), 3230–3243. https://doi.org/10.1175/1520-0469(1998)055%3C3230:DTPOED%3E2.0.CO;2

Fraisse, C. W., Cabrera, V. E., Breuer, N. E., Baez, J., Quispe, J., & Matos, E. (2008). El Niño-Southern Oscillation influences on soybean yields in eastern Paraguay. *International Journal of Climatology*, *28*(10), 1399–1407. https://doi.org/10.1002/joc.1641

Frauen, C., & Dommenget, D. (2010). El Niño and la Niña amplitude asymmetry caused by atmospheric feedbacks. *Geophysical Research Letters*, *37*, L18801. https://doi.org/10.1029/2010GL044444

Furtado, J. C., Di Lorenzo, E., Anderson, B. T., & Schneider, N. (2012). Linkages between the North Pacific Oscillation and central tropical Pacific SSTs at low frequencies. *Climate Dynamics*, *39*(12), 2833–2846. https://doi.org/10.1007/s00382-011-1245-4

Gagan, M. K. (2009). Paleo-El Niño-Southern Oscillation (ENSO) records. *Encyclopedia of Paleoclimatology and Ancient Environments*, 721–728. https://doi.org/10.1007/978-1-4020-4411-3_172

Gebbie, G., Eisenman, I., Wittenberg, A. T., & Tziperman, E. (2007). Modulation of westerly wind bursts by sea surface temperature: A semi-stochastic feedback for ENSO. *Journal of the Atmospheric Sciences*, *64*(9), 3281–3295. https://doi.org/10.1175/JAS4029.1

Gergis, J., Braganza, K., Fowler, A., Mooney, S., & Risbey, J. (2006). Reconstructing El Niño–Southern Oscillation (ENSO) from high-resolution palaeoarchives. *Journal of Quaternary Science*, *21*(7), 707–722. https://doi.org/10.1002/jqs.1070

Giese, B. S., & Ray, S. (2011). El Niño variability in simple ocean data assimilation (SODA), 1871–2008. *Journal of Geophysical Research*, *116*, C02024. https://doi.org/10.1029/2010JC006695

Glantz, M. H. (2001). *Current of change: Impacts of El Niño and La Niña on climate and society*. Cambridge, UK: Cambridge University Press.

Glynn, P. W. (1990). In P. W. Glynn (Ed.), *Global ecological consequences of the 1982–83 El Niño–Southern Oscillation* (pp. 55–126). Amsterdam: Elsevier. https://doi.org/10.1016/S0422-9894(08)70033-3

Guan, C., & McPhaden, M. J. (2016). Ocean processes affecting the twenty-first-century shift in ENSO SST variability. *Journal of Climate*, *29*(19), 6861–6879. https://doi.org/10.1175/JCLI-D-15-0870.1

Guilyardi, E., Wittenberg, A., Balmaseda, M., Cai, W., Collins, M., McPhaden, M. J., … Yeh, S.-W. (2016). Fourth CLIVAR workshop on the evaluation of ENSO processes in climate models: ENSO in a changing climate. *Bulletin of the American Meteorological Society*, *97*(5), 817–820. https://doi.org/10.1175/BAMS-D-15-00287.1

Guilyardi, E., Wittenberg, A., Fedorov, A., Collins, M., Wang, C., & Capotondi, A. (2009). Understanding el Niño in ocean-atmosphere general circulation models: Progress and challenges. *Bulletin of the American Meteorological Society*, *90*(3), 325–340. https://doi.org/10.1175/2008BAMS2387.1

Halpern, D., Menemenlis, D., & Wang, X. (2015). Impact of data assimilation on ECCO2 equatorial undercurrent and north equatorial countercurrent in the Pacific Ocean. *Journal of Atmospheric and Oceanic Technology*, *32*(1), 131–143. https://doi.org/10.1175/JTECH-D-14-00025.1

Harrison, D. E. (1987). Monthly mean island surface winds in the central tropical Pacific and el Niño events. *Monthly Weather Review*, *115*(12), 3133–3145. https://doi.org/10.1175/1520-0493(1987)115%3C3133:MMISWI%3E2.0.CO;2

Harrison, D. E., & Vecchi, G. A. (1997). Westerly wind events in the tropical Pacific, 1986–95. *Journal of Climate*, *10*(12), 3131–3156. https://doi.org/10.1175/1520-0442(1997)010%3C3131:WWEITT%3E2.0.CO;2

Harrison, D. E., & Vecchi, G. A. (1999). On the termination of El Niño. *Geophysical Research Letters*, *26*(11), 1593–1596. https://doi.org/10.1029/1999GL900316

Hendon, H. H., Lim, E., Wang, G., Alves, O., & Hudson, D. (2009). Prospects for predicting two flavors of El Niño. *Geophysical Research Letters*, *36*, L19713. https://doi.org/10.1029/2009GL040100

Hirst, A. C. (1986). Unstable and damped equatorial modes in simple coupled ocean–atmosphere models. *Journal of the Atmospheric Sciences*, *43*(6), 606–632. https://doi.org/10.1175/1520-0469(1986)043%3C0606:UADEMI%3E2.0.CO;2

Hoerling, M. P., Kumar, A., & Xu, T. Y. (2001). Robustness of the nonlinear climate response to ENSO's extreme ohases. *Journal of Climate*, *14*(6), 1277–1293. https://doi.org/10.1175/1520-0442(2001)014%3C1277:ROTNCR%3E2.0.CO;2

Hong, L. C., Ho, L., & Jin, F.-F. (2014). A Southern Hemisphere booster of super El Niño. *Geophysical Research Letters*, *41*, 2142–2149. https://doi.org/10.1002/2014GL059370

Horel, J. D. (1982). On the annual cycle of the tropical Pacific atmosphere and ocean. *Monthly Weather Review*, *110*(12), 1863–1878. https://doi.org/10.1175/1520-0493(1982)110%3C1863:OTACOT%3E2.0.CO;2

Horii, T., Ueki, I., & Hanawa, K. (2012). Breakdown of ENSO predictors in the 2000s: Decadal changes of recharge/discharge-SST phase relation and atmospheric intraseasonal forcing. *Geophysical Research Letters*, *39*, L10707. https://doi.org/10.1029/2012GL051740

Hsiang, S. M., Meng, K. C., & Cane, M. A. (2011). Civil conflicts are associated with the global climate. *Nature*, *476*(7361), 438–441. https://doi.org/10.1038/nature10311

Hu, S., & Fedorov, A. V. (2016). Exceptionally strong easterly wind burst stalling El Niño of 2014. *PNAS*, *113*(8), 2005–2010. https://doi.org/10.1073/pnas.1514182113

Hu, S., & Fedorov, A. V. (2017a). The extreme El Niño of 2015–2016: The role of westerly and easterly wind bursts, and preconditioning by the failed 2014 event. *Climate Dynamics*. https://doi.org/10.1007/s00382-017-3531-2

Hu, S., & Fedorov, A. V. (2017b). The extreme El Niño of 2015–2016 and the end of global warming hiatus. *Geophysical Research Letters*, *44*, 3816–3824. https://doi.org/10.1002/2017GL072908

Hu, S., Fedorov, A. V., Lengaigne, M., & Guilyardi, E. (2014). The impact of westerly wind bursts on the diversity and predictability of El Niño events: An ocean energetics perspective. *Geophysical Research Letters*, *41*, 4654–4663. https://doi.org/10.1002/2014GL059573

Hu, Z.-Z., Kumar, A., Ren, H. L., Wang, H., L'Heureux, M., & Jin, F. F. (2013). Weakened interannual variability in the tropical Pacific Ocean since 2000. *Journal of Climate*, *26*(8), 2601–2613. https://doi.org/10.1175/JCLI-D-12-00265.1

Huang, B., Banzon, V. F., Freeman, E., Lawrimore, J., Liu, W., Peterson, T. C., … Zhang, H.-M. (2015). Extended reconstructed sea surface temperature version 4 (ERSST.v4): Part I. Upgrades and intercomparisons. *Journal of Climate*, *28*(3), 911–930. https://doi.org/10.1175/JCLI-D-14-00006.1

Huang, B., Thorne, P., Banzon, V., Boyer, T., Chepurin, G., Lawrimore, J., … Zhang, H. (2017). Extended reconstructed sea surface temperature version 5 (ERSSTv5): Upgrades, validations, and intercomparisons. *Journal of Climate*, *30*(20), 8179–8205. https://doi.org/10.1175/JCLI-D-16-0836.1

Huang, B., Xue, Y., Wang, H., Wang, W., & Kumar, A. (2012). Mixed layer heat budget of the El Niño in NCEP climate forecast system. *Climate Dynamics*, *39*(1-2), 365–381. https://doi.org/10.1007/s00382-011-1111-4

Huang, B., Xue, Y., Zhang, D., Kumar, A., & McPhaden, M. J. (2010). The NCEP GODAS ocean analysis of the tropical Pacific mixed layer heat budget on seasonal to interannual time scales. *Journal of Climate*, *23*(18), 4901–4925. https://doi.org/10.1175/2010JCLI3373.1

Iizumi, T., Luo, J.-J., Challinor, A. J., Sakurai, G., Yokozawa, M., Sakuma, H., … Yamagata, T. (2014). Impacts of El Niño Southern Oscillation on the global yields of major crops. *Nature Communications*, *5*, 3712. https://doi.org/10.1038/ncomms4712

Ishii, M., Shouji, A., Sugimoto, S., & Matsumoto, T. (2005). Objective analyses of sea-surface temperature and marine meteorological variables for the 20th century using ICOADS and the Kobe collection. *International Journal of Climatology*, *25*(7), 865–879. https://doi.org/10.1002/joc.1169

Izumo, T., Vialard, J., Dayan, H., Lengaigne, M., & Suresh, I. (2016). A simple estimation of equatorial Pacific response from windstress to untangle Indian Ocean dipole and basin influences on El Niño. *Climate Dynamics*, *46*(7-8), 2247–2268. https://doi.org/10.1007/s00382-015-2700-4

Izumo, T., Vialard, J., Lengaigne, M., de Boyer Montegut, C., Behera, S. K., Luo, J.-J., … Masson, S. (2010). Influence of the state of the Indian Ocean dipole on the following year's El Niño. *Nature Geoscience*, *3*(3), 168–172. https://doi.org/10.1038/ngeo760

Jensen, M. H., Bak, P., & Bohr, T. (1984). Transition to chaos by interaction of resonances in dissipative systems. I. Circle maps. *Physical Review A*, *30*(4), 1960–1969. https://doi.org/10.1103/PhysRevA.30.1960

Jin, F.-F. (1997). An equatorial ocean recharge paradigm for ENSO. Part I: Conceptual model. *Journal of the Atmospheric Sciences*, *54*(7), 811–829. https://doi.org/10.1175/1520-0469(1997)054%3C0811:AEORPF%3E2.0.CO;2

Jin, F.-F., An, S.-I., Timmermann, A., & Zhao, J. (2003). Strong El Niño events and nonlinear dynamical heating. *Geophysical Research Letters*, *30*(3). 1120. https://doi.org/10.1029/2002GL016356

Jin, F.-F., Boucharel, J., & Lin, I.-I. (2014). Eastern Pacific tropical cyclones intensified by El Niño delivery of subsurface ocean heat. *Nature*, *516*(7529), 82–85. https://doi.org/10.1038/nature13958

Jin, F.-F., Kim, S., & Bejarano, L. (2006). A coupled-stability index for ENSO. *Geophysical Research Letters*, *33*, L23708. https://doi.org/10.1029/2006GL027221

Jin, F.-F., & Neelin, J. D. (1993). Modes of interannual tropical ocean-atmosphere interaction-a unified view. Part I: Numerical results. *Journal of the Atmospheric Sciences*, *50*(21), 3477–3503. https://doi.org/10.1175/1520-0469(1993)050%3C3477:MOITOI%3E2.0.CO;2

Jin, F.-F., Neelin, J. D., & Ghil, M. (1994). El Niño on the Devil's Staircase: Annual subharmonic steps to chaos. *Science*, *264*(5155), 70–72. https://doi.org/10.1126/science.264.5155.70

Jin, F.-F., Neelin, J. D., & Ghil, M. (1996). El Niño/Southern Oscillation and the annual cycle: Subharmonic frequency-locking and aperiodicity. *Physica D*, *98*(2-4), 442–465. https://doi.org/10.1016/0167-2789(96)00111-X

Jonkman, S. N. (2005). Global perspectives on loss of human life caused by floods. *Natural Hazards*, *34*(2), 151–175. https://doi.org/10.1007/s11069-004-8891-3

Kajtar, J., Santoso, A., England, M. H., & Cai, W. (2017). Tropical climate variability: Interactions across the Pacific, Indian, and Atlantic Oceans. *Climate Dynamics*, *48*(7-8), 2173–2190. https://doi.org/10.1007/s00382-016-3199-z

Kalnay, K., Kanamitsu, M., Kistler, R., Collins, W., Deaven, D., Gandin, L., … Saha, S. (1996). The NCEP/NCAR 40-year reanalysis project. *Bulletin of the American Meteorological Society*, *77*(3), 437–471. https://doi.org/10.1175/1520-0477(1996)077%3C0437:TNYRP%3E2.0.CO;2

Kang, I.-S., & Kug, J.-S. (2002). El Niño and La Niña sea surface temperature anomalies: Asymmetry characteristics associated with their wind stress anomalies. *Journal of Geophysical Research*, *107*(D19), 4372. https://doi.org/10.1029/2001JD000393

Kao, H.-Y., & Yu, J.-Y. (2009). Contrasting eastern-Pacific and central Pacific types of ENSO. *Journal of Climate*, *22*(3), 615–632. https://doi.org/10.1175/2008JCLI2309.1

Karnauskas, K. B. (2013). Can we distinguish canonical El Niño from Modoki? *Geophysical Research Letters*, *40*, 5246–5251. https://doi.org/10.1002/grl.51007

Kennedy, J. J. (2014). A review of uncertainty in in situ measurements and data sets of sea surface temperature. *Reviews of Geophysics*, *52*, 1–32. https://doi.org/10.1002/2013RG000434

Kent, E. C., Kennedy, J. J., Smith, T. M., Hirahara, S., Huang, B., Kaplan, A., … Atkinson, C. P. (2017). A call for new approaches to quantifying biases in observations of sea surface temperature. *Bulletin of the American Meteorological Society*, *98*(8), 1601–1616. https://doi.org/10.1175/BAMS-D-15-00251.1

Kessler, W. S. (2002). Is ENSO a cycle or a series of events? *Geophysical Research Letters*, *29*(23), 2125. https://doi.org/10.1029/2002GL015924.

Khalil, A. F., Kwon, H.-H., Lall, U., Miranda, M. J., & Skees, J. (2007). El Niño-Southern Oscillation-based index insurance for floods: Statistical risk analyses and application to Peru. *Water Resources Research*, *43*, W10416. https://doi.org/10.1029/2006WR005281

Kiladis, G. N., Storch, H. V., & Loon, H. V. (1989). Origin of the South Pacific convergence zone. *Journal of Climate*, *2*(10), 1185–1195. https://doi.org/10.1175/1520-0442(1989)002%3C1185:OOTSPC%3E2.0.CO;2

Kim, S.-T., Cai, W., Jin, F.-F., Santoso, A., Wu, L., Guilyardi, E., & An, S.-I. (2014). Response of el Niño sea surface temperature variability to greenhouse warming. *Nature Climate Change*, *4*(9), 786–790. https://doi.org/10.1038/nclimate2326

Kim, W., Cai, W., & Kug, J.-S. (2015). Migration of atmospheric convection coupled with ocean currents pushes el Niño to extremes. *Geophysical Research Letters*, *42*, 3583–3590. https://doi.org/10.1002/2015GL063886

Kim, S.-T., & Jin, F.-F. (2011). An ENSO stability analysis. Part II: Results from the twentieth and twenty-first century simulations of the CMIP3 models. *Climate Dynamics*, *36*(7-8), 1609–1627. https://doi.org/10.1007/s00382-010-0872-5

Kim, S. T., & Yu, J.-Y. (2012). The two types of ENSO in CMIP5 models. *Geophysical Research Letters*, *39*, L11704. https://doi.org/10.1029/2012GL052006

Kirtman, B., & Schopf, P. S. (1998). Decadal variability in ENSO predictability and prediction. *Journal of Climate*, *11*(11), 2804–2822. https://doi.org/10.1175/1520-0442(1998)011%3C2804:DVIEPA%3E2.0.CO;2

Klein, S. A., Soden, B. J., & Lau, N. C. (1999). Remote sea surface temperature variations during ENSO: Evidence for a tropical atmospheric bridge. *Journal of Climate*, *12*(4), 917–932. https://doi.org/10.1175/1520-0442(1999)012%3C0917:RSSTVD%3E2.0.CO;2

Kosaka, Y., & Xie, S.-P. (2013). Recent global-warming hiatus tied to equatorial Pacific surface cooling. *Nature*, *501*(7467), 403–407. https://doi.org/10.1038/nature12534

Kucharski, F., Parvin, A., Rodriguez-Fonseca, B., Farneti, R., Martin-Rey, M., Polo, I., … Losada, T. (2016). The teleconnection of the tropical Atlantic to indo-Pacific sea surface temperatures on inter-annual to centennial time scales: A review of recent findings. *Atmosphere*, *7*(2), 29. https://doi.org/10.3390/atmos7020029

Kug, J., Jin, F., & An, S. (2009). Two types of El Niño events: Cold tongue El Niño and warm pool El Niño. *Journal of Climate*, *22*(6), 1499–1515. https://doi.org/10.1175/2008JCLI2624.1

Kug, J.-S., Li, T., An, S.-I., Kang, I.-S., Luo, J.-J., Masson, S., & Yamagata, T. (2006). Role of the ENSO–Indian Ocean coupling on ENSO variability in a coupled GCM. *Geophysical Research Letters*, *33*, L09710. https://doi.org/10.1029/2005GL024916

Kunii, O., Nakamura, S., Abdur, R., & Wakai, S. (2002). The impact on health and risk factors of the diarrhoea epidemics in the 1998 Bangladesh floods. *Public Health*, *116*(2), 68–74. https://doi.org/10.1016/S0033-3506(02)00506-1

L'Heureux, M. L., Lee, S., & Lyon, B. (2013). Recent multidecadal strengthening of the Walker circulation across the tropical Pacific. *Nature Climate Change*, *3*, 571–576. https://doi.org/10.1038/nclimate1840

L'Heureux, M. L., Takahashi, K., Watkins, A. B., Barnston, A. G., Becker, E. J., Di Liberto, T. E., … Gottschalck, J. (2017). Observing and predicting the 2015/16 El Niño. *Bulletin of the American Meteorological Society*, *98*(7), 1363–1382. https://doi.org/10.1175/BAMS-D-16-0009.1

Larkin, N. K., & Harrison, D. E. (2005). On the definition of El Niño and associated seasonal average U.S. weather anomalies. *Geophysical Research Letters*, *32*, L13705. https://doi.org/10.1029/2005GL022738

Latif, M., Anderson, D. L. T., Barnett, T., Cane, M., Kleeman, R., Leetmaa, A., … Rosati, A. (1998). A review of the predictability and prediction of ENSO. *Journal of Geophysical Research*, *103*(C7), 14,375–14,393. https://doi.org/10.1029/97JC03413

Latif, M., & Keenlyside, N. S. (2009). El Nino/Southern Oscillation response to global warming. *PNAS*, *106*(49), 20,578–20,583. https://doi.org/10.1073/pnas.0710860105

Lau, N.-C., & Nath, M. J. (2003). Atmosphere–ocean variations in the Indo-Pacific sector during ENSO episodes. *Journal of Climate*, *16*(1), 3–20. https://doi.org/10.1175/1520-0442(2003)016%3C0003:AOVITI%3E2.0.CO;2

Lee, T., & McPhaden, M. J. (2010). Increasing intensity of El Niño in the central-equatorial Pacific. *Geophysical Research Letters*, *37*, L14603. https://doi.org/10.1029/2010GL044007

Lengaigne, M., Guilyardi, E., Boulanger, J.-P., Menkes, C., Delecluse, P., Inness, P., … Slingo, J. M. (2004). Triggering of El Niño by westerly wind events in a coupled general circulation model. *Climate Dynamics*, *23*(6), 601–620. https://doi.org/10.1007/s00382-004-0457-2

Lengaigne, M., & Vecchi, G. A. (2010). Contrasting the termination of moderate and extreme el Niño events in coupled general circulation models. *Climate Dynamics*, *35*(2-3), 299–313. https://doi.org/10.1007/s00382-009-0562-3

Levine, A. F. Z., Jin, F.-F., & McPhaden, M. J. (2016). Extreme noise-extreme El Niño: How state-dependent noise forcing creates El Niño-La Niña asymmetry. *Journal of Climate*, *29*(15), 5483–5499. https://doi.org/10.1175/JCLI-D-16-0091.1

Levine, A. F. Z., & McPhaden, M. J. (2015). The annual cycle in ENSO growth rate as a cause of the spring predictability barrier. *Geophysical Research Letters*, *42*, 5034–5041. https://doi.org/10.1002/2015GL064309

Levine, A. F. Z., & McPhaden, M. J. (2016). How the July 2014 easterly wind burst gave the 2015–2016 El Niño a head start. *Geophysical Research Letters*, *43*, 6503–6510. https://doi.org/10.1002/2016GL069204

Li, T., & Philander, G. (1996). On the annual cycle of the eastern equatorial Pacific. *Journal of Climate*, *9*(12), 2986–2998. https://doi.org/10.1175/1520-0442(1996)009%3C2986:OTACOT%3E2.0.CO;2

Li, J., Xie, S.-P., Cook, E. R., Morales, M. S., Christie, D. A., Johnson, N. C., … D'Arrigo, R. (2013). El Niño modulations over the past seven centuries. *Nature Climate Change*, *3*(9), 822–826. https://doi.org/10.1038/nclimate1936

Lin, C.-Y., Yu, J.-Y. & Hsu, H.-H. (2015). CMIP5 model simulations of the Pacific meridional mode and its connection to the two types of ENSO. *International Journal of Climatology*, *35*, 2352–2358. https://doi.org/10.1002/joc.4130

Liu, Z., & Alexander, M. (2007). Atmospheric bridge, oceanic tunnel, and global climatic teleconnections. *Reviews of Geophysics*, *45*, RG2005. https://doi.org/10.1029/2005RG000172

Lübbecke, J. F., & McPhaden, M. J. (2014). Assessing the twenty-first-century shift in ENSO variability in terms of the Bjerknes stability index. *Journal of Climate*, *27*(7), 2577–2587. https://doi.org/10.1175/JCLI-D-13-00438.1

Luo, J., Masson, S., Roeckner, E., Madec, G., & Yamagata, T. (2005). Reducing climatology bias in an ocean–atmosphere CGCM with improved coupling physics. *Journal of Climate*, *18*(13), 2344–2360. https://doi.org/10.1175/JCLI3404.1

Lyle, M., Barron, J., Bralower, T. J., Huber, M., Olivarez Lyle, A., Ravelo, A. C., … Wilson, P. A. (2008). Pacific Ocean and Cenozoic evolution of climate. *Reviews of Geophysics*, *46*, RG2002. https://doi.org/10.1029/2005RG000190

MacMynowski, D. G., & Tziperman, E. (2008). Factors affecting ENSO's period. *Journal of the Atmospheric Sciences*, *65*(5), 1570–1586. https://doi.org/10.1175/2007JAS2520.1

Mantua, N. J., Hare, S. R., Zhang, Y., Wallace, J. M., & Francis, R. C. (1997). A Pacific interdecadal climate oscillation with impacts on salmon production. *Bulletin of the American Meteorological Society*, *78*(6), 1069–1079. https://doi.org/10.1175/1520-0477(1997)078%3C1069:APICOW%3E2.0.CO;2

Manucharyan, G. E., & Fedorov, A. (2014). Robust ENSO across a wide range of climates. *Journal of Climate*, *27*(15), 5836–5850. https://doi.org/10.1175/JCLI-D-13-00759.1

Marshall, J., Ferreira, D., Campin, J. M., & Enderton, D. (2007). Mean climate and variability of the atmosphere and ocean on an aquaplanet. *Journal of the Atmospheric Sciences*, *64*(12), 4270–4286. https://doi.org/10.1175/2007JAS2226.1

McGregor, S., Ramesh, N., Spence, P., England, M. H., McPhaden, M. J., & Santoso, A. (2013). Meridional movement of wind anomalies during ENSO events and their role in event termination. *Geophysical Research Letters*, *40*, 749–754. https://doi.org/10.1002/grl.50136

McGregor, S., Timmermann, A., England, M. H., Timm, O., & Wittenberg, A. T. (2013). Inferred changes in El Niño–Southern Oscillation variance over the past six centuries. *Climate of the Past*, *9*(5), 2269–2284. https://doi.org/10.5194/cp-9-2269-2013

McGregor, S., Timmermann, A., Schneider, N., Stuecker, M. F., & England, M. H. (2012). The effect of the South Pacific convergence zone on the termination of el Niño events and the meridional asymmetry of ENSO. *Journal of Climate*, *25*(16), 5566–5586. https://doi.org/10.1175/JCLI-D-11-00332.1

McPhaden, M. J. (1999). Genesis and evolution of the 1997-98 El Niño. *Science*, *283*(5404), 950–954. https://doi.org/10.1126/science.283.5404.950

McPhaden, M. J. (2003). Tropical Pacific Ocean heat content variations and ENSO persistence barriers. *Geophysical Research Letters*, *30*(9), 1480. https://doi.org/10.1029/2003GL016872

McPhaden, M. J. (2012). A 21st century shift in the relationship between ENSO SST and warm water volume anomalies. *Geophysical Research Letters*, *39*, L09706. https://doi.org/10.1029/2012GL051826

McPhaden, M. J. (2015). Playing hide and seek with El Niño. *Nature Climate Change*, *5*(9), 791–795. https://doi.org/10.1038/nclimate2775

McPhaden, M. J., Busalacchi, A. J., Cheney, R., Donguy, J.-R., Gage, K. S., Halpern, D., … Julian, P. (1998). The Tropical Ocean-global atmosphere observing system: A decade of progress. *Journal of Geophysical Research*, *103*(C7), 14,169–14,240. https://doi.org/10.1029/97JC02906

McPhaden, M. J., Zebiak, S. E., & Glantz, M. H. (2006). ENSO as an integrating concept in earth science. *Science*, *314*(5806), 1740–1745. https://doi.org/10.1126/science.1132588

McPhaden, M. J., & Zhang, X. B. (2009). Asymmetry in zonal phase propagation of ENSO sea surface temperature anomalies. *Geophysical Research Letters*, *36*, L13703. https://doi.org/10.1029/2009GL038774

Medhaug, I., Stolpe, M. B., Fischer, E. M., & Knutti, R. (2017). Reconciling controversies about the 'global warming hiatus'. *Nature*, *545*, 41–47, https://doi.org/10.1038/nature22315

Meehl, G. A., Covey, C., Taylor, K. E., Delworth, T., Stouffer, R. J., Latif, M., … Mitchell, J. F. B. (2007). The WCRP CMIP3 multimodel dataset: A new era in climate change research. *Bulletin of the American Meteorological Society*, *88*(9), 1383–1394. https://doi.org/10.1175/BAMS-88-9-1383

Meehl, G. A., Hu, A., & Teng, H. (2016). Initialized decadal prediction for transition to positive phase of the Interdecadal Pacific Oscillation. *Nature Communications*, *7*, 11,718. https://doi.org/10.1038/ncomms11718

Meinen, C. S., & McPhaden, M. J. (2000). Observations of warm water volume changes in the equatorial Pacific and their relationship to el Niño and la Niña. *Journal of Climate*, *13*(20), 3551–3559. https://doi.org/10.1175/1520-0442(2000)013%3C3551:OOWWVC%3E2.0.CO;2

Menemenlis, D., Campin, J., Heimbach, P., Hill, C., Lee, T., Nguyen, A., … Zhang, H. (2008). ECCO2: High resolution global ocean and sea ice data synthesis. *Mercator Ocean Quarterly Newsletter*, *31*, 13–21.

Menkes, C., Lengaigne, M., Vialard, J., Puy, M., Marchesiello, P., Cravatte, S., & Cambon, G. (2014). About the role of westerly wind events in the possible development of an El Niño in 2014. *Geophysical Research Letters*, *41*, 6476–6483. https://doi.org/10.1002/2014GL061186

Merle, J. (1980). Variabilité thermique annuelle et interannuelle de l'océan Atlantique équatorial Est. L'hypothése d'un "El Niño" Atlantique. *Oceanologica Acta*, *3*, 209–220.

Merlen, G. (1984). The 1982–83 El Niño: Some of its consequences for Galapagos wildlife. *Oryx*, *18*(04), 210–214. https://doi.org/10.1017/S0030605300019244

Meyers, G., McIntosh, P., Pigot, L., & Pook, M. (2007). The years of El Niño, La Niña, and interactions with the tropical Indian Ocean. *Journal of Climate*, *20*(13), 2872–2880. https://doi.org/10.1175/JCLI4152.1

Monahan, A. H., & Dai, A. (2004). The spatial and temporal structure of ENSO nonlinearity. *Journal of Climate*, *17*(15), 3026–3036. https://doi.org/10.1175/1520-0442(2004)017%3C3026:TSATSO%3E2.0.CO;2

Münnich, M., Cane, M. A., & Zebiak, S. E. (1991). A study of self-excited oscillations of the tropical ocean-atmosphere system. Part II: Nonlinear cases. *Journal of the Atmospheric Sciences*, *48*(10), 1238–1248. https://doi.org/10.1175/1520-0469(1991)048%3C1238:ASOSEO%3E2.0.CO;2

Murty, T. S., Scott, D., & Baird, W. (2000). The 1997 El Niño, Indonesian forest fires, and the Malaysian smoke problem: A deadly combination of natural and man-made hazard. *Natural Hazards*, *21*(2/3), 131–144. https://doi.org/10.1023/A:1008141003518

Neelin, J. D., Battisti, D. S., Hirst, A. C., Jin, F.-F., Wakata, Y., Yamagata, T., & Zebiak, S. E. (1998). ENSO theory. *Journal of Geophysical Research*, *103*(C7), 14,261–14,290. https://doi.org/10.1029/97JC03424

Neelin, J. D., Jin, F.-F., & Syu, H.-H. (2000). Variations in ENSO phase locking. *Journal of Climate*, *13*(14), 2570–2590. https://doi.org/10.1175/1520-0442(2000)013%3C2570:VIEPL%3E2.0.CO;2

Newman, M., Alexander, M. A., Ault, T. R., Cobb, K. M., Deser, C., Di Lorenzo, E., … Miller, A. J. (2016). The Pacific Decadal Oscillation, revisited. *Journal of Climate*, *29*(12), 4399–4427. https://doi.org/10.1175/JCLI-D-15-0508.1

Okumura, Y., & Deser, C. (2010). Asymmetry in the duration of El Niño and La Niña. *Journal of Climate*, *23*(21), 5826–5843. https://doi.org/10.1175/2010JCLI3592.1

Paek, H., Yu, J.-Y., & Qian, C. (2017). Why were the 2015/2016 and 1997/1998 extreme El Niños different? *Geophysical Research Letters*, *44*, 1848–1856. https://doi.org/10.1002/2016GL071515

Philander, S. G. H. (1983). El Niño Southern Oscillation phenomena. *Nature*, *302*(5906), 295–301. https://doi.org/10.1038/302295a0

Philander, S. G. H., Yamagata, T., & Pacanowski, R. C. (1984). Unstable air–sea interactions in the tropics. *Journal of the Atmospheric Sciences*, *41*(4), 604–613. https://doi.org/10.1175/1520-0469(1984)041%3C0604:UASIIT%3E2.0.CO;2

Picaut, J., Masia, F., & du Penhoat, Y. (1997). An advective–reflective conceptual model for the oscillatory nature of the ENSO. *Science*, *277*(5326), 663–666. https://doi.org/10.1126/science.277.5326.663

Power, S. B., & Callaghan, J. (2016). Variability in severe coastal flooding, associated storms, and death tolls in southeastern Australia since the mid-nineteenth century. *Journal of Applied Meteorology and Climatology*, *55*(5), 1139–1149. https://doi.org/10.1175/JAMC-D-15-0146.1

Power, S., Casey, T., Folland, C., Colman, A., & Mehta, V. (1999). Inter-decadal modulation of the impact of ENSO on Australia. *Climate Dynamics*, *15*(5), 319–324. https://doi.org/10.1007/s003820050284

Power, S., Delage, F., Chung, C., Kociuba, G., & Keay, K. (2013). Robust twenty-first-century projections of El Niño and related precipitation variability. *Nature*, *502*(7472), 541–545. https://doi.org/10.1038/nature12580

Power, S. P., Delage, F., Chung, C., Ye, H., & Murphy, B. (2017). Humans have already increased the risk of major disruptions to Pacific rainfall. *Nature Communications*, *8*. https://doi.org/10.1038/ncomms14368

Puy, M., Vialard, J., Lengaigne, M., & Guilyardi, E. (2016). Modulation of equatorial Pacific westerly/easterly wind events by the Madden–Julian oscillation and convectively-coupled Rossby waves. *Climate Dynamics*, *46*(7-8), 2155–2178. https://doi.org/10.1007/s00382-015-2695-x

Rasmusson, E. M., & Carpenter, T. H. (1982). Variations in tropical sea surface temperature and surface wind fields associated with the Southern Oscillation/El Niño. *Monthly Weather Review*, *110*(5), 354–384. https://doi.org/10.1175/1520-0493(1982)110%3C0354:VITSST%3E2.0.CO;2

Rayner, N. A., Parker, D. E., Horton, E. B., Folland, C. K., Alexander, L. V., Rowell, D. P., … Kaplan, A. (2003). Global analyses of sea surface temperature, sea ice, and night marine air temperature since the late nineteenth century. *Journal of Geophysical Research*, *108*(D14), 4407. https://doi.org/10.1029/2002JD002670

Ren, H.-L., & Jin, F.-F. (2013). Recharge oscillator mechanisms in two types of ENSO. *Journal of Climate*, *26*(17), 6506–6523. https://doi.org/10.1175/JCLI-D-12-00601.1

Rodríguez-Fonseca, B., Polo, I., J. García-Serrano, Losada, T., Mohino, E., Mechoso, C. R., & Kucharski, F. (2009). Are Atlantic Niños enhancing Pacific ENSO events in recent decades? *Geophysical Research Letters*, *36*, L20705. https://doi.org/10.1029/2009GL040048

Rosenthal, Y., & Broccoli, A. J. (2004). In search of paleo-ENSO. *Science*, *304*(5668), 219–221. https://doi.org/10.1126/science.1095435

Saji, N. H., Goswami, B. N., Vinayachandran, P. N., & Yamagata, T. (1999). A dipole mode in the tropical Indian Ocean. *Nature*, *401*(6751), 360–363. https://doi.org/10.1038/43854

Saji, N. H., Xie, S.-P., & Yamagata, T. (2006). Tropical Indian Ocean variability in the IPCC twentieth-century climate simulations. *Journal of Climate*, *19*(17), 4397–4417. https://doi.org/10.1175/JCLI3847.1

Santoso, A., Cai, W., Collins, M., McPhaden, M., Jin, F.-F., Guilyardi, E., … Wang, G. (2015). ENSO extremes and diversity: Dynamics, teleconnections, and impacts. *Bulletin of the American Meteorological Society*, *96*(11), 1969–1972. https://doi.org/10.1175/BAMS-D-15-00141.1

Santoso, A., Cai, W., England, M. H., & Phipps, S. J. (2011). The role of the Indonesian throughflow on ENSO dynamics in a coupled climate model. *Journal of Climate*, *24*(3), 585–601. https://doi.org/10.1175/2010JCLI3745.1

Santoso, A., England, M. H., & Cai, W. (2012). Impact of Indo-Pacific feedback interactions on ENSO dynamics diagnosed using ensemble climate simulations. *Journal of Climate*, *25*(21), 7743–7763. https://doi.org/10.1175/JCLI-D-11-00287.1

Santoso, A., McGregor, S., Jin, F.-F., Cai, W., England, M. H., An, S.-I., … Guilyardi, E. (2013). Late-twentieth-century emergence of the El Niño propagation asymmetry and future projections. *Nature*, *504*(7478), 126–130. https://doi.org/10.1038/nature12683

Schneider, T., Bischoff, T., & Haug, G. H. (2014). Migrations and dynamics of the intertropical convergence zone. *Nature*, *513*(7516), 45–53. https://doi.org/10.1038/nature13636

Sen Gupta, A., McGregor, S., van Sebille, E., Ganachaud, A., Brown, J., & Santoso, A. (2016). Future changes to the Indonesian throughflow and Pacific circulation: The differing role of wind and deep circulation changes. *Geophysical Research Letters*, *43*, 1669–1678. https://doi.org/10.1002/2016GL067757

Smith, T. M., & Reynolds, R. W. (2004). Improved extended reconstructions of SST (1854–1997). *Journal of Climate*, *17*(12), 2466–2477. https://doi.org/10.1175/1520-0442(2004)017<2466:IEROS>2.0.CO;2

Solomon, A., & Newman, M. (2012). Reconciling disparate twentieth-century Indo-Pacific ocean temperature trends in the instrumental record. *Nature Climate Change*, *2*(9), 691–699. https://doi.org/10.1038/nclimate1591

Song, Q., Vecchi, G. A., & Rosati, A. J. (2007). The role of the Indonesian throughflow in the Indo-Pacific climate variability in the GFDL coupled climate model. *Journal of Climate*, *20*(11), 2434–2451. https://doi.org/10.1175/JCLI4133.1

Stein, K., Schneider, N., Timmermann, A., & Jin, F.-F. (2010). Seasonal synchronization of ENSO events in a linear stochastic model. *Journal of Climate*, *23*(21), 5629–5643. https://doi.org/10.1175/2010JCLI3292.1

Stein, K., Timmermann, A., Schneider, N., Jin, F.-F., & Stuecker, M. F. (2014). ENSO seasonal synchronization theory. *Journal of Climate*, *27*(14), 5285–5310. https://doi.org/10.1175/JCLI-D-13-00525.1

Stephens, D. J., Meuleners, M. J., van Loon, H., Lamond, M. H., & Telcik, N. P. (2007). Differences in atmospheric circulation between the development of weak and strong warm events in the southern oscillation. *Journal of Climate*, *20*(10), 2191–2209. https://doi.org/10.1175/jcli4131.1

Strong, E., Goreau, T. J., & Hayes, R. L. (1998). Ocean hotspots and coral reef bleaching, January-July 1998. *Reef Encounter*, *24*, 20–22.

Stuecker, M. F., Timmermann, A., Jin, F. F., McGregor, S., & Ren, H. L. (2013). A combination mode of the annual cycle and the El Niño/Southern Oscillation. *Nature Geoscience*, *6*(7), 540–544. https://doi.org/10.1038/ngeo1826

Su, J., Zhang, R., Li, T., Rong, X., Kug, J.-S., & Hong, C.-C. (2010). Causes of the El Niño and La Niña amplitude asymmetry in the equatorial eastern Pacific. *Journal of Climate*, *23*(3), 605–617. https://doi.org/10.1175/2009JCLI2894.1

Suarez, M. J., & Schopf, P. S. (1988). A delayed action oscillator for ENSO. *Journal of the Atmospheric Sciences*, *45*(21), 3283–3287. https://doi.org/10.1175/1520-0469(1988)045%3C3283:ADAOFE%3E2.0.CO;2

Sun, D.-Z., Zhang, T., Sun, Y., & Yu, Y. (2014). Rectification of El Niño–Southern Oscillation into climate anomalies of decadal and longer time scales: Results from forced ocean GCM experiments. *Journal of Climate*, *27*(7), 2545–2561. https://doi.org/10.1175/JCLI-D-13-00390.1

Takahashi, K., & Dewitte, B. (2016). Strong and moderate nonlinear El Niño regimes. *Climate Dynamics*, *46*(5-6), 1627–1645. https://doi.org/10.1007/s00382-015-2665-3

Takahashi, K., Montecinos, A., Goubanova, K., & Dewitte, B. (2011). ENSO regimes: Reinterpreting the canonical and Modoki El Niño. *Geophysical Research Letters*, *38*, L10704. https://doi.org/10.1029/2011GL047364

Takahashi, T., Nakagawa, H., Satofuka, Y., & Kawaike, K. (2001). Flood and sediment disasters triggered by 1999 rainfall in Venezuela; a river restoration plan for an alluvial fan. *Journal of Natural Disaster Science*, *23*, 65–82.

Tang, Y., Deng, Z., Zhou, X., Cheng, Y., & Chen, D. (2008). Interdecadal variation of ENSO predictability in multiple models. *Journal of Climate*, *21*(18), 4811–4833. https://doi.org/10.1175/2008JCLI2193.1

Taschetto, A. S., Sen Gupta, A., Jourdain, N., Santoso, A., Ummenhofer, C. C., & England, M. H. (2014). Cold tongue and warm pool ENSO events in CMIP5: Mean state and future projections. *Journal of Climate*, *27*(8), 2861–2885. https://doi.org/10.1175/JCLI-D-13-00437.1

Taylor, K. E., Stouffer, R. J., & Meehl, G. A. (2012). An overview of CMIP5 and the experiment design. *Bulletin of the American Meteorological Society*, *93*(4), 485–498. https://doi.org/10.1175/BAMS-D-11-00094.1

Terray, P., Masson, S., Prodhomme, C., Roxy, M. K., & Sooraj, K. P. (2016). Impacts of Indian and Atlantic oceans on ENSO in a comprehensive modeling framework. *Climate Dynamics*, *46*(7-8), 2507–2533. https://doi.org/10.1007/s00382-015-2715-x

Timmermann, A., An, S.-I., Krebs, U., & Goosse, H. (2005). ENSO suppression due to weakening of the North Atlantic thermohaline circulation. *Journal of Climate*, *18*(16), 3122–3139. https://doi.org/10.1175/JCLI3495.1

Timmermann, A., Jin, F.-F., & Abshagen, J. (2003). A nonlinear theory for El Niño bursting. *Journal of the Atmospheric Sciences*, *60*(1), 152–165. https://doi.org/10.1175/1520-0469(2003)060%3C0152:ANTFEN%3E2.0.CO;2

Timmermann, A., Lorenz, S., An, S.-I., Clement, A., & Xie, S.-P. (2007). The effect of orbital forcing on the mean climate and variability of the tropical Pacific. *Journal of Climate*, *20*(16), 4147–4159. https://doi.org/10.1175/JCLI4240.1

Timmermann, A., Oberhuber, J., Bacher, A., Esch, M., Latif, M., & Roeckner, E. (1999). Increased El Niño frequency in a climate model forced by future greenhouse warming. *Nature*, *398*(6729), 694–697. https://doi.org/10.1038/19505

Trenberth, K. E., & Hurrel, J. W. (1994). Decadal atmosphere-ocean variations in the Pacific. *Climate Dynamics*, *9*(6), 303–319. https://doi.org/10.1007/BF00204745

Trenberth, K. E., & Stepaniak, D. P. (2001). Indices of El Niño evolution. *Journal of Climate*, *14*(8), 1697–1701. https://doi.org/10.1175/1520-0442(2001)014%3C1697:LIOENO%3E2.0.CO;2

Tseng, Y.-H., Ding, R., & Huang, X.-M. (2017). The warm Blob in the northeast Pacific—The bridge leading to the 2015/16 El Niño. *Environmental Research Letters*, *12*(5), 054019. https://doi.org/10.1088/1748-9326/aa67c3

Tudhope, A. W., Chilcott, C. P., McCulloch, M. T., Cook, E. R., Chappell, J., Ellam, R. M., … Shimmield, G. B. (2001). Variability in the El Niño-Southern Oscillation through a glacial-interglacial cycle. *Science*, *291*, 1511. https://doi.org/10.1126/science.1057969 pmid:11222850

Tziperman, E., Zebiak, S. E., & Cane, M. A. (1997). Mechanisms of seasonal–ENSO interaction. *Journal of the Atmospheric Sciences*, *54*(1), 61–71. https://doi.org/10.1175/1520-0469(1997)054%3C0061:MOSEI%3E2.0.CO;2

Tziperman, E., Stone, L., Cane, M. A., & Jarosh, H. (1994). El Niño chaos: Overlapping of resonances between the seasonal cycle and the Pacific Ocean-atmosphere oscillator. *Science*, *264*(5155), 72–74. https://doi.org/10.1126/science.264.5155.72

Valle, C. A., Cruz, F., Cruz, J. B., Merlen, G., & Coulter, M. C. (1987). The impact of the 1982–1983 E1 Niño-Southern Oscillation on seabirds in the Galapagos Islands, Ecuador. *Journal of Geophysical Research*, *92*(C13), 14,437–14,444. https://doi.org/10.1029/JC092iC13p14437

Vecchi, G. A., & Soden, B. J. (2007). Global warming and the weakening of the tropical circulation. *Journal of Climate*, *20*(17), 4316–4340. https://doi.org/10.1175/JCLI4258.1

Vecchi, G. A., Soden, B. J., Wittenberg, A. T., Held, I. M., Leetmaa, A., & Harrison, M. J. (2006). Weakening of tropical Pacific atmospheric circulation due to anthropogenic forcing. *Nature*, *441*(7089), 73–76. https://doi.org/10.1038/nature04744

Vimont, D. J., Alexander, M. A., & Newman, M. (2014). Optimal growth of central and east Pacific ENSO events. *Geophysical Research Letters*, *41*, 4027–4034. https://doi.org/10.1002/2014GL059997

Vos, R., Velasco, M., and de Labastida, E. (1999). Economic and social effects of El Niño in Ecuador, 1997–1998, Inter-American Development Bank, Sustainable Development Dept. Tech. Papers Series, POV-107.

Wang, C. (2001). A unified oscillator model for the El Niño-Southern Oscillation. *Journal of Climate*, *14*(1), 98–115. https://doi.org/10.1175/1520-0442(2001)014%3C0098:AUOMFT%3E2.0.CO;2

Wang, B., & An, S. (2002). A mechanism for decadal changes of ENSO behavior: Roles of background wind changes. *Climate Dynamics*, *18*(6), 475–486. https://doi.org/10.1007/s00382-001-0189-5

Wang, G., Cai, W., Gan, B., Wu, L., Santoso, A., Lin, X., … McPhaden, M. (2017). Continued increase of extreme El Nino frequency long after 1.5°C warming stabilization. *Nature Climate Change*, *7*(8), 568–572. https://doi.org/10.1038/nclimate3351

Wang, S. Y., Hipps, L., Gillies, R. R., & Yoon, J. H. (2014). Probable causes of the abnormal ridge accompanying the 2013–2014 California drought: ENSO precursor and anthropogenic warming footprint. *Geophysical Research Letters*, *41*, 3220–3226. https://doi.org/10.1002/2014GL059748

Webster, P. J., & Yang, S. (1992). Monsoon and ENSO: Selectively interactive systems. *Quarterly Journal of the Royal Meteorological Society*, *118*(507), 877–926. https://doi.org/10.1002/qj.49711850705

Weller, E., Min, S., Lee, D., Kug, J., Cai, W., & Yeh, S. (2015). Human contribution to the 2014 record high sea surface temperatures over the western tropical and northeast Pacific Ocean. *Bulletin of the American Meteorological Society. 96*(12), S100–S104. https://doi.org/10.1175/BAMS-D-15-00055.1

Weisberg, R. H., & Wang, C. (1997). A western Pacific oscillator paradigm for the El Niño–Southern Oscillation. *Geophysical Research Letters*, *24*(7), 779–782. https://doi.org/10.1029/97GL00689

Wittenberg, A. T. (2009). Are historical records sufficient to constrain ENSO simulations? *Geophysical Research Letters*, *36*, L12702. https://doi.org/10.1029/2009GL038710

Woodruff, S. D., Worley, S. J., Lubker, S. J., Ji, Z., Eric Freeman, J., Berry, D. I., … Wilkinson, C. (2011). ICOADS release 2.5: Extensions and enhancements to the surface marine meteorological archive. *International Journal of Climatology*, *31*(7), 951–967. https://doi.org/10.1002/joc.2103

Worley, S. J., Woodruff, S. D., Reynolds, R. W., Lubker, S. J., & Lott, N. (2005). ICOADS release 2.1 data and products. *International Journal of Climatology*, *25*(7), 823–842. https://doi.org/10.1002/joc.1166

Wu, R., & Kirtman, B. P. (2004). Understanding the impacts of the Indian Ocean on ENSO variability in a coupled GCM. *Journal of Climate*, *17*(20), 4019–4031. https://doi.org/10.1175/1520-0442(2004)017%3C4019:UTIOTI%3E2.0.CO;2

Xiang, B., Wang, B., & Li, T. (2013). A new paradigm for the predominance of standing central Pacific warming after the late 1990s. *Climate Dynamics*, *41*(2), 327–340. https://doi.org/10.1007/s00382-012-1427-8

Xie, P., & Arkin, P. A. (1997). Global precipitation: A 17-year monthly analysis based on gauge observations, satellite estimates, and numerical model outputs. *Bulletin of the American Meteorological Society*, *78*(11), 2539–2558. https://doi.org/10.1175/1520-0477(1997)078%3C2539:GPAYMA%3E2.0.CO;2

Xie, S.-P., Deser, C., Vecchi, G. A., Ma, J., Teng, H., & Wittenberg, A. (2010). Global warming pattern formation: Sea surface temperature and rainfall. *Journal of Climate*, *4*, 966–986.

Xue, Y., & Kumar, A. (2017). Evolution of the 2015/16 el Niño and historical perspective since 1979. *Science China Earth Sciences*, *60*(9), 1572–1588. https://doi.org/10.1007/s11430-016-0106-9

Yan, X.-H., Ho, C.-R., Zheng, Q., & Klemas, V. (1992). Temperature and size variabilities of the western Pacific warm pool. *Science*, *258*(5088), 1643–1645. https://doi.org/10.1126/science.258.5088.1643

Yeh, S.-W., Kug, J.-S., Dewitte, B., Kwon, M.-H., Kirtman, B. P., & Jin, F.-F. (2009). El Niño in a changing climate. *Nature*, *461*(7263), 511–514. https://doi.org/10.1038/nature08316

Yu, J.-Y., Kao, H.-Y., & Lee, T. (2010). Subtropics-related interannual sea surface temperature variability in the equatorial central Pacific. *Journal of Climate*, *23*, 2869–2884, https://doi.org/10.1175/2010JCLI3171.1

Yu, X., & McPhaden, M. J. (1999). Seasonal variability in the equatorial Pacific. *Journal of Physical Oceanography*, *29*(5), 925–947. https://doi.org/10.1175/1520-0485(1999)029%3C0925:SVITEP%3E2.0.CO;2

Yuan, D., Wang, J., Xu, T., Xu, P., Hui, Z., Zhao, X., … Yu, Y. (2011). Forcing of the Indian Ocean dipole on the interannual variations of the tropical Pacific Ocean: Roles of the Indonesian throughflow. *Journal of Climate*, *24*(14), 3593–3608. https://doi.org/10.1175/2011JCLI3649.1

Zebiak, S. E. (1993). Air–-sea interaction in the equatorial Atlantic region. *Journal of Climate*, *6*(8), 1567–1586. https://doi.org/10.1175/1520-0442(1993)006%3C1567:AIITEA%3E2.0.CO;2

Zebiak, S. E., & Cane, M. A. (1987). A model El Niño-Southern Oscillation. *Monthly Weather Review*, *115*(10), 2262–2278. https://doi.org/10.1175/1520-0493(1987)115%3C2262:AMENO%3E2.0.CO;2

Zhang, H., Clement, A., & Di Nezio, P. (2014). The South Pacific meridional mode: A mechanism for ENSO-like variability. *Journal of Climate*, *27*(2), 769–783. https://doi.org/10.1175/JCLI-D-13-00082.1

Zhang, W., Wang, Y., Jin, F.-F., Stuecker, M. F., & Turner, A. G. (2015). Impact of different El Niño types on the El Niño/IOD relationship. *Geophysical Research Letters*, *42*, 8570–8576. https://doi.org/10.1002/2015GL065703

Zhao, M., Hendon, H. H., Alves, O., Liu, G., & Wang, G. (2016). Weakened eastern Pacific El Niño predictability in the early twenty-first century. *Journal of Climate*, *29*(18), 6805–6822. https://doi.org/10.1175/JCLI-D-15-0876.1

Zheng, X.-T., Xie, S.-P., & Liu, Q. (2011). Response of the Indian Ocean basin mode and its capacitor effect to global warming. *Journal of Climate*, *24*(23), 6146–6164. https://doi.org/10.1175/2011JCLI4169.1